AN ABSTRACT OF THE THESIS OF

Silas Shields for the degree of Master of Science in Civil Engineering presented on June 8, 2017.

Title: Assessing Durability of Reinforced Concrete and Ductile Iron

Abstract approved:

_____

O. Burkan Isgor   Jason H. Ideker

The first goal of this master's thesis was to investigate the linkage between a non-destructive testing method, surface resistivity, and premature concrete deterioration brought on by chloride ingress and/or freeze-thaw cycling. The experimental method for this project consists of taking surface resistivity measurements of reinforced concrete slabs after they were ponded with a magnesium chloride de-icing solution, containing a corrosion inhibitor. Reinforced concrete slabs and companion concrete cylinders also underwent freeze/thaw cycling to observe its effect on surface resistivity in conjunction with exposure to chlorides. Many factors such as internal and ambient temperature and relative humidity affect surface resistivity measurements so this data was also collected. To compare the surface resistivity to the rate of chloride ingress, cores were taken from the slabs. As expected, the surface resistivity of the concrete slabs initially increased while the concrete cured and lost moisture due to the hydration process and to the environment. Once ponding of the chloride solution started, however, there began to be a decrease in surface resistivity. This decrease in surface resistivity is believed to be caused by the increase of free chlorides present in the slabs after being saturated with the de-icing solution. The surface resistivity of the corresponding slabs that were ponded with tap water remained constant.

These results show that surface resistivity measurements are a potential indicator of chloride ingress and, therefore, may correlate to risk of corrosion in reinforced concrete. The effect of freeze/thaw cycling on surface resistivity, according to this study, is that it increases the surface resistivity. This is due to the micro-cracking in the concrete matrix, caused by the freeze-thaw damage.

In the second part of this master's thesis the corrosion susceptibility of ductile iron pipe (DIP) was investigated. Ductile iron pipe has been used mostly in the water transmission field since the 1950s. At that time, ductile iron pipe replaced traditional cast iron pipe, due to ductile iron's superior strength properties. More recently, ductile iron pipe has been considered as a replacement for traditional timber poles for power transmission. While there are benefits to using ductile iron such as its strength and sustainability, ductile iron suffers from pitting corrosion due to the nodular structure of its free graphite. This type of corrosion can lead to severe deterioration of the pipe in localized areas. Due to this, researchers have been studying ductile iron durability and developing solutions for its durability issues. In this research study ductile iron was tested for its susceptibility to corrosion. Samples were subjected to an accelerated corrosion process inside a salt fog chamber. After the samples had corroded, mass loss measurements were taken. Tensile strength tests were also done before and after corrosion. Stainless steel samples were tested alongside the ductile iron for comparison. In addition to the corrosion chamber and strength tests, electrochemical tests were done to characterize the corrosion kinetics of ductile iron. Stainless steel samples showed almost no change in mass loss and tensile strength after corrosion. Ductile iron samples, on the other hand, had a corrosion rate of approximately 52.6 mpy (1.3 mmy), and a 10 ksi (69 MPa) decrease in ultimate tensile strength after corrosion. Open circuit potential results showed that the ductile iron samples

had a higher potential, and thus, lower corrosion resistance than the stainless steel samples. Similarly, electrochemical impedance spectroscopy showed that stainless steel had a greater impedance than ductile iron, which correlates to increased corrosion resistance. Analysis of cyclic polarization curves showed that the ductile iron samples had much higher corrosion rates than stainless steel samples. However, the corrosion products which formed on the ductile iron samples appeared to be protective in nature. This indicates that ductile iron may have good field performance.

Assessing Durability of Reinforced Concrete and Ductile Iron

by

Silas Shields

A THESIS

submitted to

Oregon State University

in partial fulfillment of

the requirements for the

degree of

Master of Science

Presented June 8, 2017

Commencement June 2017

Master of Science thesis of Silas Shields presented on June 8, 2017

APPROVED:

_____

Co-major Professor, representing Civil Engineering

_____

Co-major Professor, representing Civil Engineering

_____

Head of the School of Civil and Construction Engineering

_____

Dean of the Graduate School

I understand that my thesis will become part of the permanent collection of Oregon State University libraries. My signature below authorizes release of my thesis to any reader upon request.

_____

Silas Shields, Author

ACKNOWLEDGEMENTS

I would like to sincerely thank my co-advisors Jason Ideker and Burkan Isgor for your guidance and mentorship throughout my time as a graduate student. Thank you for giving me the opportunity to be a part of the important research being done by your research groups. The experience and knowledge you have provided me with will be invaluable throughout my engineering career. It has truly been an honor to have worked with both of you.

Thank you to my committee members, Dr. Jason H. Ideker, O. Burkan Isgor, Dr. Andre Barbosa, and Dr. Julie Tucker for taking the time to review this project, and giving me your guidance.

Thank you to all my fellow graduate research assistants who have been incredibly supportive throughout both my research and coursework. Thank you to Vahid Azad for the hours you spent assisting me with programming. Thank you, David Rodriguez, for laying the groundwork for my research on the ODOT project, and thank you, Pratik Murkute for your hard work and assistance on the PGE project.

To all the undergraduate students who have assisted me, thank you very much for the hours of hard work you put into this project. Walter Webster, Christine Baker, Suellen Nerone, and Brianna Velasquez, thank you for your support.

Thank you to my parents, James and Angela Shields, for teaching me to work hard and go after every opportunity. I truly would not be where I am today without the love and support I received from you both.

Finally, thank you to my best friend and wife, Naomi Shields. You are a constant encouragement and inspiration to me. Thank you so much for all you have done to support me during my time as a graduate student. I am so excited for this next stage in our lives, as I start a new career and we raise our family together. I adore you both.

CONTRIBUTION OF AUTHORS

Drs. O. Burkan Isgor and Jason H. Ideker advised on data collection, analysis, interpretation, and writing of chapters 1, 2, 3, and 4. David Rodriguez assisted in data collection, analysis, interpretation, and writing of chapter 2. Dr. Vahid Jafari Azad assisted in writing and data interpretation of chapter 2. Pratik Murkute assisted in data collection, analysis, interpretation, and writing of chapter 3.

TABLE OF CONTENTS

TABLE OF CONTENTS (Continued)

TABLE OF CONTENTS (Continued)

TABLE OF CONTENTS (Continued)

TABLE OF CONTENTS (Continued)

LIST OF FIGURES

LIST OF FIGURES (Continued)

LIST OF TABLES

LIST OF EQUATIONS

1. General Introduction and Literature Reviews

1.1 Scope and Layout of Thesis

The format chosen for this thesis is the manuscript option. This thesis follows the guidelines provided by the Oregon State University Graduate School Thesis Guide 2016-2017. The scope of this thesis covers the effects of certain exposure conditions on infrastructure materials (*i.e.*, reinforced concrete and ductile iron pipe). Specifically, the use of a non-destructive testing method (*i.e.*, surface resistivity) to monitor chloride ingress in reinforced concrete that has been exposed to deterioration mechanisms (*i.e.*, freeze-thaw and chloride de-icing solutions) is studied. This thesis also explores the durability and corrosion resistance of ductile iron pipe. There are four chapters and an appendix, which make up this thesis.

Chapter 1 contains an introduction on the research subjects presented in this thesis. Two literature reviews are also provided in this chapter. Two separate literature reviews were done due to the difference in topics between manuscript 1 and manuscript 2.

Chapter 2 contains the first manuscript. The first manuscript is titled "Experimental Investigation of the Effects of Chloride Ingress and Freeze-Thaw Attack on Electrical Surface Resistivity Measurements". This manuscript presents how surface resistivity measurements on various reinforced concrete slabs are affected by chloride de-icing solutions and freeze-thaw cycling in combination. Different slab mixtures and rebar positions are investigated.

Chapter 3 contains the second manuscript. The second manuscript is titled "Experimental Investigation of the Effects of Accelerated Corrosion on Ductile Iron". This manuscript presents

the results of accelerated testing of ductile iron and stainless steel in an accelerated corrosion chamber. Mass loss tests, electrochemical tests, and tensile strength tests are also done to quantify the effects of corrosion.

Chapter 4 provides a summary and conclusions for the two manuscripts. Recommendations for field practices related to the research findings are presented here. Also, suggestions for future work as well as current work planned for these research areas are discussed.

The appendix contains the cement composition and SCMs used, as well as images of various types of deterioration observed throughout the experimental studies.

1.2   Background for Manuscript 1

Performing reinforced concrete bridge deck inspections is an important yet difficult task for the Oregon Department of Transportation (ODOT). Several concrete durability issues can potentially shorten the service life of a bridge deck and often multiple deterioration mechanisms combine to cause damage. It is critical to implement mitigation strategies in a timely manner to increase service-life. Therefore, early detection by frequent and effective inspections is crucial. In the case of concrete bridge decks, two of the leading deterioration mechanisms are corrosion and freeze-thaw damage.

The current methods for monitoring corrosion-induced deterioration involve visual inspections as well as intrusive field sampling and subsequent laboratory tests, such as coring followed by chloride profiling. This time consuming process is less than ideal. These destructive methods not only require prolonged access to the bridge decks, resulting in traffic closures, but they also only provide a snapshot of the concrete's current condition. It is also difficult to get a comprehensive view of the potential deterioration of a structure, using destructive techniques. Using non-

destructive testing methods may be a quicker, more effective way of inspecting bridge decks. Due to these methods being non-invasive and relatively fast, more measurements can be taken and a more thorough inspection can be achieved.

One of these non-destructive methods is the surface resistivity test. Surface resistivity measurements have been shown to relate to chloride ingress rate. However, there are several factors that could potentially influence these measurements. Specifically, there is a gap in knowledge on how freeze-thaw cycling along with chloride ingress effects surface resistivity measurements. This is an important piece of missing information since concrete bridge decks that are exposed to chloride containing de-icing chemicals also experience freezing and thawing. The goal of this research was to study how freeze-thaw damage affects the surface resistivity of reinforced concrete slabs that have been ponded with de-icing chlorides. This additional data will be used in a model which could be used to predict whether or not corrosion is an impending issue in a given reinforced concrete bridge deck.

1.3   Literature Review for Manuscript 1

The use of surface resistivity measurements as a non-destructive test method is a very quick and efficient way to monitor concrete, and has many benefits over other test methods. However, it also has its limitations and there are several factors that influence the measurements. It is important to understand these influencing factors so that accurate predictions can be made. Deterioration of concrete is a major influencing factor and can affect surface resistivity in different ways depending on the deterioration mechanism. This literature review will cover the following:

- Common deterioration mechanisms of reinforced concrete bridge decks;

- Overview of destructive and non-destructive test methods used to evaluate concrete condition;

- The effects of chloride ingress and freeze-thaw damage on surface resistivity measurements.

1.3.1   Deterioration Mechanisms

1.3.1.1 Chloride Ingress

Exposure to chlorides from sources such as marine salts or de-icing chemicals is one of the main mechanisms for corrosion initiation in reinforced concrete bridge decks. The ability and time it takes for chlorides to travel from the surface of the concrete to the embedded reinforcement is affected by several concrete properties. The tortuosity of the concrete pore structure is a leading factor because the porosity and the connectivity of that porosity (e.g. permeability) are where the chlorides are transported. Therefore, properties that have an effect on the pore structure also affect chloride ingress. These include cement type and cement content, water to cementitious materials ratio and water content, concrete age, use of supplementary cementitious materials, and consolidation. Adjusting these factors will make the concrete more or less permeable, thus harder or easier for chlorides to penetrate. Increasing the distance the chlorides have to travel before they reach the reinforcement, in other words the concrete cover, will also decrease the time to corrosion initiation.

Chloride ions travel in concrete via four processes; permeation, advection, diffusion, and electrical migration. Permeation is the movement of ions due to a hydraulic pressure gradient. In advection, the ions move due to a moisture gradient. Ions move due to a concentration gradient in diffusion, and due to an electrical potential gradient in electrical migration. In

concrete, these mechanisms influence chloride ingress at different stages, and are inter related (Basheer et al. 2001). For example, a chloride containing solution ponded at the surface of the concrete will begin to push chlorides into the concrete through permeation. If the concrete is dry, there will also be advection influencing chloride movement. Once the chlorides are inside the concrete, diffusion will move the chlorides deeper as there is a difference in chloride concentration.

In order to predict chloride movement in concrete, a standard nomenclature has been developed which combines all of the transport mechanisms into a diffusion-like process, called the apparent diffusion coefficient, D_a. ASTM C1556 provides the standard method for determining D_a using a closed form solution to Fick's second law:

$$(x, t) = Cs - (Cs - C_i) \cdot erf (x \sqrt{4 \cdot Da \cdot t}) \tag{1.1}$$

The chloride concentration in mass percent, C(x,t), is measured at a depth, x, and exposure time, t. C_s is the surface concertation on concrete, C_i is the initial chloride concentration of the cementitious mixture prior to submersion in the exposure solution, x is the depth below the exposed surface measured in millimeters, D_a is the apparent chloride diffusion coefficient, t is the exposure time in seconds, and erf is the error function. Surface concertation, C_s, and apparent diffusion coefficient, D_a, are obtained through the nonlinear regression analysis (ASTM C1556). The apparent diffusion coefficient represents how the chlorides are moving specifically in the concrete from which the core was taken, therefore, it should not be used to make predictions about any other concrete structure.

1.3.1.1.1 Bound and Free Chlorides

A percentage of the chloride ions traveling through the concrete can become physically or chemically bound to the concrete's hydration products. This means that the chloride ions that eventually reach the reinforcement are the free chlorides that did not become bound. Due to this, the capacity of the concrete to bind chloride ions has a significant effect on corrosion initiation (Martin-Perez et al. 2000). The most common forms of chemical chloride binding are in the reaction of tricalcium aluminate, C_3A, and the formation of Calcium aluminum chlorohydroxide, known as Friedel's salt (Neville 1996). Determining chloride content is an important procedure for service life prediction and corrosion mitigation strategies. Therefore, knowing the amount of free and bound chlorides is essential. The two ASTM standards for determining free and total chlorides are ASTM C1218 and ASTM C1152, respectively. ASTM C1218 uses a hot water extraction process to assess the free chlorides from a finely ground concrete sample. ASTM C1152 uses acids to extract total chlorides within the concrete sample. It has been found that the severity of the extraction process determines the type and amount of chlorides obtained in the procedure (Sirivivatnanon et al. 2012). This is why if only the free chlorides are desired to be extracted, a much gentler process of boiling water is used. The fineness of the ground concrete sample is also a factor since a larger surface area will allow for more of the chlorides to be extracted.

1.3.1.2 Sources of Chloride: Deicing Solutions

Anti-icers and de-icing chemicals are commonly used by transportation departments to remove ice from concrete and other pavement surfaces. Anti-icers work by lowering the freezing point of the pavement surface so that water does not freeze when it falls on it. De-icers also lower the freezing point, but are placed on the pavement after ice has already formed to melt it away.

Since the 1930's when de-icing chemicals were first used, several types of de-icing chemicals

have been developed (Lord 1988). These include sodium chloride (NaCl), calcium chloride

($CaCl_2$), and magnesium chloride ($MgCl_2$). Although these ice removing chemicals are helpful in

providing safer roads to drive on, they also have some deleterious effects on the concrete,

especially when combined with freeze-thaw and wet-dry cycling (Wang et al. 2005). When

chloride containing de-icing solutions are placed on the concrete, the chlorides begin

penetrating down towards the reinforcement, which eventually leads to corrosion. Wet-dry

cycles can accelerate this process through advection. The difference in moisture between the

surface and the interior of the concrete will encourage chloride transportation. Freeze-thaw

damage also worsens the effect of de-icing chemicals because cracks and pores are what

chlorides travel through. A study found that under both wet-dry and freeze-thaw cycling,

calcium chloride de-icing solutions led to more damage than sodium chloride solutions (Wang et

al. 2005). This damage included mass loss, scaling damage, and strength loss. Several studies

also found that magnesium chloride solutions had greater deleterious effects on durability than

other chloride solutions such as sodium chloride (Sutter et al. 2008; Cody et al.1994; Cody et

al. 1996; Mussato 2004; Kozikowski et al. 2007). Other factors that control the rate of chloride

ingress are chloride concentration of the de-icing chemical, permeability of the concrete, and

weather conditions (Conciatori 2008). A greater concentration of chlorides means more

potential for chlorides to reach the reinforcement and initiate corrosion. It was found that

in higher temperature concrete, chlorides are able to diffuse at a greater rate (Yuan 2008).

1.3.1.3 Freeze-Thaw Action

Repeated freezing and thawing of moisture in and around concrete can lead to various damages

to the concrete, including cracking, scaling, and aggregate pop-outs. When concrete is overly

saturated the water that freezes can lead to damage. When water freezes it expands by 9% of its original volume. This expansion of water inside concrete pores creates internal tensile stresses that leads to cracks when the stress exceeds the tensile strength of the concrete. Continual cycles of freezing and then thawing, further weakens and deteriorates the concrete with each cycle. To prevent freeze-thaw damage in concrete a process called air-entrainment is done. When a concrete mixture is air-entrained, very small air voids are added to the concrete in the size range of 10 to 1000 microns, with a space factor less than 0.2 mm (PCA). These small air voids allow space for the capillary pore water to expand into when it freezes. Therefore, the stresses created by the expanding pore water are minimized. ASTM C666 is the standard test method for determining concrete resistance to rapid freezing and thawing. Two procedures are used in this method. One is for rapid freezing and thawing in water, and the other is for rapid freezing in air and thawing in water. These procedures are used to determine how variations in concrete properties effect its resistance to freeze-thaw damage. The test method calls for the concrete samples to be measured for mass and fundamental transverse frequency at least every 36 cycles. The samples are to be tested until they reach either 300 cycles or 60% of their initial relative dynamic modulus of elasticity. Measurements after every 10 cycles is recommended for samples that are expected to deteriorate rapidly.

Relating freeze-thaw damage to surface resistivity is an important task if surface resistivity is to be used to monitor chloride ingress in concrete. Concrete that is exposed to chlorides in the form of de-icing chemicals is typically undergoing freeze-thaw cycles at the same time. Therefore, the effects of freeze-thaw damage will likely need to be accounted for while taking surface resistivity measurements. There is a lack of research specifically observing the effects of freeze-thaw damage and chloride ingress on surface resistivity. One study found that decreased

temperature led to increased concrete resistivity (Wang et al. 2014, 2015). As freeze-thaw cycles were continued, the concrete resistivity steadily increased during freezing periods, and decreased during thawing periods.

1.3.2 Destructive and Non-destructive Testing

1.3.2.1 Destructive Testing

There are various testing methods and technologies used to assess the condition of reinforced concrete bridge decks. These methods all vary in ease of use and their ability to deliver accurate data. Many traditional testing methods are destructive, meaning they require altering the structure in a destructive manner. This would include taking cores for chloride testing, in situ chloride profiling, or accessing the reinforcement for half-cell potential mapping.

1.3.2.1.1 Laboratory Tests

1.3.2.1.1.1 Rapid Chloride Penetration and Acid Soluble Chloride Content Tests

Rapid Chloride Penetration (RCP) (ASTM C1202) and acid-soluble chloride content (ASTM C1152) tests both require taking cores from the structure to be evaluated. RCP testing determines the concrete sample's resistance to chloride ion penetration through a surrogate electrical charge resistivity. The test procedure involves passing a current through the concrete and observing the charge that is able to pass through. The entire procedure is tedious and takes approximately 24 hours. Plus there are many known drawbacks to this test method including sample heating which changes the results of the test, and an inability to test mixtures with low w/cm and/or those containing supplementary cementitious materials. Determining the chloride content in concrete via ASTM C1152 is also a very time consuming and tedious task. The core must first be ground into powders by layer, then the powders are prepared to extract the chlorides. The

solutions containing the chlorides are then titrated to determine the chloride content in each layer. This process takes several hours to complete and requires the use of hazardous chemicals.

1.3.2.1.1.2 Scanning Electron Microscopy

Scanning electron microscopy (SEM) has long been used in concrete research to characterize samples and observe microstructural responses to environmental changes. In the case of freeze-thaw damage, SEM has been used to observe cracking and other microstructural changes within a concrete sample (Jacobsen, Stefan et al. 1995). An SEM instrument fires accelerated electrons at a solid sample, and then uses the various energy signals that are produced when the electrons hit the sample to create different images. Secondary electrons, backscattered electrons, and diffracted backscattered electrons are all examples of these energy signal responses. From secondary electrons, the topography of a sample can be seen. Backscattered electron signal detections are proportional to the average atomic number in a given area of the sample. A brighter intensity from the signal means that there are larger atoms with a greater average atomic number, causing more backscattered electrons. The signal intensity is mapped out across the entire sample, producing a greyscale image, which is useful for showing the contrast in phases of a sample. Backscattered electrons produce a greyscale image in which air voids, cement grains, aggregate, and hydrated cement phases can all be distinguished from each other. For example, in hydrated concrete, the C-S-H phase can be distinguished from the CH phase and from portions of unreacted cement grains.

SEM can produce greatly magnified images, allowing the observer to view areas as small as 50 nanometers. These images can usually be obtained in under five minutes making it a very time efficient method. While data collection is relatively quick, sample preparation can be tedious

and time consuming. In order for the sample to readily produce secondary electrons, it is often finely coated with a conductive metal such as a gold/palladium mixture.

While SEM produces detailed images, it is important to take care when interpreting the information. The sample preparation process can often lead to fracturing and shrinkage cracking of the sample (Jacobsen, Stefan et al. 1995). Also, the small size of the sample leads to it not necessarily being representative of the larger bulk structure. For example, a sample that shows no indication of freeze-thaw damage may have just been taken from an undamaged area of the concrete structure.

1.3.2.1.2 In Situ Tests

Another destructive method for identifying the potential for corrosion in reinforced concrete is half-cell potential mapping (ASTM C876). The potential of the reinforcement is mapped out by moving an electrode around the surface of the concrete, while one end of the electrode is attached to the reinforcement. A very negative potential indicates that there is possible corrosion. This test is limited by the amount of locations that can be reached by the electrode. If the majority of the concrete structure cannot be tested then small areas of corrosion could be missed. Research has shown that increased grid size, mixed moisture conditions, and concrete resistivity all caused the detectability of corroding, anodic areas to decrease (Kessler et al. 2016).

1.3.2.2 Non-Destructive Testing

Non-destructive testing (NDT) methods are a desirable alternative to destructive methods, as they are usually quicker, more cost effective, and do not carry the risk of damage to the structural integrity of the bridge. A study done by the Transportation Research Board of the

National Academies determined the performance of NDT technologies based on accuracy,

precision, ease of use, speed, and cost (Gucunski et al. 2013). It was found that for each type of

deterioration there were technologies that sufficiently provided detection, but there was not a

single technology that could assess all deterioration types (Gucunski et al. 2013). Non-

Destructive Test methods which are in use and being researched include rebound hammer test

(ASTM C805), chain drag test (ASTM D4580), ultrasonic pulse velocity test (ASTM C597), ground

penetrating radar (ASTM D6432), impact echo test (ASTM C1383), and surface resistivity

(AASHTO TP 95). Rebound hammer tests are used to estimate the quality of the concrete as well

as its compressive strength. While it is a simple test, studies have shown that it is unsuitable as

an individual test for compressive strength (Qasrawi 2000). Ultrasonic pulse velocity has been

used to detect discontinuities in concrete as well as estimate the dynamic modulus of elasticity.

This test is also limited as it is sensitive to the concrete's internal properties and density. Impact

echo testing utilizes stress waves to detect flaws within the concrete. A study done to determine

the accuracy of impact echo tests found that it gave a false positive prediction of a flaw 19% of

the time (Chaudhary 2013). While this means that impact echo can accurately detect flaws most

of the time, there is still a chance for inaccurate predictions. The chain drag method of

inspection requires a trained inspector to listen for hollow sounds as a chain is dragged across

the concrete. This method is inexpensive but primitive, time consuming, and subjective. It is also

difficult to do this test in areas with loud ambient noises such as near a highway or construction

site (Oh 2013). A major drawback with the chain drag method is that if a flaw is detected it is

indicative a major corrosion problem. A hollow noise means that the corrosion is already so

severe that a delamination has occurred between the reinforcing steel bars and the concrete. At

this stage of corrosion repairs are needed, and there was never a chance to identify the

corrosion before it caused severe damage. Ground penetrating radar is another method for

detecting subsurface objects and flaws. It sends high frequency radio waves into the concrete and uses the reflected signals to image the subsurface. Ground penetrating radar can produce useful images of the concrete, which separate the reinforcement from the possible defects in the concrete. However, gathering data can take hours and requires closing off traffic to the tested areas. Also, irregularities in cover depth can lead to misleading variations in reflection amplitudes. This will decrease the accuracy of deterioration analysis, if the reflection amplitudes are not properly normalized for depth.

1.3.2.2.1 Electrical Surface Resistivity

One of the main mechanisms for corrosion of reinforced concrete is the transport of charged chloride ions through the concrete microstructure. When these chloride ions reach the reinforcing steel, they de-passivate it due to the lowering of the surrounding pH. Because of this, a correlation can be made between chloride ion transport and the resistivity of the concrete. As the resistivity of the concrete increases, the corrosion rate decreases (Hornbostel et al. 2013). It has also been found that a low resistivity correlates with a low critical chloride threshold (Polder 2009). The resistivity of concrete is affected by several factors that must be taken into consideration when interpreting values. Concrete characteristics such as pore saturation, water-to-cement ratio, chloride concentration, and water content can all change concrete resistivity (Hussain et al. 1995, Neville 1996, Morris et al. 2004, Song et al. 2007). There are many ways to measure concrete resistivity such as by electrode disc or simply by passing a current through a concrete core (Polder 2001). However, few methods are as practical as the four-point Wenner probe. The Wenner probe is able take surface resistivity measurements in only seconds, and can be placed directly on the surface of the concrete. There is no need for access to the reinforcement or for taking cores. The Wenner probe contains four equally

spaced electrodes. The two outer electrodes induce a current, while the two inner electrode measure the drop in potential. Figure 1.1 below shows a schematic for how four point Wenner probes measure resistivity.
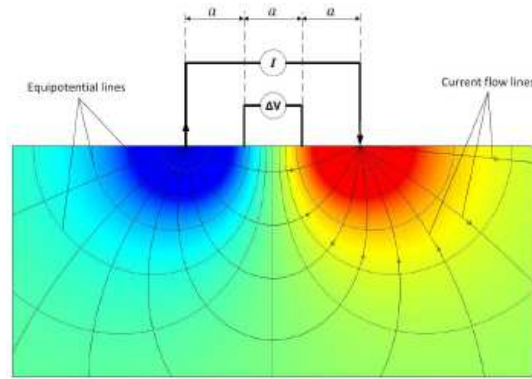
Figure 1.1: Function schematic of four point Wenner probe.

Resistance can be calculated using ohm's law, being the ratio of the change in potential to the current. Resistivity takes into account the spacing between the electrodes and can be found using the equation below, where V is the potential drop, *a* is the spacing between the electrodes, I is the current, and ρ is the resistivity:

$$\rho = 2\pi\, a\, \frac{\Delta V}{I} \tag{1.2}$$

1.3.2.2.1.1 Limitations of Electrical Surface Resistivity

While surface resistivity measurements seem to be quick and effective, there are some limitations that require careful consideration. Just as there are many factors that affect concrete resistance, there are similar factor that affect surface resistivity measurements. These include concrete moisture; temperature; relative humidity; and reinforcement bar size, spacing, depth, and orientation.

Surface resistivity measurements taken at one temperature will be different than if it were taken at another temperature. For example at higher temperatures, ions in the solution become more mobile, and therefore the solution becomes more conductive. This leads to lower resistivity values. The opposite is true for low temperatures. Due to this, each measurement needs to be normalized using the Hinrichsen-Rasch law (Hope 1987) given by:

$$\rho_2 = \rho_1 * \exp\left[2900\left(\frac{1}{T_1} - \frac{1}{T_2}\right)\right]$$
(1.3)

where ρ_1 is the measured resistivity, ρ_2 is the normalized resistivity, T_1 (K) is the temperature of the concrete during the measurement, and T_2, is the normalized temperature. The moisture content of the concrete is also an important influencing factor. An electrical current will move faster through liquid than it will through a solid, therefore, if the concrete is more saturated with a liquid it will have a lower resistivity. This result has been found to be true even when the concrete samples have the same degree of chloride ingress (Neville 1996, Hussain 2011, Ryu et al. 2011, Wang et al. 2014). A correction factor to account for moisture content needs to be developed to ensure surface resistivity measurements are comparable across a concrete bridge deck with varying moisture conditions.

The reinforcing bars themselves can influence surface resistivity measurements due to the metal interfering with the current emitted by the electrode probes. While the rebar depth, size, and orientation with respect to the probe can all have an effect, the greatest influencing factor is the distance from the rebar to the measured location (Gowers et al. 1999, Weydert et al. 1999, Presuel-Moreno et al. 2009, Sengul 2009, Salehi 2013, Garzon et

al. 2014, Morales 2015). If the rebar is near the measurement probe it will have a greater interference with the reading. The size of the rebar has little effect on measurements. It is necessary to take these factors into consideration when choosing measurement locations. The optimal location for taking surface resistivity measurements with a Wenner probe has been found to be with the probe oriented perpendicular to the topmost rebar and parallel to the bottommost rebar (Morales 2015). This orientation minimizes the rebar's interference with the probe's current.

1.3.3 De-icing Solutions, Chloride Ingress, and Electrical Surface Resistivity

Determining the chloride content in concrete is an important inspection process for identifying possible corrosion. Unfortunately, most standard methods for doing so are expensive, time consuming, damaging, and difficult. A non-destructive technique such as surface resistivity measurements would be a much more efficient method for determining chloride content. The relationship between concrete resistivity and chloride ingress has been studied, but more work needs to be done, especially when factoring in the effects of freeze-thaw damage. A crucial value for predicting corrosion initiation is the chloride threshold. The chloride content at the surface of the reinforcement needs to reach a certain threshold value before it is believed that corrosion can initiate. A study by Morris et al. (2004), aimed to correlate chloride threshold values with resistivity values. Since rebar corrosion parameters such as corrosion potential and corrosion current density correlate with concrete resistivity and chloride concentration, the researchers proposed that resistivity and chloride threshold were also related. It was generally found that resistivity is a good indicator of concrete quality. Therefore, concrete with higher resistivity values or of better quality, also had higher chloride threshold values. Some suggested causes for this relationship, given by the researchers, were that lower resistivity values were

associated with high concentrations of free chlorides and that low resistivity could mean low degrees of pore saturation. It was speculated that low pore saturation prevents active corrosion of the reinforcement. While this research is beneficial in establishing a relationship, more needs to be done if surface resistivity is to be used as a non-destructive technique to determine chloride ingress.

1.3.4 Summary and Gaps in Literature

Thorough inspections of reinforced concrete bridge decks are time consuming, challenging, and expensive for departments of transportation. Standard methods of identifying potential corrosion damage such as chloride profiling or half-cell potential mapping are not ideal. The industry needs an easier method for detecting the potential for corrosion that can be used to determine whether further testing needs to be done. Electrical surface resistivity measurements have shown good correlation with chloride ion movement in concrete. Surface resistivity measurements coupled with a prediction model may be able to give estimates for what the chloride concentration at a particular location of the concrete is. While these predictions may not be completely accurate, they provide useful information for deciding whether or not to proceed with further testing. Because surface resistivity measurements take only seconds take and are not destructive, inspectors can take several measurements at several locations in a much shorter amount of time then if using other methods. Research has found that there are several factors affecting surface resistivity measurements. These include porosity, temperature, moisture, and rebar placement in the concrete. The effect of these factors on surface resistivity values is well understand for the most part, but these factors vary when the concrete is exposed to deterioration mechanisms. There have been studies on how surface resistivity values change when concrete is exposed to deicing chemicals, but there has not been a study where the

effects of de-icing chemicals coupled with freeze-thaw damage were investigated. This is an

important exposure condition to understand since de-icing chemicals are only used when the

concrete is subjected to freeze-thaw conditions. This research study will investigate this

exposure condition and observe the effects on surface resistivity of the concrete. With this new

information, better prediction models can be developed, which will make surface resistivity a

more viable non-destructive test method for monitoring corrosion in reinforced concrete

structures.

1.3.5 References

ASTM C597-09 Standard test method for pulse velocity through concrete. (2010). ASTM International, West Conshohocken, PA.

ASTM C666/C666M-15 Standard test method for resistance of concrete to rapid freezing and thawing. (2015). ASTM International, West Conshohocken, PA.

ASTM C1152 Standard test method for acid-soluble chloride in mortar and concrete. (2012). ASTM International, West Conshohocken, PA.

Amini, Kamran, Mehdi Jalalpour, and Norbert Delatte. (2016) "Advancing concrete strength prediction using non-destructive testing: Development and verification of a generalizable model." Construction and Building Materials 102: 762-68.

Andrade, C., M. Prieto, P. Tanner, F. Tavares, R. d'Andrea. (2013). "Testing and modelling chloride penetration into concrete." Construction and Building Materials 39: 9-18.

Blackburn, R., D. Amsler, K. Bauer (2004). Snow removal and ice control technology. Sixth International Symposium on Snow Removal and Ice Control Technology, Transportation Research Board of the National Academies, Spokane, WA.

Brencich, A., G. Cassini, D. Pera, G. Riotto (2013). "Calibration and Reliability of the Rebound (Schmidt) Hammer Test." Civil Engineering and Architecture 1(3): 66-78.

Chaudhary, Muhammad Tariq A. (2013) "Effectiveness of Impact Echo testing in detecting flaws in prestressed concrete slabs." Construction and Building Materials 47: 753-59.

Conciatori, D, H. Sadouki, E. Brühwiler. (2008). "Capillary suction and diffusion model for chloride ingress into concrete." Cement and Concrete Research 38(12): 1401-1408.

Garzon, A. J., J. Sanchez, C. Andrade, N. Rebolledo, E. Menéndez, J. Fullea. (2014). "Modification of four point method to measure the concrete electrical resistivity in presence of reinforcing bars." Cement and Concrete Composites 53: 249-257.

Koch, G.H., M. Brongers, N. Thompson, Y. Virmani, J. Payer. (2002). "Corrosion Costs and Preventive Strategies in the United States." FHWA-RD-01-156 (Final Report): 773 pp.

Gowers, K. R., S. G. Millard. (1999). "Measurement of concrete resistivity for assessment of corrosion severity of steel using Wenner technique." ACI Materials Journal 96(5): 536-541.

Gucunski, N., I. Arezoo; F. Romero, S. Zanarian, D. Yuan, H. Wiggenhauser, P. Shokouhi, A. Taffe, D. Kutrubes. (2013). Nondestructive testing to identify concrete bridge deck deterioration. Transportation Research Board. Washington, D.C.

Hong, K. (1999). Cyclic wetting and drying and its effects on chloride ingress in concrete. National Library of Canada, Ottawa, ON. 22

Hope, B, A. Ip. (1987). "Chloride Corrosion Threshold in Concrete." Materials Journal 84(4): 306-314.

Huang, J., W. Shaowei, J. Chaudhari, S. Soltesz, X. Shi. (2014). Deicer Effect on Concrete Bridge Decks: Practitioners Perspective and a Method of Developing Exposure Maps. Transportation Research Board Annual Meeting: 1-13. Washington, DC.

Hussain, R. R. (2011). "Effect of moisture variation on oxygen consumption rate of corroding steel in chloride contaminated concrete." Cement and Concrete Composites 33(1): 154-161.

Hussain, S., E.,Rasheeduzzafar, A. Almusallam, A. S. Algahtani. (1995). "Factors affecting threshold chloride for reinforcement corrosion in concrete." Cement and Concrete Research 25(7): 1543-1555.

Jackson, L. (2013). "Surface resistivity test evaluation as an Indicator of the Chloride Permeability of Concrete." Tech brief. Publication no. FHWA-HRT-13-024, McLean, VA.

Jacobsen, Stefan, Jacques Marchand, and Hugues Hornain. (1995) "Sem observations of the microstructure of frost deteriorated and self-healed concretes." Cement and Concrete Research 25.8: 1781-790.

Jaegermann, C. (1990). "Effect of water-cement ratio and curing on chloride penetration into concrete exposed to Mediterranean Sea climate." Materials Journal 87(4): 333-339.

Ji, Y., T. Zan, Y. Yuan. (2009). "Chloride Ion Ingress in Concrete Exposed to a Cyclic Wetting and Drying Environment." American Society of Agricultural and Biological Engineers 52(1): 239-245.

Jianhong, C., B. Dylan, J. Frank, H. Dryver. (2008). Concrete bridge deck condition assessment with automated multisensor techniques. Bridge Maintenance, Safety Management, Health Monitoring and Informatics. Burlington, VT, Taylor & Francis.

Kessler, Sylvia, and Christoph Gehlen. (2017) "Reliability Evaluation of Half-Cell Potential Measurement Using POD." Journal of Infrastructure Systems 23.2: n. pag.

Khalim, A. R., D. Sagar, M. D. Kumruzzaman, A. S. M. Z. Hasan. (2011). "Combination of nondestructive evaluations for reliable assessment of bridge deck." Facta universitatis - series: Architecture and Civil Engineering 9(1): 11-22.

Kosmatka, S. H., M. L. Wilson. (2011). "Design and Control of Concrete Mixtures." 15th Edition: 444, Portland Cement Association, Washington, D.C.

Lingen, R. T. (1998). "Concrete in coastal structures." 301. London, U.K., Thomas Telford Limited.

López, W., J. A. González. (1993). "Influence of the degree of pore saturation on the resistivity of concrete and the corrosion rate of steel reinforcement." Cement and Concrete Research 23(2): 368-376.

Lord, B. N. (1988). "Program to reduce deicing chemical usage." Federal Highway Administration: 13 pp., McLean, VA. 23

Martín-Pérez, B., H. Zibara, R.d Hooton, and M.d.a Thomas. (2000) "A study of the effect of chloride binding on service life predictions." Cement and Concrete Research 30.8: 1215-223.

Morales, M. T. (2015). Experimental investigation of the effects of embedded rebar, cracks, chloride ingress and corrosion on electrical resistivity measurements of reinforced concrete: 174 pp.

Morris, W., A. Vico, M. Vázquez. (2004). "Chloride induced corrosion of reinforcing steel evaluated by concrete resistivity measurements." Electrochimica Acta 49(25): 4447-4453.

Mussato, B. T., O. K. Gepraegs and G. Farnden (2004). "Relative effects of sodium chloride and magnesium chloride 0n reinforced concrete: state of the art." Transportation research record. (1866): 59-66.

Mutale, L. (2014). An investigation into the relationship between surface concrete resistivity and chloride conductivity tests: 105 pp.

Neville, A. M. (1996). Properties of Concrete: Fourth Edition. 844. Hoboken, NJ, Wiley.

Prassianakis, I.n., and N.i. Prassianakis. (2004) "Ultrasonic testing of non-metallic materials: concrete and marble." Theoretical and Applied Fracture Mechanics 42.2: 191-98.

Presuel-Moreno, F., Y. Liu, M. Paredes (2009). Understanding The Effect Of Rebar Presence And/Or Multilayered Concrete Resistivity On The Apparent Surface Resistivity Measured Via The Four-Point Wenner Method. Corrosion Conference 2009. Atlanta, GA, NACE International.

Oh, Taekun, Seong-Hoon Kee, Ralf W. Arndt, John S. Popovics, and Jinying Zhu. (2013) "Comparison of NDT Methods for Assessment of a Concrete Bridge Deck." JOURNAL OF ENGINEERING MECHANICS 139.3: 305-14

Qiang, Y., A. Katrien, S. Caijun, S. Geert De. (2008). Effect of temperature on transport of chloride ions in concrete. Concrete Repair, Rehabilitation and Retrofitting II, CRC Press: 159-160.

Rupnow, T., I. Patrick. (2011). Evaluation of surface resistivity measurements as an alternative to the rapid chloride permeability test for quality assurance and acceptance. Louisiana Transportation Research Center: 68 pp.

Ryu, D, W. Ko, T. Noguchi. (2011). "Effects of simulated environmental conditions on the internal relative humidity and relative moisture content distribution of exposed concrete." Cement and Concrete Composites 33(1): 142-153.

Sadowski, L. (2013). "Methodology for assessing the probabilty of corrosion in concrete structures on the basis of half-cell potential and concrete resistivity measurements." Scientific World Journal. 2013: 8. Article ID 714501.

Salehi, M. (2013). Numerical investigation of the effects of cracking and embedded reinforcement on surface concrete resistivity measurements using Wenner probe. Civil and Environmental Engineering. Ottawa, ON, Carleton University. Master of Applied Science in Civil Engineering: 155 pp. 24

Sengul, O. G., E. Odd. (2009). "Effect of Embedded Steel on Electrical Resistivity Measurements on Concrete Structures." 106 (1): 11-18.

Shariati, M., H. Sulong, M. Arabnejad, P. Shafigh, H. Sinaei. (2011). "Assessing the strength of reinforced concrete structures through ultrasonic pulse velocity and Schmidt Rebound Hammer tests." Scientific Research and Essays 6 (1): 213-220.

Sirivivatnanon, V., W. A. Thomas, K. Waye. (2012). Determination of free chlorides in aggregates and concrete. Australian Journal of Structural Engineering. 151-158.

Song, H. W., V. Saraswathy. (2007). "Corrosion monitoring of reinforced concrete structures - A review." International Journal of Electrochemical Scienc. 2(1): 1-28.

Swanstrom, J., T. Rogers, G. Bowling, S. Tuttle (2013). ODOT bridge inspection program manual 2013. Oregon Department of Transportation: 1-381, OR.

Wang, Kejin, Daniel E. Nelsen, and Wilfrid A. Nixon. (2006) "Damaging effects of deicing chemicals on concrete materials." Cement and Concrete Composites 28.2: 173-88.

Wang, Z., Q. Zeng, L. Wang, Y. Yao, K. Li. (2014). "Effect of moisture content on freeze–thaw behavior of cement paste by electrical resistance measurements." Journal of Materials Science. 49(12): 4305-4314.

Weydert, R., C. Gehlen. (1999). "Electrolytic resistivity of cover concrete: Relevance, measurement and interpretation." Proceedings of the 8th International Conference on Durability of Building Materials and Components. 409-419. NRC Research Press, Vancouver, Canada.

Wang, Q. Z., L. Wang, Y. Yao, K. Li. (2015). "Electrical resistivity of cement pastes undergoing cyclic freeze-thaw action." Journal of Materials in Civil Engineering. 27(1).

1.4   Background for Manuscript 2

Ductile iron pipe is a fairly recent (1950s) modification to the traditional gray iron pipe that has

been in use for many centuries. The applications of grey iron pipe and later ductile iron pipe

(DIP) are centered on water and wastewater conveyance. Since ductile iron pipe has only been

in use for about 60 years the durability of this material is still under investigation (Carpenter,

2010). While the majority of use is for water exposure, there has been limited use of ductile

iron pipe in the power transmission industry. The main use of ductile iron pipe in this field is to

replace the traditionally used timber poles for local/regional power transmission (e.g. substation

to home, home to home, small business, etc.). There are still many questions about the

durability of DIP in the arena of power transmission. Much of this literature review focuses on

the experience with DIP in water and wastewater. The largest question about durability is

related to corrosion of the pipe and its susceptibly to corrosive agents in water, wastewater, and

soil.

1.4.1   Historical Use

Iron pipe was first used in Germany in 1455 for water piping in the Dillenberg Castle in Germany

(Carpenter 2010). Almost two centuries later iron pipe was again used to run water to the

French Palace of Versaille by Louis XIV. This piping network was over 24 km long and lasted for

over 330 years; a testament to the potential for long-term durability in such application. In 1834

the first cast iron pipe was produced in the US in Philadelphia, Pennsylvania and in 1915 the Cast

Iron Pipe Research Association (CIPRA) was established (Noble 1940). Three main

breakthroughs in grey iron and ductile iron pipe have led to its further long history of

satisfactory performance: 1) introduction of cement mortar lining in 1922, 2) invention of

ductile iron pipe in 1948, followed by first field usage in 1955 and 3) introduction of the design

decision model (DMM) in 2004 (Carpenter 2010).

1.4.2   Introduction of cement mortar lining in 1922

One of the most important qualities for a pipe conveying water is for good clear flow. It is

desired to avoid tuberculation which can results in a loss in flow efficiency. The introduction of

cement mortar linings for iron pipe in 1922 resulted in very good Hazen-Williams flow

coefficients of 140 or higher (American pipe manual 2004). This indicates a pipe with good

flowability. It was also shown that corrosion is unlikely if the lining was properly placed and

cured prior to the pipe being put in service (American pipe manual 2004).

1.4.3   Invention of ductile iron pipe in 1948, followed by first field usage in 1955

In 1948 ductile iron was invented by a team of metallurgists. The main difference between grey

iron and ductile iron is that the free graphite is found in spheroidal or nodular form in DIP rather

than in the flaky form in grey iron. This provides continuity to the metal matrix resulting in a

stronger, tougher more ductile material. Ductile iron pipe typically contains 85-90% recycled

material, improving the sustainability of this material as well (Carpenter 2010).

1.4.4   Introduction of the design decision model (DMM) in 2004 (1958)

Two events that occurred 50 years apart led to the third breakthrough for iron pipe. In 1952

CIPRA installed a gray iron pipe with a polyethylene (PE) sleeve (American pipe manual 2004).

Six years later they buried similar samples in aggressive soil sites. After 50 years of experience

the PE has proven its ability to protect the grey iron pipe from aggressive soils. In 2004 a Design

Decision Model (DMM) was developed that takes into consideration the likelihood of failure due

to aggressive environments and the consequences of failure occurring. Then five possible

recommendations for corrosion protection are given. These recommendations are 1) installing

the pipe as-manufactured with its standard shop coating, 2) encasing the pipe in polyethylene,

3) encasing the pipe in polyethylene or encasing the pipe in polyethylene and providing bonded

joints, 4) encasing the pipe in polyethylene and providing bonded joints or providing cathodic

protection, and 5) providing cathodic protection (American pipe manual 2004). The results of

the earlier study were crucial to developing and validating the DMM. For assessment of piping

in aggressive soils it is important to know if the pipe was installed with the PE encasement or

just the bare shop coating (Carpenter 2010).

1.5   Literature Review for Manuscript 2

1.5.1   Corrosion Mechanisms

Corrosion is an electrochemical reaction that requires four main concurrent steps to create an

electrochemical cell. These are an anodic reaction, a cathodic reaction, an electron movement

from metal, and ionic movement within an electrolyte (Uhlig and Revie 2008). The anode is the

electrode where oxidation (metal loss) occurs and electrons are produced. The positive metal

ions dissolve from the anode to the electrolyte, while the electrons travel through the metal to

the cathode. At the cathode, there is a reduction reaction where electrons are consumed. These

reduction reactions are most commonly gas reactions such as oxygen reduction or hydrogen

evolution (Marcus 2012). When dissimilar metals are in contact with each other, galvanic

corrosion might occur as one metal might acts as the anode and the other act as the cathode

(Roberge 2008). In the case of galvanic corrosion, the reduction may be on the surface of the

metal. The electrolyte is a conductive solution that allows the flow of ions from the anode to the

cathode. This reduction and oxidation reaction cycle is what drives the electrochemical

corrosion cell.

1.5.1.1 Pitting Corrosion on Ductile Iron

Pitting corrosion is the result of a local action corrosion cell (Marcus 2012). In a local action cell there are more active areas on the surface of the metal which act as anodes. The less active areas then act as cathodes in the corrosion cell. These anodic areas can be the result of alloys in the metal, microstructural differences, or defects (Marcus 2012). In the case of ductile iron, the discrete graphite nodes create less active areas on the surface of the metal. The small areas of iron adjacent to the graphite then preferentially corrode because they are more active. In order to provide sufficient current density to drive the corrosion cell, the metal is oxidized in a vertical pit rather than spread out across the surface. Pitting corrosion is detrimental to many structural metals because of how it increases the penetration depth (Uhlig and Revie 2008). Corrosion rate is typically measured in mils per year. One mil being a thousandth of an inch. In uniform corrosion, the corrosion rate will be less than pitting corrosion because it is spread out across the surface of the metal. Pitting corrosion will have a higher rate of corrosion because it will penetrate deep in a small area.

1.5.2   Ductile Iron Characteristics

Ductile iron was first developed in 1948, and was considered to be one of the most significant breakthroughs in metallurgy of the century (Carpenter 2010). Ductile iron pipe is an iron alloy containing approximately 3% carbon and .035% magnesium. Depending on the manufacturer, the exact composition of DIP can vary in order to adjust certain properties. The carbon content of DIP, places it in between steel and cast iron. Therefore, it is stiffer than steel, but more ductile than cast iron.

1.5.2.1 Ductile Iron Microstructure

Research has shown that steel pipe exhibits elongations 2 to 4 times that of ductile iron pipe when tested in tension (Keil and Devletian 2011). Steel also has Charpy impact values 3 to 30 times higher than ductile iron (Keil and Devletian 2011). The ductile iron is stronger, more ductile, and can withstand higher impacts than cast iron, however (Carpenter 2010). The reason ductile iron performs better than cast iron is due to its unique microstructure. The addition of magnesium causes the free graphite to form nodular deposits rather than flakes. Figure 1.2 below compares the microstructure of cast iron to that of ductile iron.
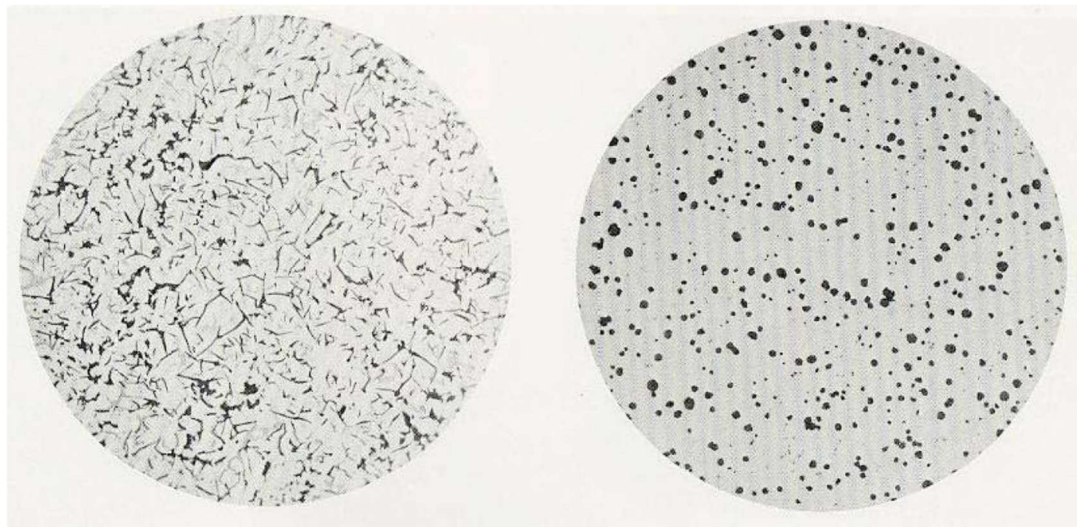
Figure 1.2: Microstructure of cast iron (left) and ductile iron (right) (Carpenter, Ralph 2010).

The figure clearly shows the difference in graphite formation. The cast iron has very flaky graphite, while the ductile iron graphite forms in nodes or spheroids. While this nodular graphite structure gives the ductile iron increased strength and ductility, it is also responsible for ductile iron's propensity towards pitting corrosion.

1.5.2.2 Strength Properties

Keil and Devletian showed that the tensile strength of DIP is around 55,000 psi with approximately 5% elongation. Results of Charpy impact testing show about 5 ft-lbs at 70 F. All testing was done according to ASTM C370. They also concluded that AWWA standards for design using steel and DIP were sufficient (Keil and Devletian 2011).

1.5.2.3 Durability

The largest research focus on DIP to date is on its performance in regard to corrosion. A literature review from 2012 by Cole and Marney summarized the current state-of-the-art in regard to corrosion performance of DIP. They focused on soil exposure, oxygen transport and solute movement in soils. They also looked closely at historical analysis and surveys of buried metal/pipe in the field, buried sensors and lab studies. In 1992, 19% of water pipes were ductile iron (Cole and Marney 2012). Pitting corrosion is a significant problem when dealing with water transmission pipes. In the 1960's the thinnest 12 inch cast iron pipe used in water transmission was 0.54 inches thick (Szeliga 2012). The thinnest 12 inch ductile iron pipe at the time was 0.31 inches thick (Szeliga 2012). The industry at the time believed that since ductile iron had higher strength and ductility that it could be made thinner than the cast iron pip, while still maintaining the required durability. However, the effects of pitting corrosion were not well understood. The thinner pipe allows for pitting corrosion to deteriorate through the walls of the pipe much faster. In fact, since the 1960's there have been many documented cases of ductile iron pipe failing faster than cast iron pipe (Szeliga 2012).

1.5.2.3.1 Environmental Impact

In order to have a corrosion cell there has to be an anode, cathode, metal, and electrolyte. The environment in which a metal is placed will determine whether or not these requirements for corrosion are met, and if so, how fast the corrosion will occur. In the case of ductile iron pipe used in water transmission, the environment will typically be the soil in which the pipe is buried.

There are many soil properties which will affect how well electrons and ions can transfer during the corrosion reactions. These properties include soil pH, oxygen concentration, chloride concentration, sulfate concentration, moisture content, and resistivity. A low pH causes the corrosion rate to increase, while a pH above 5 will not significantly contribute to the corrosion rate of ductile iron pipe (Szeliga and Simpson 2003). Chlorides and sulfates will have an effect on the pH of the soil, thus changing the corrosion rate. Also, if the oxygen in the soil is low than it may be consumed quickly by the oxygen reduction reaction, thus being a limiting factor and slowing down the corrosion rate. Studies on soil properties have shown that soil resistivity is the most critical characteristic when evaluating corrosion potential (Szeliga and Simpson 2003). Table 1.1 shows the corrosivity of soil based on its resistivity.

Table 1.1: Corrosivity of soil vs. soil resistivity and how they affect
ductile iron pipe (Szeliga and Simpson 2003).

Resistivity	Corrosivity	Failures Have Been Reported in
Less than 1,000 ohm-cm	Extremely Corrosive	5 Years or Less (See Figure 5)
1,000 to 5,000	Very Corrosive	15 Years or Less (See Figure 6)
5,001 to 10,000	Corrosive	20 Years or Less (See Figure 7)
10,001 to 25,000	Moderately Corrosive	25 Years or Less
Over 25,000	Mildly Corrosive	Over 25 Years

This table suggests that soils with a resistivity less than 1,000 ohm-cm should be considered

extremely corrosive. Ductile iron pipe located in soils such as this have been reported to fail in

under 5 years. Another problem that can occur with ductile iron pipe buried in soil is if the soil

type or properties vary significantly along the length of the pipe. For example, if the salt

concentration in the soil along one section of the pipe is very different from an adjacent section

of soil, a concentration cell can develop. The problem is that soil properties do vary quite a bit

and can often be corrosive. The properties of soil cannot be easily controlled or monitored. In

order to protect the ductile iron pipe from corrosion, there needs to be a way to protect the

pipe from the internal and external environments.

1.5.3 Field Studies

A 2003 study by Szeliga and Simpson describes the proper procedure for examining pipe and soil

conditions. They recommended that soil samples should be analyzed for resistivity, pH,

chlorides, and sulfate concentration. Soil with resistivity less than 1000 ohm-cm should be

considered extremely corrosive. They also purported that soils with a pH below 5 will contribute

to accelerated corrosion. Further soils with a chloride concentration above 150 ppm will increase the corrosion rate and can also de-passivate the DIP. They also stressed that stray current from impressed current cathodic protection systems or other sources can cause corrosion at areas near non-metallic joints along the pipe (Szeliga and Simpson 2003).

In a 2012 article Szeliga highlighted that corrosion engineers reported active corrosion occurring in over less than 10% of most DI pipelines. He also emphasized that random testing for corrosion along pipelines is not helpful as it is very likely that no corrosion will be found as the most severe corrosion can be very localized. He recommended using cell-to-cell potential measurements to locate active corrosion areas in the field (Szeliga 2012).

In a 2013 study by Kleiner et al., DIP samples were taken from water utilities in four different North American cities: Kansas City, Kansas, St. Louis, Missouri, Louisville, Kentucky and Calgary, Alberta (Canada). After the samples were sand blasted they were laser scanned to generate data regarding corrosion pit area, depth and volume. Samples were also sliced into thin sections referred to as rings. The pitting population on each ring was analyzed and the data was fitted using statistical models. The right-truncated Gumbel probability distribution best fit the frequency distribution of maximum pit depth whereas, the Weibull distribution best fit the frequency distribution of pit area and volume (Kleiner et al. 2013). Table 1.2 shows the results of fitting the data with these statistical models.

Table 1.2: Statistical analysis results of pit geometries in ductile iron pipe ring populations (Kleiner et al. 2013)

Ring		Pit depth maxima, truncated Gumbel			Pit area, Weibull			Pit volume, Weibull		
Length (mm)	Count	Scale	Location	P-value	Scale	Shape	P-value	Scale	Shape	P-value
Kansas City										
25	2,718	1.11	1.12	0.000	67	0.27	0.000	89	0.26	0.000
50	1,380	1.16	1.33	0.000	169	0.32	0.000	226	0.31	0.000
100	645	1.23	1.61	0.000	451	0.38	0.000	607	0.36	0.000
150	456	1.29	1.85	0.000	862	0.44	0.000	1,178	0.42	0.000
300	181	1.43	2.23	0.050	2,215	0.53	0.000	3,091	0.51	0.000
450	95	1.56	2.56	0.003	4,013	0.61	0.000	5,766	0.57	0.000
600	84	1.71	2.62	0.006	4,519	0.59	0.001	6,252	0.56	0.001
Louisville										
25	2,738	1.04	0.94	0.000	38	0.24	0.000	50	0.23	0.000
50	1,440	1.14	1.19	0.000	111	0.27	0.000	148	0.26	0.000
100	684	1.28	1.49	0.000	313	0.32	0.000	432	0.30	0.000
150	455	1.37	1.74	0.000	596	0.35	0.000	844	0.33	0.000
300	220	1.62	2.38	0.000	1,965	0.47	0.000	2,959	0.44	0.000
450	141	1.83	2.80	0.000	3,615	0.55	0.000	5,608	0.50	0.000
600	78	1.68	2.99	0.003	4,480	0.60	0.000	6,916	0.55	0.000
Calgary										
25	2,297	1.45	1.41	0.000	13	0.29	0.000	21	0.27	0.000
50	1,192	1.56	1.99	0.000	41	0.37	0.000	69	0.34	0.000
100	585	1.69	2.71	0.000	117	0.43	0.000	207	0.40	0.000
150	388	1.87	3.19	0.000	205	0.45	0.000	370	0.41	0.000
300	189	2.09	4.22	0.000	532	0.48	0.000	1,008	0.44	0.000
450	83	2.06	4.59	0.007	824	0.47	0.001	1,651	0.42	0.002
600	83	2.64	5.70	0.014	1,289	0.51	0.002	2,609	0.46	0.002

Note: The mean wall thickness of the Kansas City, Louisville, and Calgary samples were 10.89, 8.89, and 8.44 mm, respectively.

The Gumbel and Weibull models fit their respective data well as can be seen by the low P-values. Soil data for each location was analyzed to compare with the pitting corrosion data. Results found that soil property data did not improve their ability to predict corrosion pit properties (Kleiner et al. 2013).

1.5.4   Laboratory Studies

In a 2013 study, DIP samples were exposed to different corrosion environments for 6 months to observe and compare corrosion rates. Initial results showed that samples exposed to a salty environment had the highest weight loss (in Ota, Nigeria). The samples in the A/C environment had no corrosion (Oke and Ukoba 2013a). Table 1.3 shows the weight loss of ductile iron in different environments over the exposure time.

Table 1.3: Weight loss of ductile iron in different exposure environments (Oke and Ukoba 2013a)

EXPO-SURE TIME (DAYS)	WEIGHT OUTSIDE (g)	WEIGHT LOSS (OUTSIDE)	WEIGHT (NaOH) (g)	WEIGHT LOSS (NaOH)	WEIGHT A/C (g)	WEIGHT LOSS A/C (g)	WEIGHT BRACKISH (NaCl) (g)	WEIGHT LOSS (NaCl) (g)
1	21.451	-	21.451	-	21.451	-	21.451	-
30	20.6521	0.7989	20.59	0.861	21.451	0	20.6309	0.8201
60	20.6062	0.0459	20.584	0.006	21.451	0	20.5658	0.0651
90	20.5603	0.0459	20.59	-0.006	21.451	0	20.5007	0.0651
120	20.5144	0.0459	20.584	0.006	21.451	0	20.4356	0.0651
150	20.4685	0.0459	20.59	-0.006	21.451	0	20.3705	0.0651
180	20.4226	0.0459	20.584	0.006	21.451	0	20.3054	0.0651

It can be seen that ductile iron samples exposed to the outside and sodium chloride environments had the greatest weight loss indicating environments more conducive to corrosion.

In a 2012 study by Zheng and co-workers a non-destructive evaluation (NDE) technique relying on pulse thermography was used to assess pitting corrosion of DIP. This is considered an active indirect NDE method because an external input, in this case heat, is applied to aid in damage detection. A schematic of the method is shown in Figure 1.3. They investigated five signal features: amplitude, phase, first and second derivative, and principal component. All features showed the presence of corrosion pitting, but none were able to accurately quantify the depth of pitting corrosion (Zheng et al. 2012).
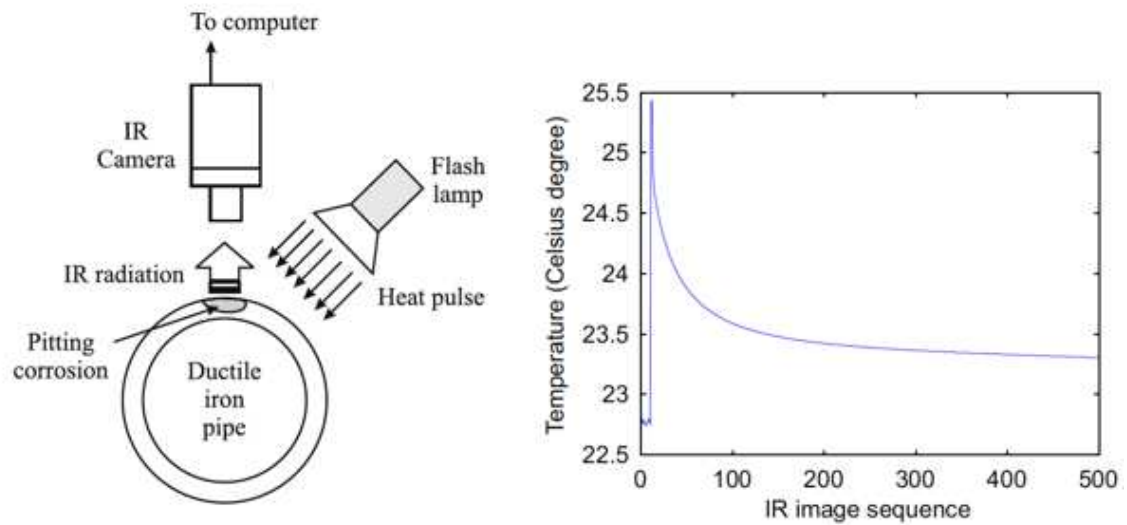
Figure 1.3: Pulsed thermography inspection schematic for ductile iron pipe (Zheng et al. 2012)

Figure 1.4 shows an example of the results of pulse thermography.
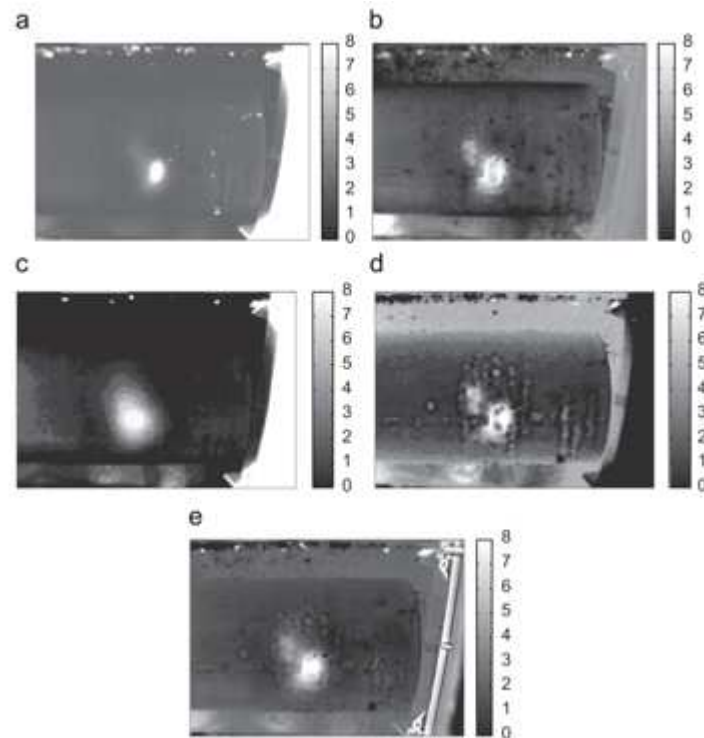
Figure 1.4: Estimation of pitting depth from thermal features (unit of the color bar is in mm). (a) amplitude (b) phase (c) first derivative (d) second derivative and (e) principal component. (Zheng et al. 2012)

They found that the second principle component gave the best estimate of pit depth across the range of 0-8 mm (for this study). They also showed that the amplitude and phase features can allow the researcher to know if there is corrosion pitting present over a certain threshold depth. It was noted that during field inspection pipes would still need to be sand blasted or fully cleaned. The researchers pointed out that while the technology is promising it is not yet ready for the field. (Zheng et al. 2012)

1.5.5   Practical Tests

Two different test methods for assessing whether pipe is of the grey iron or ductile type are outlined in a 2010 article by Carpenter. This follows either a destructive test method using ¼" drill bits and drilling into the subject pipe or a non-destructive sounding test. Both tests are outlined below:

1. Drill test - using a ¼" cutting bit

    a) Ductile iron should be noticeably more difficult to drill. This is due to the increased strength of ductile iron vs. gray iron and the slight increase in lubricity of the flake formation of the graphite in the microstructure.

    b) Ductile iron should have longer, more contiguous chip formations,

    c) while the gray iron will have small, discontinuous chips. (Carpenter, 2010)

2. Sounding test

    a) Using a small small ball peen hammer, the outside of the pipe is tapped and the sound will provide a unique signature for the material type.

b) Ductile iron should have a noticeable "ring" due to the spheroidal graphite what allows the sound waves to reverberate through the microstructure

a) Gray iron should have an audible and distinct "KLUNK" as the flake graphite will attenuate the sound waves (Carpenter 2010).

1.5.6   Corrosion Mitigation Techniques for Ductile Iron Pipe

There are several methods that have been developed over the years to prevent corrosion on ductile iron pipe. These range from coatings to cathodic protection. The goal of these methods is to provide efficient ways of protecting the pipe from the surrounding corrosive environment. The following section will explain some of these methods as well as identify the best mitigation techniques to be used with ductile iron pipe.

1.5.6.1 Cement-Mortar Lining

One of the most significant improvements for corrosion protection of iron pipe was the use of cement-mortar linings for cast iron and ductile iron pipe (Carpenter 2010). While not directly applicable to power transmission usage for DIP, there may be valuable information learned which can be applied to durability improvement for DIP. This may be especially true for DIP buried in aggressive soils, where a protective barrier could be realized with a cement-mortar lining and/or coating. Cement-mortar linings may be applied by either the centrifugal or projection process (American pipe manual 2004). In 1939 cement-mortar linings were first recognized under the designation of A21.4 (AWWA C104) "Specifications for Cement-Mortar Lining for Cast Iron Pipe and Fittings." Over time this important standard has been updated include cements other than OPC, increases to the size pipe covered in the specification and to

cover different types of manufacturing processes. In a review by Bonds, seal coating was

highlighted as a way to retain moisture and aid in curing, but issues with VOCs in the seal coat

which could be released during manufacture resulted in changes to the specification that in turn

have manufacturers developing low or non VOC seal coats (Bonds 2015). It was also found that

seal coated linings are limited for temperatures below 150 to avoid softening of the seal coat.

Limitations to durability for cement-mortar linings mainly include cracking or issues with initial

manufacturer that limit the bond between the lining and the metal (Bonds 2015). Two types of

cracks can exist – surface crazing or circumferential cracks. It has been shown that self-healing

can occur where initially formed hairline cracks during the manufacture process are "healed" or

will close up once in contact with water. Furthermore, initial shrinkage may also be overcome

by water uptake and swelling of C-S-H. It was also shown that porosity can be limited or

reduced by: (Bonds 2015)

a) calcium hydroxide reacting with calcium bicarbonate in the water to precipitate
   calcium carbonate which fills porosity and limits further ingress

b) sulfates will also precipitate as calcium sulfate to block porosity

c) some initial iron dissolution may also react with free lime to form iron hydroxide

1.5.6.2 Polyethylene Encasement

Polyethylene encasement has been promoted by the ductile iron pipe industry as the primary

corrosion control method (Szeliga 2012). It is simply a loose, plastic sheeting that is wrapped

around the pipe and held with duct tape. The benefits of this protection method are that it is

easy to install and repair and is relatively less expensive. There are, however, many issues with

this method. First, the installation of polyethylene encasement requires an amount of care that

is simply not practiced by most construction workers. It is common for folds and tears in the

plastic to develop during installation, which defeats the purpose of the wrapping. In fact, having these small areas of pipe exposed to the soil at these holes can cause more severe corrosion. Even if the polyethylene sheeting were installed perfectly, case studies have shown that the rocky backfill, coupled with the weight of the water filled pipe will cause tears and holes to form (Szeliga 2012). Overall this method is difficult to ensure 100% protection of the pipe, and will likely leave small areas of pipe exposed to the soil. In the case of power transmission pipes, polyethylene encasement is somewhat impractical since much of the pipe is exposed and the plastic could easily become damaged. However, polyethylene encasement could be considered for the section of pipe that is buried in the soil.

1.5.6.3 Coatings

There are many coatings that are used in pipes. These coatings can generally be split into two categories, metal coatings and plastic coatings (Uhlig and Revie 2008). Common metal coatings would include zinc and aluminum. These type of coatings work by creating sacrificial anodes, which corrode instead of the iron. Common plastic coatings are epoxies, vinyl, and polyurethanes. These type of coatings act as barriers, which prevent contact between interfaces. In the case of ductile iron pipe used for power transmission, a zinc coating would be appropriate for external protection. The zinc coating would be more resistant to scratches and rubbing than an epoxy.

1.5.6.4 Cathodic Protection

Cathodic protection is a widely used method for protecting metals from corrosion. There are two types of cathodic protection (Roberge 2008). One method is done by applying a current to the metal which raises its potential, pushing it into the immunity zone in the case of ferrous

metals. The other method is by connecting the protected metal to a more anodic metal that will corrode sacrificially.

When dealing with ductile iron pipe, impressed current cathodic protection is ill advised (Szeliga and Simpson 2003). Ductile iron pipe is electrically discontinuous. At every joint, there is a non-metallic connection that prevents the flow of electrons from proceeding through the pipe. If there are stray currents due to nearby cathodic protection systems or power lines, they can enter the pipe and exit near the joints. Near these joints, where current is flowing in and out there can be high rates of corrosion. Because of this, it is best to not use an impressed current system in most cases.

Sacrificial anode cathodic protection is a more appropriate method for corrosion protection of ductile iron pipe (Szeliga and Simpson 2003). This type of cathodic protection will not produce stray currents that could lead to corrosion. The problem with using sacrificial anodes is that a large amount of the anodic metal is needed to drive a current large enough to protect the ductile iron. The anodes will also need to be placed frequently along the length of the pipe. This makes it more difficult to install and repair.

1.5.7   Summary and Gaps in Literature

Since the 1960s, it has become clear that pitting corrosion is a problem with ductile iron pipe that needs to be solved. The nodular microstructure of DIP make it stronger and more ductile than cast iron pipe, but also causes it to corrode in pits. Many protection methods have been developed that have varying levels of practicality and effectiveness. The polyethylene encasement method is less expensive and easy to install, but its effectiveness is questionable. Coatings are good for protecting the exterior of the pipe, although it is important that they are

applied properly so that there are no defects. Cement-mortar linings are effective in protecting the interior of the pipe, and seem to improve with age due to their self-healing properties. Cathodic protection can be used if using sacrificial anodes, although it may not be practical in some cases since large amounts of the anodic material are needed to protect a large ductile iron pipeline. Currently, the best way to protect a ductile iron pipe transmitting water seems to be to apply a cement-mortar lining to the interior, and apply a zinc coating on the exterior.

Further research should be done to investigate alternative protection methods, pitting corrosion rate, and other uses for ductile iron pipe. For example, ductile iron pipe that is used as power transmission poles will require different types of corrosion protection. There may be concentration cells developing due to part of the pipe being buried in the ground, while the rest is exposed to the air. There could also be more severe corrosion at the joints of the ductile iron pipe. Stray current corrosion could also be an issue since the pole is transmitting power. With most of these applications, it seems that the best way of mitigating corrosion is to use two or three protection methods. These could include both coatings and a polyethylene encasement or cement mortar lining. Corrosion is inevitable and difficult to counter so providing multiple barriers and inhibitors is usually beneficial.

1.5.8   References

Ahn, Tae-Ho, and Toshiharu Kishi. (2010) "Crack Self-healing Behavior of Cementitious Composites Incorporating Various Mineral Admixtures." Journal of Advanced Concrete Technology ACT 8.2: 171-86.

American pipe manual. (2004). Birmingham, Ala.: American Cast Iron Pipe Co.

Bonds, Richard W. (2015) "Cement-Mortar Linings for Ductile Iron Pipe." Ductile Iron Pipe Research Association.

Carpenter, Ralph. (2010) "Gray Iron and Ductile Iron Pipe—Some Historical Benchmarks Impacting Condition Assessment." World Environmental and Water Resources Congress.

Keil, Brent, and Jack Devletian. (2011) "Comparison of the Mechanical Properties of Steel and Ductile Iron Pipe Materials." Pipelines.

Kleiner, Yehuda, Balvant Rajani, and Dennis Krys. (2013) "Performance of Ductile Iron Pipes. I: Characterization of External Corrosion Patterns." Journal of Infrastructure Systems 19.1: 108-19.

Kleiner, Yehuda, and Balvant Rajani. (2013) "Performance of Ductile Iron Pipes. II: Sampling Scheme and Inferring the Pipe Condition." Journal of Infrastructure Systems 19.1: 120-28.

Kramek, N., & Loh, L. (2007). "The History of Philadelphia's Water Supply and Sanitation System. Lessons in Sustainability of Developing Urban Water Systems." *Master of Environmental Studies. Philadelphia, University of Pennsylvania, Philadelphia Global Water Initiative, junio*.

Liu, Zheng, Marc Genest, and Dennis Krys. (2012) "Processing thermography images for pitting corrosion quantification on small diameter ductile iron pipe." NDT & E International 47: 105-15.

Marcus, P. (2012). "Corrosion mechanisms in theory and practice." Boca Raton: CRC Press.

Noble, H. J. (1940). "History of the Cast Iron Pressure Pipe Industry in the United States of America." Printed at Birmingham publishing Company.

Oke, P.k., and O.k. Ukoba. (2013) "Analysis of Corrosion Growth of Ductile Iron in Different Environments." Advanced Materials Research 824: 327-31.

Oke, P.k., and O.k. Ukoba. (2013) "Analysis of Property Changes of Ductile Iron in Different Environments." Advanced Materials Research 824: 332-38.

Roberge, P. R. (2008). "Corrosion engineering: principles and practice." New York: McGraw-Hill.

Szeliga, Michael J. (2012) "Ductile Iron Corrosion Theories and Science." Pipelines.

Szeliga, Michael J., and Debra M. Simpson. (2003) "Evaluating Ductile Iron Pipe Corrosion." New Pipeline Technologies, Security, and Safety.

Uhlig, H. H., & Revie, R. W. (2008). *Corrosion and corrosion control: an introduction to corrosion science and engineering*. Hoboken, NJ: J. Wiley.

2   First Manuscript

Experimental Investigation of the Effects of Chloride Ingress and Freeze-Thaw Attack on the Electrical Surface Resistivity Measurements of Reinforced Concrete

Silas Shields[1], O. Burkan Isgor[1], Jason H. Ideker[1], David Rodriguez[1],

Vahid Jafari Azad[1]

Abstract: Early detection of corrosion in reinforced concrete bridge decks is important for affective prevention and rehabilitation strategies. Current testing methods are expensive and time-consuming. There is a need for testing methods that are relatively quick and that can be done with minimal effort. This goal of this study is to research a non-destructive testing method, surface resistivity, and the effects premature concrete deterioration brought on by chloride ingress and/or freeze-thaw cycling have on it. The experimental method for this project consists of taking surface resistivity measurements of reinforced concrete slabs after they have been ponded with a magnesium chloride de-icing solution, containing a corrosion inhibitor. Reinforced concrete slabs and companion concrete cylinders also underwent freeze-thaw cycling to observe its effect on surface resistivity in conjunction with exposure to chlorides. Many factors such as internal and ambient temperature and relative humidity affect surface resistivity measurements so this data was also collected. To compare the surface resistivity to the rate of chloride ingress, cores were taken from the slabs. As expected, the surface resistivity of the concrete slabs initially increased while the concrete cured and lost moisture due to the hydration process and to the environment. Once ponding of the chloride solution started,

however, there began to be a decrease in surface resistivity. This decrease in surface resistivity

is believed to be caused by the increase of free chlorides present in the slabs after being

saturated with the de-icing solution. The surface resistivity of the corresponding slabs that were

ponded with tap water remained constant. These results show that surface resistivity

measurements are a potential indicator of chloride ingress and, therefore, may correlate to risk

of corrosion in reinforced concrete. The effect of freeze-thaw cycling on surface resistivity,

according to this study, is that it increases the surface resistivity. This is due to the micro-

cracking in the concrete matrix, caused by the freeze-thaw damage.

_____

[1]Oregon State University, School of Civil and Construction Engineering, Corvallis, Oregon, USA

2.1   Introduction

One of the most common forms of deterioration in concrete structures is corrosion of the

reinforcing steel. Corrosion in concrete structures is often initiated by chlorides penetrating the

concrete and reaching the reinforcement. These chlorides mainly come from marine salts or de-

icing chemicals. Once the chloride concentration at the reinforcement depth surpasses a certain

threshold, corrosion will initiate, propagate, and deteriorate the steel. Another deterioration

mechanism often present when de-icing chemical are used is freeze-thaw attack. The cycling of

temperature between warm and freezing will cause the pore solution within the concrete to

constantly freeze and expand. This can cause serious damage to concrete if the mixture was not

designed to mitigate these effects. The spalling and cracking caused by freeze-thaw attack,

allows more moisture and potentially more chlorides to travel down through the concrete to the

reinforcing steel.

Detecting corrosion in reinforced concrete can be very difficult since it is not visible when it

initiates. By the time corrosion is evident by visible rust staining on the outside of the structure,

serious damage has already been done, and expensive rehabilitation or replacement plans need

to be made. The earlier potential corrosion can be detected in a concrete structure, the less

expensive and easier it is to repair or prevent from initiating. The problem with many current

methods of corrosion detection is that they are expensive and time consuming. Many

departments of transportation (DOT) extract cores from bridges and do chloride depth profiles

to determine corrosion risks in concrete structures. This requires closing off traffic, having an

inspector take several cores from various locations, and then spending many hours in the lab

determining the chloride concentrations at various depths of the concrete. This process is not

ideal, and will likely not be done unless a serious corrosion issue is suspected. There needs to be

a more cost-effective and efficient method of monitoring chloride ingress so that more bridges can be regularly inspected, thus detecting corrosion before it becomes a serious issue.

Electrical resistivity of concrete has been found to correlate with concrete durability (Alfonso et al. 1988). Many studies have established a relationship between electrical resistivity and the corrosion rate of the reinforcing steel. One of these relationships is that concrete resistivity and corrosion rate are inversely proportional (Lopez et al. 1993) (Gowers et al. 1999). There are also concrete characteristics that affect concrete resistivity. For example, high water-to-cement ratio and/or high moisture contents correlate with low resistivity values (Neville 1981, Morris et al. 2004). Degree of saturation and chloride concentration have also been found to affect concrete resistivity (Hussain et al. 1995, Morris et al. 2004, Song et al. 2007).

Rapid Chloride Permeability Tests (RCPT) have been a common method for measuring concrete resistivity, but recently, surface resistivity (SR) measurements have started to replace them. Both test methods measure the concrete's resistance to ionic movement under an applied electrical potential difference, but SR measurements can be taken in seconds, while RCPT measurements take hours. Plus there are many known drawbacks to the RCPT test method including sample heating which changes the results of the test, and an inability to test mixtures with low w/cm and/or those containing supplementary cementitious materials. Studies have shown that the measurements taken by the two methods have good correlation (Rupnow 2011, Hooton et al. 2012, Jackson 2013).

All these developments have led to increased efforts to standardize SR measurement procedures (AASHTO TP 095-11-UL; CAN/CSA A23.2 2009; ASTM WK37880). A number of jurisdictions even started requiring resistivity measurements as part of ongoing construction

and maintenance procedures (FM 5-578 2004; MTO LS-444 2013). Consequently, a number of companies producing SR measurement devices have been increasing, while the cost of units for SR measurements has been declining.

The most commonly used method for measuring surface resistivity in the field is the four-point Wenner probe technique (ASTM 2014). This method is simple and fast, and can be done not only on cores but also directly on the surface of concrete structures. This is a major advantage since it does not require damaging the structure by taking cores or having to access the reinforcement. There are several factors which alter the measurements and require corrections to me made, however. SR values can be affected by the density, depth, diameter, type, and orientation of the steel reinforcement (Gowers et al. 1999, Weydert et al. 1999, Presuel-Moreno et al. 2009, Sengul et al. 2009, Salehi 2013). These affects need to be corrected for so that accurate predictions can be made. Morales (2015) did a detailed literature review on these factors and gave guidelines for taking SR measurements in a way that minimizes errors stemming from them.

The ability to map the amount of chloride ingress across a large area, without having to take cores or access the reinforcement is a major advantage of SR measurements. If SR measurements can be couple with time-to-corrosion prediction models then DOTs can use them as a more efficient tool to inspect more bridge decks. While SR measurements do not give an actual chloride depth profile, they could be used with prediction models to determine if there is a potential problem that may require further investigation. With this tool, DOTs will not have to sacrifice thorough and frequent inspections because of limited

time and resources. This increases the likelihood of identifying potential corrosion early on, which can be more easily mitigated in the early stages.

Chloride prediction models become much more accurate when environmental factors such as salt exposure, temperature, relative humidity, and moisture are known. Temperature can be corrected for using the Hinrichsen-Rasch law. Moisture and salts will decrease the resistivity of the concrete. This study will include gathering this data so that they can be taken into account in the predictive models. SR measurements coupled with chloride ingress prediction models could be a very useful tool for determining at risk areas of reinforced concrete. This research study is focused on gathering experimental data on how applications of chloride-containing de-icing solutions coupled with freeze-thaw cycling affect SR values.

2.2 Materials and Methods

2.2.1 General Information

The experimental work for this study involved gathering temperature, relative humidity, chloride ingress, and surface resistivity data to observe how surface resistivity of concrete slabs changed when undergoing freeze and thaw cycling. This data will be used to calibrate a predictive model which is being developed as a part of this project, but is the subject of a different manuscript. These concrete slabs were designed to represent existing Oregon concrete bridge decks, and thus have mixture proportions that range from 1960s era concrete to currently specified concrete. An ordinary Portland cement mixture (OPC-47) was proportioned according to 1960s specifications for air-entrained concrete. Another ordinary Portland cement mixture (OPC-53) was proportioned according to 1960s specifications for non-air-entrained

concrete, and a high performance concrete mixture (HPC-43) follows current day concrete mixture proportions for air-entrained concrete. Each slab was approximately 48 inches by 40 inches and had a cover depth of 2.5 inches.

2.2.2 Materials

2.2.2.1 Concrete

All concrete mixtures were manufactured at a local ready-mix plant and cast at an outdoor exposure site located just outside of Oregon State University's Hinsdale wave lab. The three slab types underwent the same exposure regimes both at the outdoor exposure site and in the freeze-thaw chamber.

2.2.2.1.2 Concrete Mixture Designs

Nine concrete slabs were cast for this study. Three of these slabs were only ponded with a chloride de-icing solution, three of them were only ponded with tap water, and three of them were ponded with chlorides and underwent freeze-thaw cycling. The detailed mixture proportions used for this research study are shown in Table 2.1. Values of slump, air content, and unit weight are also given.

Table 2.1: Mixture design for STA, STB, and STC

	OPC-47	OPC-53	HPC-43
w/cm ratio	0.47	0.53	0.43
Measured Slump, in. (cm)	6.25 (15.9)	5.5 (14.0)	3.5 (8.9)
Measured Air, %	5	1	2.5
Measured Unit Weight, lb/ft^3 (kg/m^3)	142.16 (2277.2)	148 (2370.7)	145.88 (2336.8)
Cement, lbs. (kg)	512 (232.2)	515 (233.6)	461 (209.1)
Fly Ash, lbs. (kg)	0	0	204 (92.5)
Silica Fume, lbs. (kg)	0	0	25 (11.3)
Water, lbs. (kg)	240 (108.9)	275 (124.7)	300 (136.1)
3/4'' - No.4, lbs. (19.1mm - 4.76mm, kg)	1690 (766.6)	1693 (767.9)	1714 (777.5)
Sand, lbs. (kg)	1196 (542.5)	1401 (635.5)	617 (279.9)
Total, lbs. (kg)	3638 (1750.2)	3884 (1761.8)	3321 (1506.4)

OPC-47 and OPC-53 are both designed according to 1960s specifications and, thus, contain no supplementary cementitious materials. The OPC-47 slab is air entrained, while OPC-53 is not. The HPC-43 slab is a modern high performance concrete mixture. In this mixture, the class F fly ash replacement percentage was 30%, and for silica fume it was 4%. The target air content for the two air-entrained mixtures was 6%. Neither of these mixtures actually reached this target

due to complications at the ready-mix plant. It was decided that the study would proceed with the existing air contents. In addition to the concrete slabs, fifteen 4in. x 8 in. concrete cylinders from each mixture type were also cast. These cylinders were used for mechanical property and performance testing, and underwent the same freeze-thaw cycling regime as the slabs.

2.2.2.1.3 Reinforcement

Steel reinforcement bars were placed in all slabs according to Oregon bridge deck design standards. ASTM A615 carbon steel #5 (5/8 in., 16mm) reinforcement is used in most bridge decks, although #4 is also occasionally used. The important factor is the rebar's effect on surface resistivity, and studies have shown that these two rebar sizes do not affect surface resistivity measurements differently (Salehi 2013). According to historical data, the concrete cover thickness on many of Oregon's bridge decks is 2.5 inches (6.35 cm), therefore this cover was used. The rebar in each slab was placed in an orthogonal grid with 8 inch center-to-center spacing. A section of each slab was left unreinforced for the purpose of comparing surface resistivity measurements.
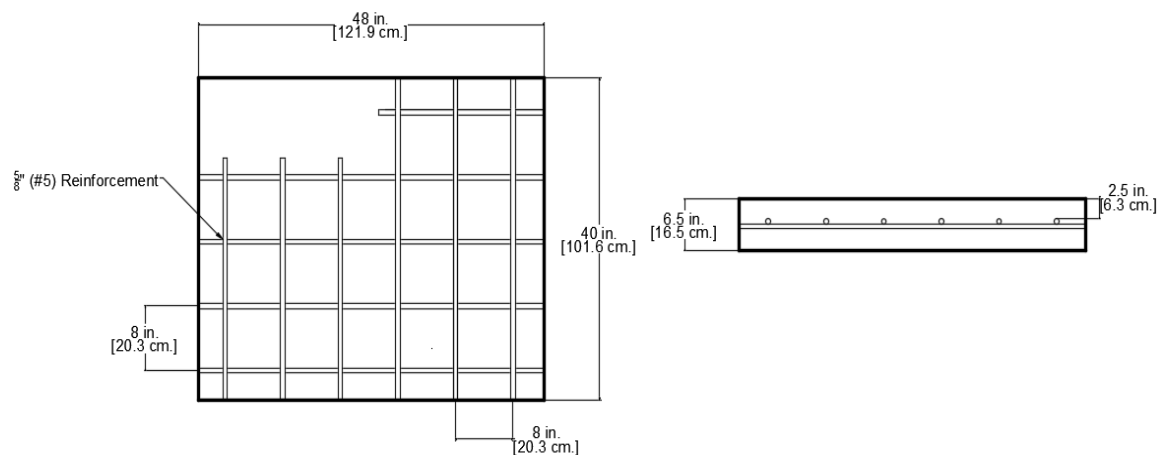
(a)
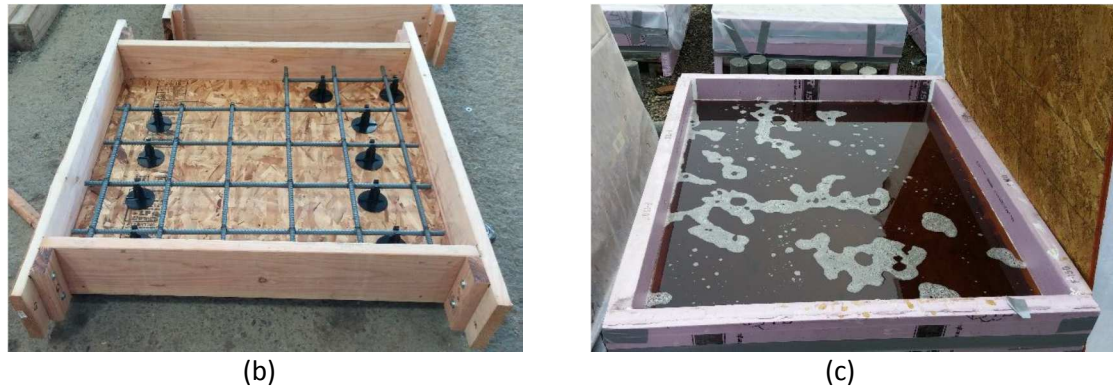
Figure 2.1 – (a) Geometrical details of the concrete slabs; (b) a sample slab with placed reinforcement before casting of concrete; (c) a sample concrete slab during ponding with the deicing solution. The section that is unreinforced was used to take measurements and to extract cores for additional testing.

2.2.3 Exposure Regime

2.2.3.1 Initial Curing

Curing of the slabs and cylinders occurred under wet burlap for 28 days after they were cast. A portion of the cylinders were used for strength tests at 28 and 90 days, in accordance with ASTM C39.

2.2.3.2 Ponding

In order to mimic the exposure of concrete bridge decks to deicing salts, the test slabs were exposed to a commercially available 30% magnesium chloride ($MgCl_2$) solution, used by ODOT. This solution also contained a corrosion inhibitor, the specific chemical composition was not disclosed by the manufacturer. The ponding regime consisted of wet/dry cycles in order to encourage chloride ingress through advection. See figure 2.1.c above for example ponded slab. The test slabs were ponded with the $MgCl_2$ solution for 96 hours, after which the solution was vacuumed out and a 10 day dry period began. The test slabs were exposed to natural ambient

conditions during the dry cycle. This exposure regime was chosen based on previous studies that showed that these wet/dry cycling times increased chloride ingress, while still being representative of field exposure (Hong 1999). Control slabs were ponded with water, during this exposure regime. After 7 ponding cycles, it was determined that the chlorides were penetrating the slabs too rapidly. Therefore, ponding was paused for ten weeks. Ponding with the $MgCl_2$ solution began once again after this. Three of the slabs underwent both chloride ponding cycles and freeze-thaw cycling. Ponding was stopped on all the slabs after the freeze-thaw slabs had been through 300 freeze-thaw cycles in the environmental chamber.

2.2.3.3 Internal and Atmospheric Conditions

Internal and ambient weather conditions are important variables when considering surface resistivity data. Changes in weather conditions can affect surface resistivity measurements. In order to support the predictive model being developed alongside this project and to normalize the surface resistivity data being collected, temperature and relative humidity conditions were monitored. A weather station was set up at the outdoor exposure site to collect ambient temperature, relative humidity, precipitation, wind speed, wind direction, and other weather conditions. To monitor the slabs specifically, Wagner Rapid RH® probes were installed into the slabs at two unique depths. These probes gave internal relative humidity and internal temperature data. A probe was placed at a one inch (2.54 cm) depth from the surface of the slab, and another probe was place at a two and a half inch (6.35 cm) depth from the surface of the slab. At a one-inch depth, the probes were less likely to cause any cracking at the surface. The two and a half inch deep probe was used to compare changes in internal relative humidity and internal temperature to the one-inch probe. The surface temperature of the slabs were measured using an infrared temperature gun.

2.2.3.4 Freeze-Thaw Cycles

Freeze-thaw cycles were administered on both the three designated concrete slabs and their

corresponding cylinders, according to ASTM C666-15 Procedure B. Before the freeze-thaw

cycles began, the slabs had been exposed to 8 chloride ponding cycles. ASTM C666-15

Procedure B requires that the slabs and cylinders be exposed to 300 freeze-thaw cycles. These

cycles were broken up into 5 segments of 60 cycles each. In between each segment, the slabs

and cylinders were returned to the outdoor exposure site and underwent 3 additional ponding

cycles before returning to the freeze-thaw chamber. One freeze-thaw cycle inside the chamber

lasted 3 hours. The first half hour was a ramping period in which the temperature decreased to

3.2^{o}F (-16°C). This was followed by an hour maintaining this freezing temperature. Next, there

was another half hour ramping period, which brought the temperature up to 60.8^{o}F (+16°C). The

last hour maintained this thawing temperature. The goal of this exposure regime was to achieve

an approximate cycling range of 14°F to 50°F (-10°C to 10°C) at 1.5-inch (3.81cm) depth. An

additional set of cylinders were subjected to 300 freeze-thaw cycles inside of a Scientemp

chamber to be compared with the cylinders that were placed in the large freeze-thaw chamber

with the slabs. ASTM C666-15 Procedure B requires freezing in air and thawing in water, as

opposed to Procedure A, which requires freezing in water and thawing in water. Procedure B

was used for the cylinders in the Scientemp chamber in order to keep the environment

consistent with the cylinders in the large freeze-thaw chamber. At the end of the 300 freeze-

thaw cycles, there was not a significant enough difference in surface resistivity measurements

between the freeze-thaw slabs and their controls. Therefore, it was decided to continue testing

with an additional 300 freeze-thaw cycles. These additional freeze-thaw cycles were done 10

months after the end of the first 300 cycles. Also, chloride ponding had stopped 6 months prior

to the additional freeze-thaw cycles. Accelerated freeze-thaw testing of 300 cycles is very

aggressive for many temperate environments where the concrete may only experience around

50 cycles during its service life. Therefore, the environment in which the reinforced concrete

structure is servicing should be taken into consideration when comparing and analyzing results.

2.2.4 Testing Methods

Throughout the study, several tests were done to analyze both the concrete cylinder and slab

samples. These tests were done to determine the internal conditions, compressive strength, and

degree of chloride ingress among other things. The following section describes each test that

was done during this research study.

2.2.4.1 Chloride Profiling

In order to determine chloride ingress for comparison with the surface resistivity data and for

use in the predictive model, chloride profiles were taken. This began by extracting 4 in. diameter

cores from the chloride ponded slabs. These cores were then ground into powders by layer,

using a profile grinder. ASTM C1152 was followed to determine the acid-soluble chloride

content in each powdered concrete layer. This procedure gives the total amount of chlorides in

each layer. After the chloride profile was determined, ASTM C1556 was used to analyze the

chloride transport properties such as the apparent diffusion coefficient. Holes left in the slabs

from where the cores were taken were repaired with a commercial self-consolidating,

shrinkage-compensating concrete repair material.

2.2.4.2 Compressive Strength

Compressive strengths of cylindrical concrete specimens were determined, following ASTM C39.

Specimens were loaded at a rate of 500 lb/s, using a 700 kip compression machine.

2.2.4.3 Four Point Probe Surface Resistivity

Surface resistivity data was collected using a four point Wenner probe measurement device. Measurements were taken on both the reinforced and unreinforced sections of the concrete slabs. A previous study by Morales (2015) found that when taking surface resistivity measurements over reinforced concrete, the optimum orientation of the probe is perpendicular to the topmost rebar to minimize error. In the field, a rebar locator can be used to ensure proper probe orientation for measurements. Five measurements were taken on both the reinforced and unreinforced sections of the slabs and the median value was noted for each. Measurements were taken in between chloride ponding cycles. During the 8-day freeze-thaw period, measurements were taken on all slabs at the same time during a thawing cycle. Surface resistivity measurements were also taken on the concrete cylinders that were undergoing freeze-thaw cycles. These measurements were taken every 36 cycles. For the cylinders, five measurements were taken every 90 degrees around the cylindrical concrete specimen. The median value of the five measurements was used as the surface resistivity value for each cylinder.

2.2.4.4 Bulk Electrical Resistivity

Bulk resistivity measurements are often taken on concrete cylinders. The measurements involve sending a current through the entire bulk structure of the cylinder, as opposed to surface resistivity measurements, which only send a current through the surface of the concrete. Studies have shown that bulk and surface resistivity measurements have good correlation. A Giatec RCON electrical resistivity meter was used to measure the bulk resistivity of the concrete cylinder that were undergoing freeze-thaw cycles in the Scientemp chamber. These measurements were taken every 36 cycles, and were used to compare to the surface resistivity

measurements being taken with the Wenner probe. Bulk resistivity measurements taken with the Giatec meter followed the guidelines given in ASTM C1760.

2.2.4.5 Resonant Frequency Test

Studies have shown that using resonant frequency and observing the longitudinal and transverse wave velocities can be used as a non-destructive test method to identify concrete's dynamic modulus of elasticity (Prassianakis 2004). Fractures and deformations in concrete will coincide with a decrease in its dynamic modulus of elasticity. The concrete cylinders undergoing freeze-thaw cycles in the Scientemp chamber were measured according to the resonant frequency test standard specified in ASTM C215. Measurements were taken every 36 cycles, and used to identify damage caused to the cylinders by the freeze-thaw cycles.

2.2.4.6 Scanning Electron Microscope

In addition to the aforementioned tests, concrete samples were also observed under a scanning electron microscope (SEM). These images were taken to observe microstructural changes in the concrete caused by freeze-thaw damage. The OPC-47 slab was chosen for this test. One core was taken from the slab that went through freeze-thaw cycles in the large chamber and another core was taken from the same slab type that did not go through freeze-thaw cycling. Both of these slabs were ponded with chlorides. These two cores were then used to create samples appropriate for use in the SEM. For each core, two samples were taken; one at a depth of 8/10 in. and another at a depth of 2.5 in. Once these samples were cut out from the center of the cores, they were mounted in epoxy so that they could be used with the SEM. The samples were then rough polished to expose the surface of the concrete followed by fine polishing using 9, 3, and 1 micron high performance polycrystalline diamond spray for the polishing media. The

samples were polished with the 9 micron spray for 8 hours, with the 3 micron spray for 4 hours, and with the 1 micron spray for another 4 hours. Before the samples were placed under the microscope, a gold sputter coating was applied to improve the conductivity of the sample and gain a better SEM image. A Quanta 600 FEG SEM device used in backscatter mode provided the images of the concrete samples. This electron microscope was provided for use by the electron microscope facility at Oregon State University.

2.3   Experimental Results and Discussion

2.3.1 Compressive Strength

Concrete cylinders that were cast alongside the slabs that they represented were tested for compressive strength at 28 and 90 days, according to ASTM C39. Compressive strength results are shown below in table 2.2.

Table 2.2: Compressive strengths of mixtures at 28 and 90 days.

	OPC-47	OPC-53	HPC-43
28 Day, MPa (psi)	20.9 (3031.3)	28.3 (4104.6)	24.6 (3567.9)
90 Day, MPa (psi)	28.3 (4104.6)	37.3 (5409.9)	33.1 (4800.7)

The OPC-53 slab had the highest strength gain after 90 days of curing. This is likely due to the slab containing no air-entrainment. The next highest compressive strength was HPC-43, which is the modern day concrete mixture, containing fly ash and silica fume. Due to the addition of fly ash, this concrete mixture will take a longer period of time to mature and gain strength. Eventually, it is expected that this slab type will have the highest compressive strength. The

OPC-47 slab contained air-entrainment and a higher w/cm ratio, therefore it had the lowest

compressive strength after 28 and 90 days. All of the concrete mixtures were below the design

strength of 5,000 psi at 28 days. This is likely due to low casting and curing temperatures of the

slabs and cylinders. The concrete mixtures were cast and wet cured outdoors in temperatures

fluctuating around 45°F (7.2°C).

**2.3.2 Concrete Cylinders Undergoing Freeze-Thaw in Scientemp F-T chamber**

Surface and bulk electrical resistivity of concrete cylinders that underwent 300 F-T cycles

following ASTM C666 Procedure B in a Scientemp F-T chamber were compared to additional

cylinders that were placed in the F-T environmental chamber with the reinforced concrete slabs.

The SR and the bulk resistivity of the cylinders are shown in Figures 2.2.

As illustrated in Figure 2.2, even before the F-T cycles, the electrical resistivity is well correlated

with the type of concrete tested. The lower the electrical resistivity, the lower the concrete

quality and thus more prone that concrete is to various durability problems. The lowest

resistivity before the F-T cycles was the OPC with w/cm ratio of 0.53 (OPC-53), which contained

no air entrainment (air content was about 1%). These concrete cylinders did not perform well

under F-T, as expected. All cylinders from this type of concrete began to deteriorate at about 72

F-T cycles and showed spalling at 108 F-T cycles. The surface of the entire cylinder of this type of

mixture came off in chunks and only the core of the cylinder remained exposing the aggregates,

as shown in Figure 2.3. The figure shows that for these mixtures the resistivity decreased rapidly

as the specimens deteriorated until the SR measurements could not be taken any more. The

performance of the other concrete mixtures was significantly better when compared to the

mixture with no air-entrainment. Based on SR measurements alone, it can be said that SR can be

an indicator of deterioration since the values decreased for the specimens that deteriorated

below 5 kΩ-cm, however, SR measurements should be combined with other tests to verify the

extent and type of deterioration.
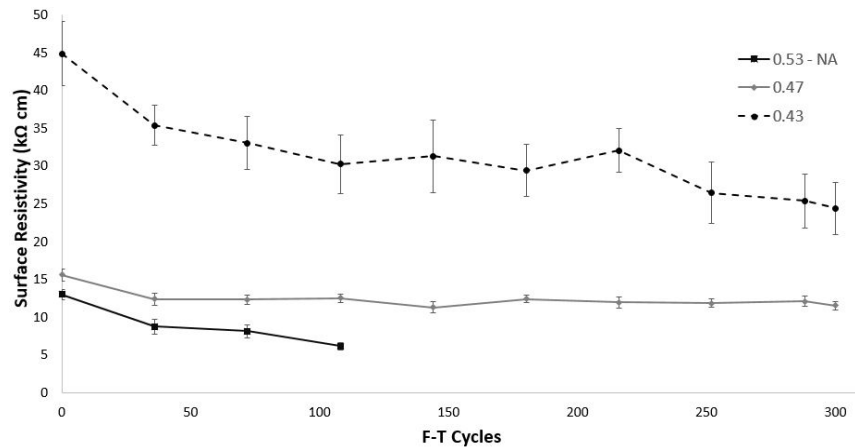
(a)
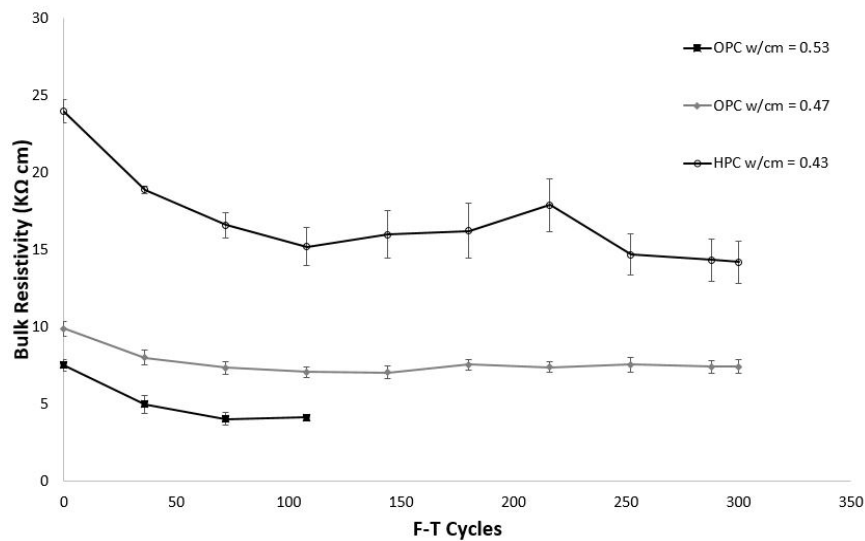
(b)

Figure 2.2: Surface (a) and bulk (b) resistivity taken on cylinders that underwent 300 F-T cycles according to ASTM C666 Procedure B. Three types of concrete were tested: 1) OPC concrete with w/c ratio of 0.53 and no air-entrainment, 2) an OPC concrete w/cm ratio of 0.47 with air-entrainment, and 3) a HPC with a w/cm ratio of 0.43 that contained silica fume, fly ash and air-entrainment. Measurements are normalized for 77°F (25 °C).

(a)   (b)
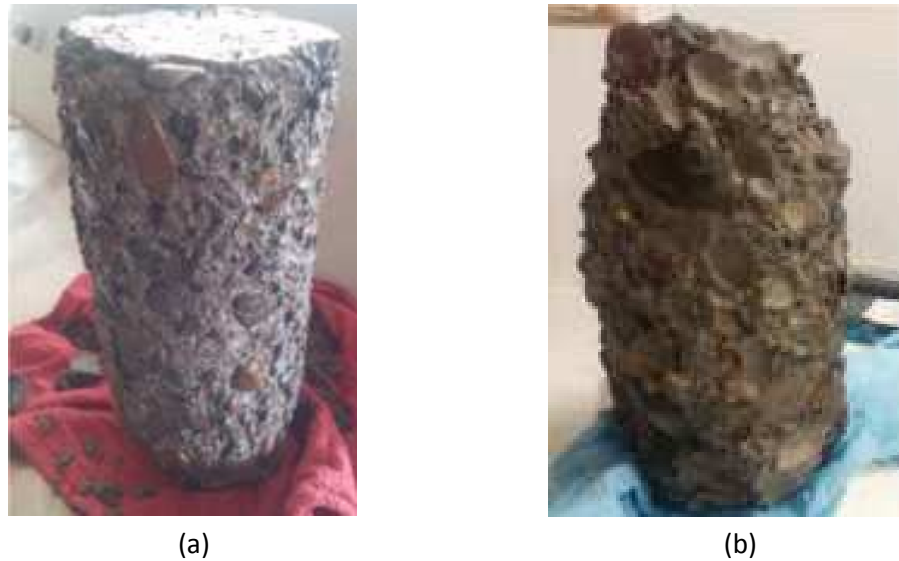
Figure 2.3: Deterioration in OPC-53 cylinders (without air entrainment) after (a) 72 F-T cycles, (b) 108 F-T cycles under ASTM C666 Procedure B protocol.

From visual inspection, the OPC-47 and HPC-43 specimens did not have any spalling or pop-outs.

The air content of the OPC-47 was 5% while the HPC-43 mixture with w/cm of 0.43 had an air

content of 2.5%. It was expected that the HPC-43 concrete would deteriorate at a faster rate than

the OPC-47 mixture due to a low percent of air content, however the specimens did not show any

visual signs of deterioration. Running an air void analysis following ASTM C457 would help

determine the true percent of air entrained in the matrix. This would help develop a better

understanding of why this concrete mixture performed well. The SR of the OPC-47 mixture with

w/cm ratio of 0.47 had a minimal change throughout the duration of the test. The SR

measurements decreased by about 2 kΩ-cm, where the SR of the HPC-43 mixture decreased by

over 15 kΩ-cm throughout the duration of the test. The bulk resistivity of the OPC-47 and HPC-43

mixtures also decreased by about 2 and 10 kΩ-cm, respectively. The general trend for all

measurements in both, bulk and SR seem to decrease over time. This is contrary to what it is expected. Resistivity should increase due to the micro-cracks that may form through F-T cycles when expansion of water molecules freeze inside the pores of the concrete matrix and create internal tensile forces. These micro cracks reduce the conductivity of the current flowing through the matrix, thus increasing resistivity. Because both figures follow the same trend for all three types of concrete and since electrical resistivity has been used in the concrete industry as an aid for durability related studies, a comparison between the two methods was made to validate the results obtained. This comparison is important to establish since the use of bulk resistivity test may not always be the most convenient since it requires taking cores or cylinders from a structure and this may not always be an option. Bulk and SR were plotted against each other and can be seen in Figure 2.4.
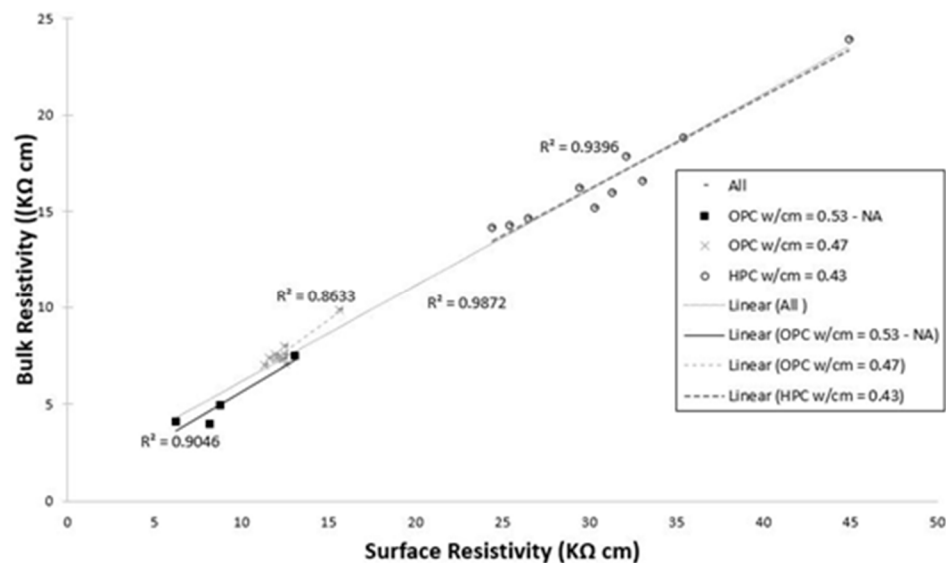

Figure 2.4: Linear regression relationship between surface resistivity and bulk resistivity taken on cylinders for each type of concrete.

Figure 2.4 shows the linear correlation coefficients (R^2) between bulk resistivity and SR. The coefficients are shown for each set of concrete samples as well as the overall group. The

coefficient for the concrete mixtures with w/cm ratio of 0.47, 0.53 and 0.43 are 0.863, 0.905 and

0.940 respectively. The correlation coefficient for the overall set of points is 0.987. These

coefficients support a strong correlation between bulk and SR and indicate that SR alone will

provide accurate information. The ratio of the theoretical bulk resistivity to the SR of the data

collected was calculated to be 0.576. A separate study done on the relationship between bulk

and SR supports this finding. Ghosh and Tran showed that the two techniques were well

correlated for different types of OPC, HPC, and control mixtures over longer periods of time

(Ghosh et al. 2015).

To further investigate the behavior of the cylinders going through F-T cycles and to better

understand the results obtained from the electrical resistivity measurements, the mass over

time and the relative dynamic modulus of the cylinders were monitored and it can be seen in

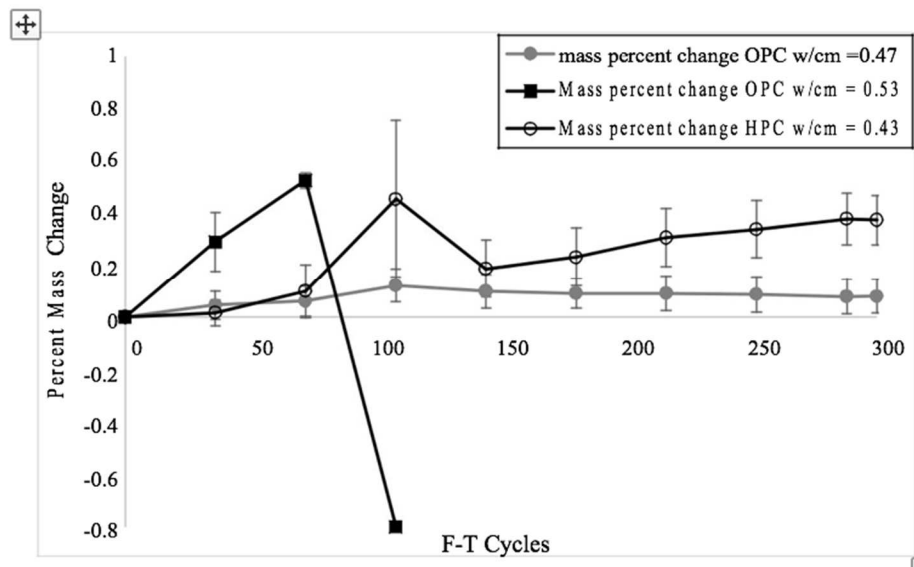Figure 2.5 and 2.6, respectively.

Figure 2.5: Percent mass change over time on cylinders that underwent 300 F-T cycles in the Scientemp chamber. Three types of concrete were tested: 1) OPC concrete with w/c ratio of 0.53 and no air-entrainment, 2) an OPC concrete w/cm ratio of 0.47 with air-entrainment and 3) a HPC with a w/cm ratio of 0.43 that contained silica fume, fly ash and air-entrainment.

Figure 2.5 shows that the three types of concrete increased in mass throughout the duration of the F-T cycles. The concrete mixture with no air (OPC w/cm = 0.53), had a steep increase in mass compared to the other two mixtures, and then deteriorated under freeze-thaw cycles rather rapidly due to spalling. This gain in mass could be explained by an increase in water content in the concrete matrix which caused expansion when the water froze to the point that it created the surface to spall off and separate from the aggregates. Literature shows contrary results when it comes to mass gain throughout the F-T cycles (Zhendi Wang 2015). In these freeze-thaw studies, the concrete decreases in mass. This is attributed to the paste on the surface separating from the aggregate due to the expansion of water when frozen. However, most studies rely on procedure A from ASTM C666 standard. Procedure A requires that the specimens undergo freezing and thawing submerged in water. Procedure B was used in this study, because it mimics the F-T cycles that the concrete slabs underwent. This provides a better understanding of what could be happening in the concrete matrix. While the F-T action is providing some damage to the microstructure of the concrete, the continuous cycles may also be driving water in the concrete further into the matrix during thawing phase, which is submerged in water, allowing for more water to be absorbed by the cracks that are newly developed. Since Procedure A of the standard requires full submersion of the samples, it does not provide the concrete surface to go through a wet and dry period, and it is well understood that wet and dry cycles provide an increase of moisture ingress into the concrete matrix. This gain in moisture also helps understand why the electrical resistivity is decreasing over time. The conductivity will increase with an increase in water available in the system. The relative dynamic modulus RDM of the cylinders was also monitored in this study and can be found in Figure 2.6.
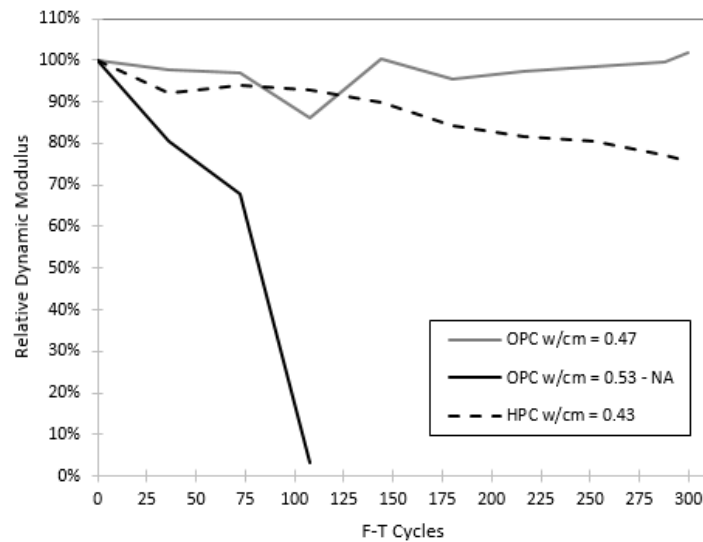
Figure 2.6: Relative dynamic modulus of elasticity on concrete cylinders after 300 F-T cycles in the in the Scientemp chamber.

The RDM of the air entrained specimens essentially experiences no decrease and indicates that these mixtures contain a properly air-entrained system and should be expected to have excellent freeze-thaw resistance in the field. This further underscores the disconnect between the measured air content of the 0.43 mixture and the high dosage rate, which further supports the need to evaluate the samples for hardened air void analysis. The non-air entrained mixture on the other hand performed poorly as was expected. The mixture experienced a very rapid decrease in RDM from the beginning and it was recorded in the first 36 cycles. After 108 cycles the mixture was completely disintegrated due to effects of freeze-thaw action.

2.3.3 Concrete Slabs under F-T Action in Environmental Chamber

Surface resistivity measurements were taken on reinforced concrete slabs that went through 28 ponding cycles of de-icer that contained 30% $MgCl_2$ solution with a corrosion inhibitor. These slabs were OPC-47 (w/cm = 0.47, with 5% air entrainment), OPC-53 (w/cm = 0.53, no air), and HPC-43 (w/cm = 0.43, with 2% air entrainment). The concrete slabs underwent ten sets of 60 F-T

cycles, which started after the 7th ponding cycle. A total of 600 F-T cycles were completed.

Figure 2.7 shows the SR measurements taken on the reinforced and unreinforced section of the

slabs. These figures show that the effect of the presence of reinforcement was negligible. SR

measurements were also taken on the control slabs, which were only ponded with water. The

control slabs did not go through F-T action. All SR measurements are corrected for temperature

and normalized to a 25°C reference temperature so that it did not have an effect on the

measurements.

(a)
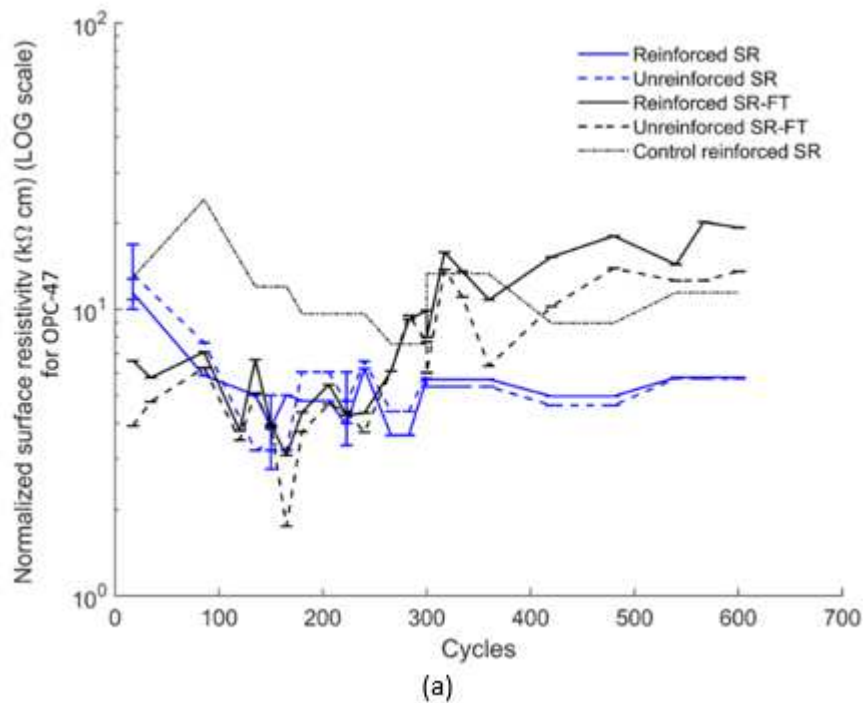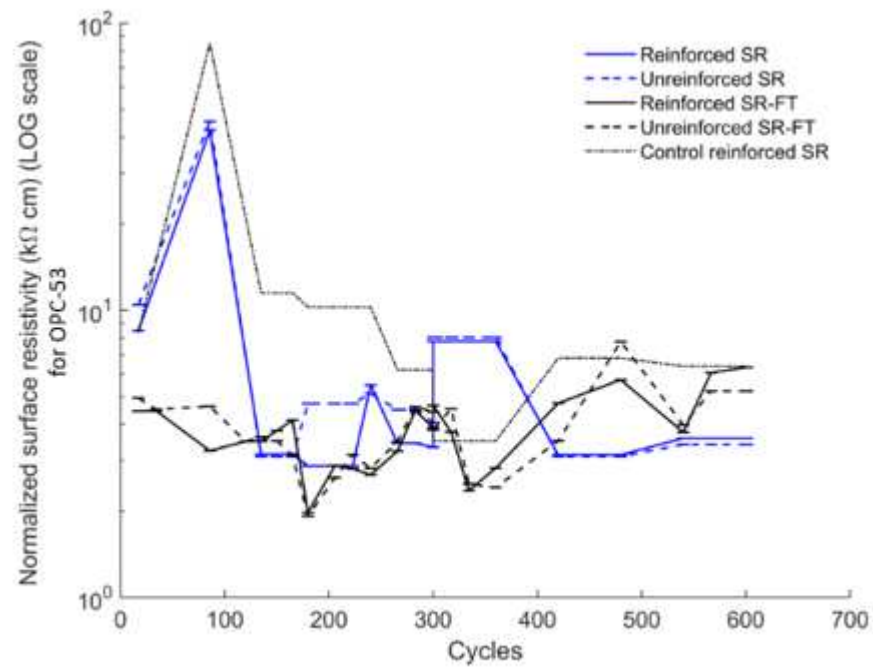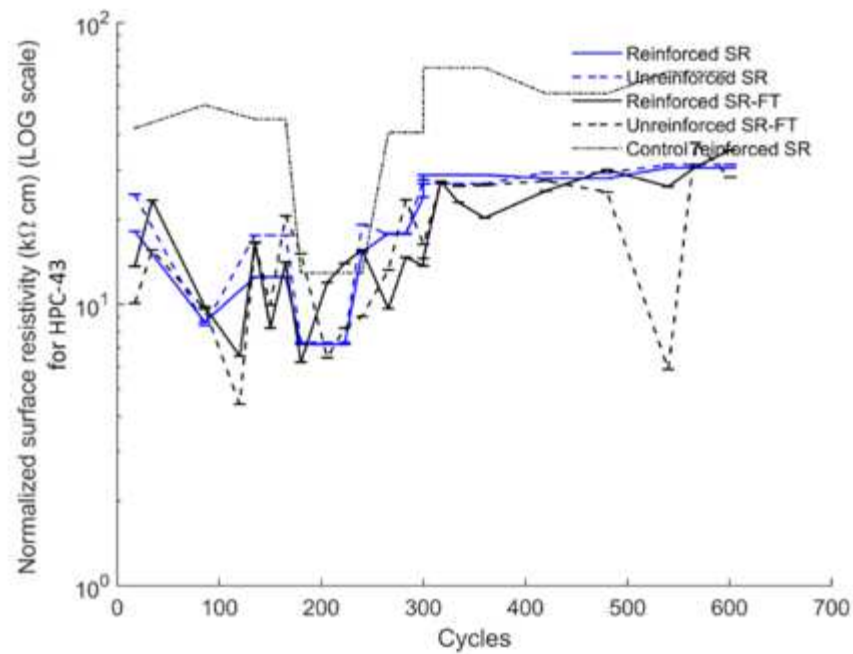
Figure 2.7: Surface resistivity values normalized to 25°C plotted against freeze-thaw cycles. The blue data represents slabs that were ponded with chlorides, but did not go through freeze-thaw. a) Resistivity values for OPC-47. b) Resistivity values for OPC-53. c) Resistivity values for HPC-43.

It can be seen from these plots that there is a significant difference between the control slabs and the chloride ponded slabs that did not go through freeze-thaw cycling. The control slabs consistently have a higher resistivity than the slabs that were ponded with the chloride deicing solution. This again demonstrates how chloride ingress decreases surface resistivity. OPC-47 (0.47 w/cm ratio) shows a decrease in SR between 0 to 300 F-T cycles. After 300 cycles the SR measurements begin to increase for the slabs that went through F-T cycles, and the SR measurements for the slabs that were chloride ponded but did not go through F-T cycles plateaued. This increase of SR for the F-T slabs may be due to micro-cracking and there no longer being moisture from the chloride ponding. This would be surprising since this slab mixture had a 5% air entrainment. These results were verified with SEM analysis, which is discussed in a following section. The OPC-53 slab shows a decrease in SR for the first 300 cycles. This is followed by an increase in SR for the F-T slabs. This result is similar to that of OPC-47, and likely occurred due to the same reasons. The SR measurements are overall smaller for OPC-53, which again demonstrates the relationship between SR and concrete permeability. OPC-53 had the highest w/cm ratio (0.53) and, therefore, had the least dense microstructure. OPC-53 showed extensive damage such as surface spalling, pop-outs, and visible corrosion of the reinforcement. Images of this damage can be found in the appendix. HPC-43 showed good resistance to F-T cycling. The SR increased after ponding stopped after 300 cycles, but the SR plateaued after that. The SR measurements between the reinforced and unreinforced sections are nearly identical. This validates the technique used to measure SR over reinforced areas of the concrete slabs.

2.3.4 Concrete Cylinders under F-T Action in Environmental Chamber

Figure 2.8 shows the SR measurements that were taken while the cylinders went through F-T cycles with the concrete slabs.
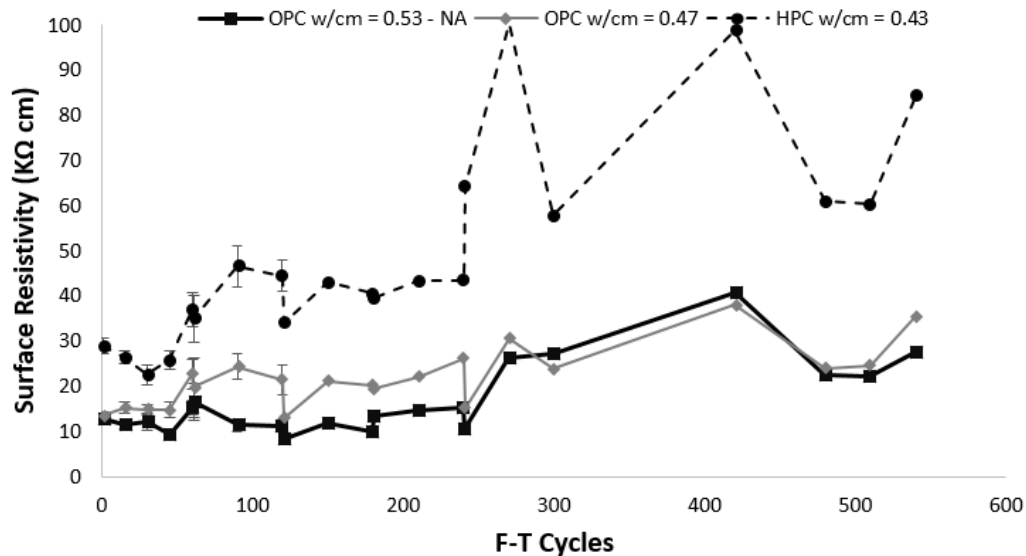
Figure 2.8: Surface resistivity taken on cylinders that underwent nine sets of 60 F-T cycles in a controlled environmental chamber. An OPC concrete with w/c ratio of 0.53 and no air-entrainment, an OPC concrete w/cm ratio of 0.47 with air-entrainment, and a HPC with a w/cm ratio of 0.43 that contained silica fume, fly ash and air-entrainment.

The figure shows an increase in SR measurements in the two types of concrete that had air entrainment, which is the opposite behavior of the measurements from the cylinders that followed ASTM C666 in a Scientemp F-T chamber. This can be attributed to the fact that the cylinders were never fully submerged under water like the ones in the Scientemp F-T chamber. The increase in SR could indicate microstructural damage due to F-T action. It can also be seen that the HPC mixture has much higher surface resistivity values then the other two. This shows that higher surface resistivity values are an indicator of better concrete quality.

2.3.5 Chloride Profiles

Figure 2.9 shows four chloride profiles for each type of concrete.
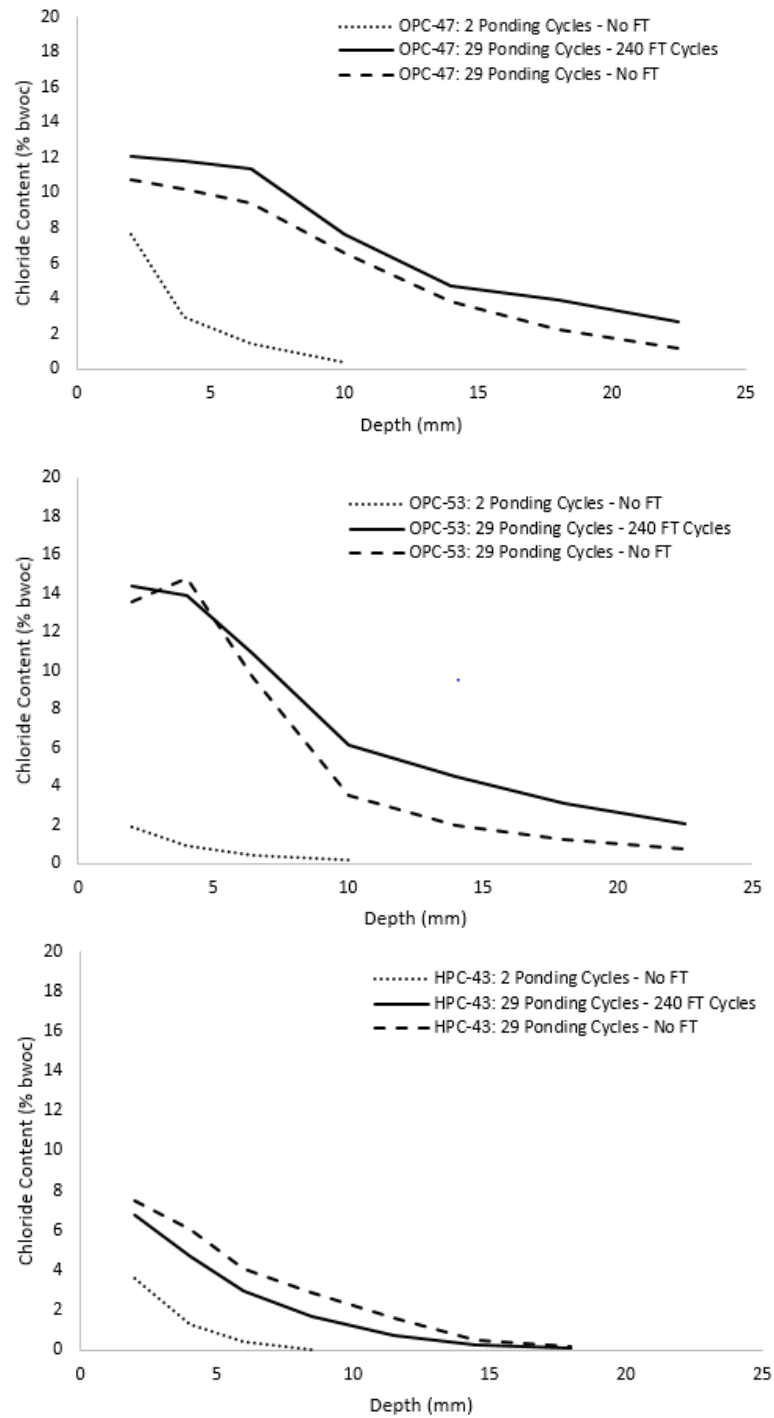
Figure 2.9: Two chloride profiles for three types of concrete are showing the effect of F-T action on chloride ingress. An OPC concrete with w/c ratio of 0.53 and no air-entrainment (OPC-53), an OPC concrete w/cm ratio of 0.47 with air-entrainment (OPC-47), and a HPC with a w/cm ratio of 0.43 (HPC-43).

The control slab, which is the slab that did not go through F-T action and only two ponding cycles, is shown with a dotted line. After 29 ponding cycles, chloride profiles were taken and are depicted with dashed lines. This shows the amount of chloride ingress after 29 ponding cycles. The freeze-thaw slabs underwent 240 F-T cycles, and were ponded for 29 cycles before chloride profiles were taken. These slabs are represented with a solid line and are labeled FT in the legend.

From Figure 2.9 it is seen that F-T action has an impact on the amount of chlorides penetrating the slab with no air entrainment (OPC-53). OPC-53 had severe deterioration on the surface of the concrete after the 240 F-T cycles. It also allowed for substantial chloride ingress. The OPC mixture with air-entrainment (OPC-47) also showed signs of deterioration with spalling and pop-outs on the surface of the slab. Although the slabs did not appear to be as deteriorated compared to the slab with no air-entrainment, the chloride profiles clearly indicate that the penetrability of the slab increased compared to the same slab that did not go through F-T action. The F-T action, on the other hand, did not affect the chloride ingress in the HPC slab (HPC-43). The HPC showed good resistance to chloride ingress due to the SCMs creating a dense, low permeable microstructure.

2.3.6 SEM Analysis

Results from the surface resistivity measurements of the freeze-thaw slabs showed an interesting increase in resistivity once chloride ponding stopped and freeze-thaw cycles continued. This behavior was especially evident in the OPC-47 slabs. It was suspected that this increase in surface resistivity was the result of freeze-thaw damage in the concrete. To verify this, cores were taken from the OPC-47 slab for observation in a scanning electron microscope.

Samples were taken at a 1-inch and 2.5-inch depth for both the chloride ponded slab and the slab that went through both chloride ponding and freeze-thaw cycling. Images of these slab samples are shown in figure 2.10 below.
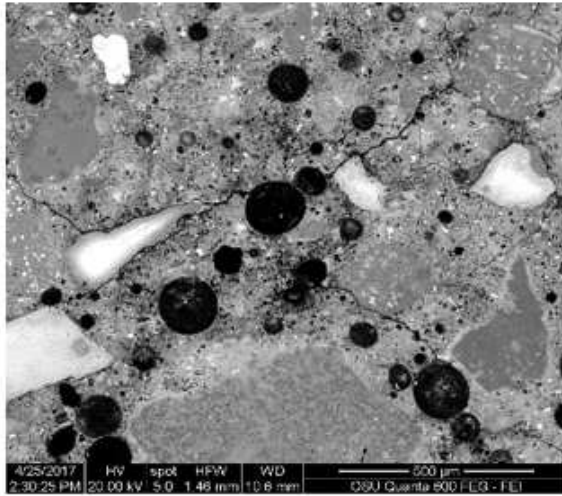
Cl and No FT (500 um)
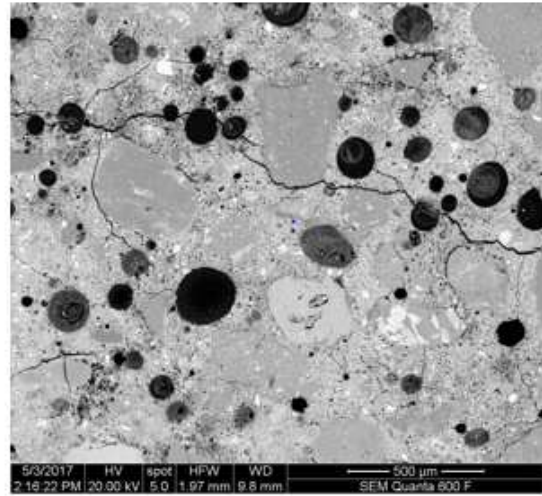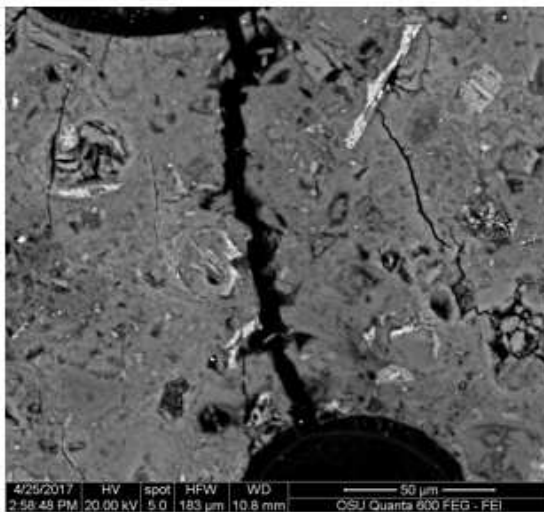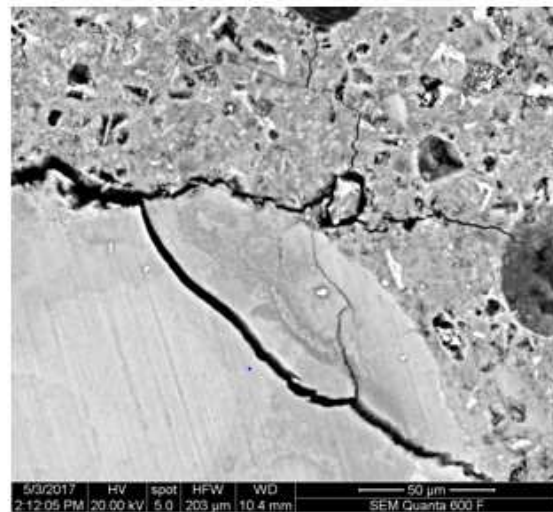
Cl and FT (500 um)

Cl and No FT (50 um)

Cl and FT (50 um)

(a)
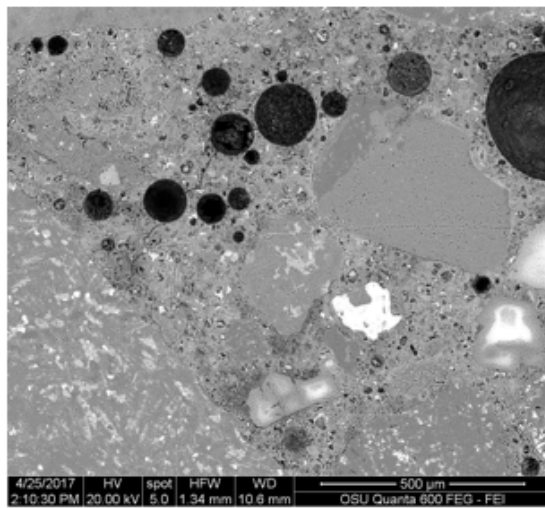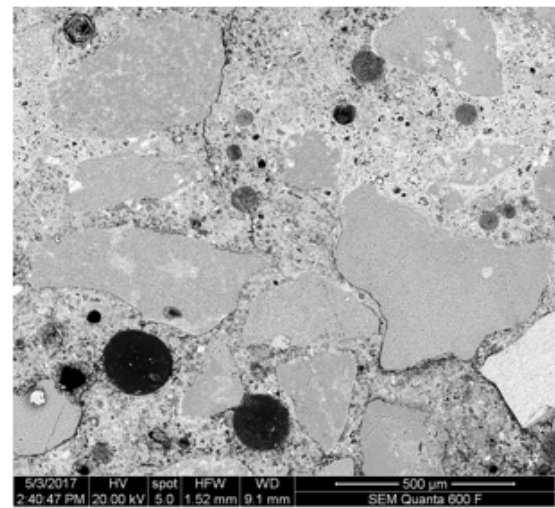
Cl and No FT (500 um)
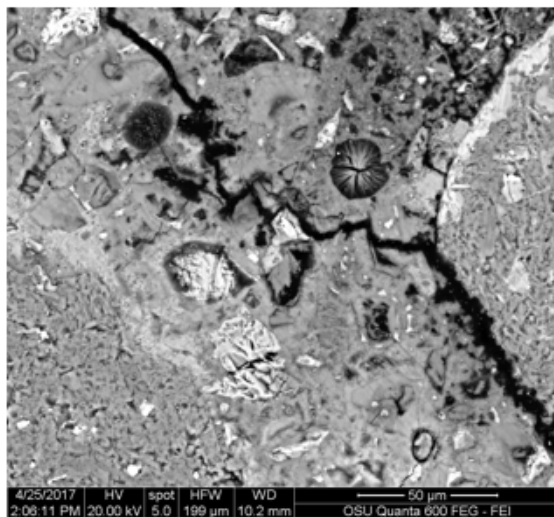
Cl and FT (500 um)

Cl and No FT (50 um)
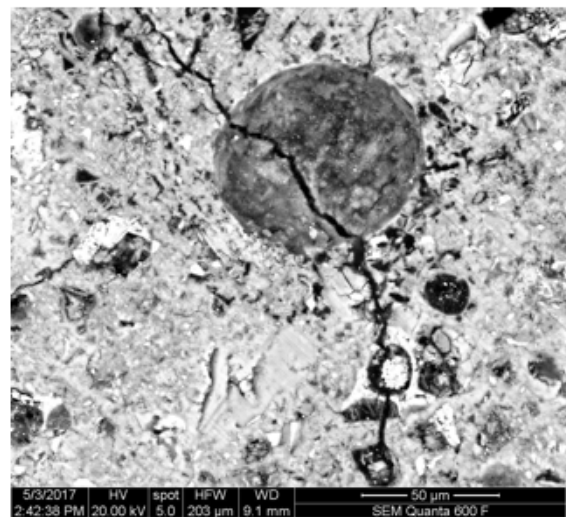
Cl and FT (50 um)

(b)

Figure 2.10: SEM images at 500 and 50-micron magnification for the OPC-47 slab at a) 1-inch depth and b) 2.5-inch depth

The OPC-47 slab contained 5% entrained air. These air voids can be seen as the dark spots in the SEM images. These entrained air voids should have mitigated freeze-thaw damage, but some micro cracking can be seen, especially near the surface of the slab at the 1-inch depth. Although

both slabs show cracking, the slab that went through both chloride ponding and freeze-thaw cycling qualitatively showed more cracking, including cracks through aggregates, which is a sign of freeze-thaw damage rather than the result of damage during sample preparation. Cracking through aggregates was not observed in the samples that only went through chloride ponding. This damage may contribute to an increase in surface resistivity, but not to the extent as was seen in the surface resistivity measurements for the OPC-47 slab. The increased surface resistivity may be due to a combination of freeze-thaw damage and moisture loss. The chloride ponding was stopped after 300 freeze-thaw cycles, after which the F-T slabs remained in a dry environment inside the environmental chamber for the second set of 300 cycles. During this dry period is when the increase in surface resistivity was seen.

2.4 Conclusions

This study provided data that helps further the understanding of the effects of magnesium chloride deicing solutions and freeze-thaw cycling on the surface resistivity of reinforced concrete. These reinforced slabs were cast to represent different eras of bridge decks, ranging from the 1960s to modern day. The exposure regime consisted of ambient temperature chloride ponding in wet/dry cycles and then a period of freeze-thaw cycling in an environmental chamber. Concrete cylinders were also cast alongside the slabs and were put through freeze-thaw cycling. A set of cylinders went through 300 freeze-thaw cycles, in accordance with ASTM C666, while another set was placed alongside the slabs undergoing 600 freeze-thaw cycles in the large environmental chamber. Routine surface resistivity measurements were taken throughout the entire study period. The experimental results yielded the following conclusions:

- It is recommended that if bulk or surface resistivity are to be used congruently with ASTM C666, to use Procedure A in the standard, to eliminate the effects that wet and

dry exposure conditions used in Procedure B may have on the specimens and measurements.

- Bulk and SR resistivity measurements taken on the cylinders showed a linear relationship which is in line with previous studies that compared the two testing methods.

- F-T action had a significant negative impact on the rate of chloride ingress on the slabs. The concrete slab with no air entrainment had severe deterioration and allowed for substantial chloride ingress after 29 ponding cycles and 240 F-T cycles.

- Although the OPC-47 mixture with air-entrainment visually did not appear to be as deteriorated compared to the slab with no air-entrainment, the chloride profiles clearly indicate that the penetrability of the slab increased compared to the same slab that did not go through F-T action.

- The HPC-43 mixture performed well under F-T action. An increase in transport of chlorides was not evident and cannot be seen in the chloride profiles, however, it would be beneficial in this study to do a hardened air void analysis on this mixture to verify the air void content since the excellent performance of this mixture under F-T action was not expected due to the low fresh concrete air content measured.

- It appears that freeze-thaw damage caused an increase in micro-cracking, especially near the surface of the OPC-47 slab. This along with the possible decrease in moisture content caused the surface resistivity of OPC-47 to increase after ponding was stopped, but freeze-thaw cycles continued.

2.5 References

ACI Committee 222R-01: (2001), Protection of Metals in Concrete against Corrosion. Reapproved 2010.

Alonso, C., C. Andrade, J. A. González. (1988). "Relation between resistivity and corrosion rate of reinforcements in carbonated mortar made with several cement types." Cement and Concrete Research 18(5): 687-698.

Andrade, C., C. Alonso (2004). "Test methods for on-site corrosion rate measurement of steel reinforcement in concrete by means of the polarization resistance method." Materials and Structures 37(9): 623-643.

Andrade, C., M. Prieto, P. Tanner, F. Tavares, R. d'Andrea. (2013). "Testing and modelling chloride penetration into concrete." Construction and Building Materials 39: 9-18.

ASTM A615-15a Standard Specification for Deformed and Plain Carbon-Steel Bars for Concrete Reinforcement. (2015). ASTM International, West Conshohocken, PA.

ASTM C1152-12 Standard test method for acid-soluble chloride in mortar and concrete. (2012). ASTM International, West Conshohocken, PA.

ASTM C1218/C1218M-15 Standard Test Method for Water-Soluble Chloride in Mortar and Concrete. (2015). ASTM International, West Conshohocken, PA.

ASTM C1556-11a Standard test method for determining the apparent chloride diffusion coefficient of cementitious mixtures by bulk design. (2012). ASTM International, West Conshohocken, PA.

ASTM C215-08 Standard Test Method for Fundamental Transverse, Longitudinal, and Torsional Resonant Frequencies of Concrete Specimens. (2014). ASTM International, West Conshohocken, PA.

ASTM C39-15 Standard Test Method for Compressive Strength of Cylindrical Concrete Specimens. (2015). ASTM International, West Conshohocken, PA.

ASTM C457-12 Standard Test Method for Microscopical Determination of Parameters of the Air-Void System in Hardened Concrete. (2012). ASTM International, West Conshohocken, PA.

ASTM C597-09 Standard test method for pulse velocity through concrete. (2010). ASTM International, West Conshohocken, PA. 102

ASTM C666/C666M-15 Standard test method for resistance of concrete to rapid freezing and thawing. (2015). ASTM International, West Conshohocken, PA.

ASTM WK37880 New Test Method for Measuring the Surfae Resistivity of Hardened Concrete Using the Wenner Four-Electrode Method. (2014). ASTM International, West Conshohocken, PA.

Backus, J., D. McPolin, A. Long, M. Basheer, N. Holmes. (2013). "Exposure of mortars to cyclic chloride ingress and carbonation." Advances in Cement Research 25(1): 3-11.

Basheer, P., P. Gilleece, A. Long, W. Mc Carter. (2002). "Monitoring electrical resistance of concretes containing alternative cementitious materials to assess their resistance to chloride penetration." Cement and Concrete Composites 24(5): 437-449.

Blackburn, R., D. Amsler, K. Bauer (2004). Snow removal and ice control technology. Sixth International Symposium on Snow Removal and Ice Control Technology, Transportation Research Board of the National Academies, Spokane, WA.

Brencich, A., G. Cassini, D. Pera, G. Riotto (2013). "Calibration and Reliability of the Rebound (Schmidt) Hammer Test." Civil Engineering and Architecture 1(3): 66-78.

Conciatori, D, H. Sadouki, E. Brühwiler. (2008). "Capillary suction and diffusion model for chloride ingress into concrete." Cement and Concrete Research 38(12): 1401-1408.

Concrete materials and methods of concrete construction/Test methods and standard practices for concrete. (2009). Canadian Standards Association, Toronto, ON.

Florida method of test for concrete resistivity as an electrical indicator of its permeability. (2004). Department of Transportation Florida, FL, USA.

Garzon, A. J., J. Sanchez, C. Andrade, N. Rebolledo, E. Menéndez, J. Fullea. (2014). "Modification of four point method to measure the concrete electrical resistivity in presence of reinforcing bars." Cement and Concrete Composites 53: 249-257.

Ghosh, P., Q. Tran. (2015). "Correlation Between Bulk and Surface Resistivity of Concrete." International Journal of Concrete Structures and Materials 9(1): 119-132.

Gowers, K. R., S. G. Millard. (1999). "Measurement of concrete resistivity for assessment of corrosion severity of steel using Wenner technique." ACI Materials Journal 96(5): 536-541.

Gowers, K., S. Millard. (1999). "Measurement of concrete resistivity for assessment of corrosion severity of steel using Wenner technique." ACI Materials Journal 96(5): 536-541. 103

Gucunski, N., I. Arezoo; F. Romero, S. Zanarian, D. Yuan, H. Wiggenhauser, P. Shokouhi, A. Taffe, D. Kutrubes. (2013). Nondestructive testing to identify concrete bridge deck deterioration. Transportation Research Board. Washington, D.C.

Hamilton, H., A. J. Boyd, E. Vivas, M. Bergin. (2007). Permeability of concrete - comparison on conductivity and diffusion methods. No. 00026899. Gainesville, FL, University of Florida.

Hong, K. (1999). Cyclic wetting and drying and its effects on chloride ingress in concrete. National Library of Canada, Ottawa, ON.

Hooton, R.D., A. Shahroodi, E. Karkar. (2012). Evaluating concretes using rapid test methods for fluid penetration resistance, ACI Fall Convention in Toronto, presented in the Emerging Technologies (Part 2); available at aci-int.org.

Hope, B., A. Ip. (1987). "Chloride Corrosion Threshold in Concrete." Materials Journal 84(4): 306-314.

Huang, J., W. Shaowei, J. Chaudhari, S. Soltesz, X. Shi. (2014). Deicer Effect on Concrete Bridge Decks: Practitioners Perspective and a Method of Developing Exposure Maps. Transportation Research Board Annual Meeting: 1-13. Washington, DC.

Hussain, R. R. (2011). "Effect of moisture variation on oxygen consumption rate of corroding steel in chloride contaminated concrete." Cement and Concrete Composites 33(1): 154-161.

Hussain, S., E.,Rasheeduzzafar, A. Almusallam, A. S. Algahtani. (1995). "Factors affecting threshold chloride for reinforcement corrosion in concrete." Cement and Concrete Research 25(7): 1543-1555.

Jackson, L. (2013). "Surface resistivity test evaluation as an Indicator of the Chloride Permeability of Concrete." Tech brief. Publication no. FHWA-HRT-13-024, McLean, VA.

Jaegermann, C. (1990). "Effect of water-cement ratio and curing on chloride penetration into concrete exposed to Mediterranean Sea climate." Materials Journal 87(4): 333-339.

Ji, Y., T. Zan, Y. Yuan. (2009). "Chloride Ion Ingress in Concrete Exposed to a Cyclic Wetting and Drying Environment." American Society of Agricultural and Biological Engineers 52(1): 239-245.

Jiang, J. H. (2013). "Relationship of moisture content with temperature and relative humidity in concrete." Magazine of Concrete Research 65(11): 685-692. 104

Jianhong, C., B. Dylan, J. Frank, H. Dryver. (2008). Concrete bridge deck condition assessment with automated multisensor techniques. Bridge Maintenance, Safety Management, Health Monitoring and Informatics. Burlington, VT, Taylor & Francis.

Julio-Betancourt, J. A. (2009). Effect of de-icer and anti-icer chemicals on the durability microstructure, and properties of cement-based materials. Graduate of Civil Engineering. Toronto, Canada, University of Toronto. Doctor of Philosophy: 854 pp.

Kessler, R., R. Powers, M. Paredes. (2005). Resistivity measurements of water saturated concrete as an indicator of permeability. NACE International.

Khalim, A. R., D. Sagar, M. D. Kumruzzaman, A. S. M. Z. Hasan. (2011). "Combination of nondestructive evaluations for reliable assessment of bridge deck." Facta universitatis - series: Architecture and Civil Engineering 9(1): 11-22.

Koch, G.H., M. Brongers, N. Thompson, Y. Virmani, J. Payer. (2002). "Corrosion Costs and Preventive Strategies in the United States." FHWA-RD-01-156 (Final Report): 773 pp.

Kosmatka, S. H., M. L. Wilson. (2011). "Design and Control of Concrete Mixtures." 15th Edition: 444, Portland Cement Association, Washington, D.C.

Kulik, D., T. Wagner, S.Dmytrieva, G. Kosakowski, F. Hingerl, K. Chudnenko, U. Berner. (2013). "GEM-Selektor geochemical modeling package: revised algorithm and GEMS3K numerical kernel for coupled simulation codes." Computational Geosciences 17(1): 1-24.

Lingen, R. T. (1998). "Concrete in coastal structures." 301. London, U.K., Thomas Telford Limited.

López, W., J. A. González. (1993). "Influence of the degree of pore saturation on the resistivity of concrete and the corrosion rate of steel reinforcement." Cement and Concrete Research 23(2): 368-376.

Lord, B. N. (1988). "Program to reduce deicing chemical usage." Federal Highway Administration: 13 pp., McLean, VA.

Martin-Perez, B. (1999). "Service life modelling of R.C. highway structures exposed to chlorides." Ph.D. thesis: 168 pp.

Method of test for determination of electrical resistivity of concrete. (2013). Ministry of Transportation Ontario, Toronto, ON.

Morales, M. T. (2015). Experimental investigation of the effects of embedded rebar, cracks, chloride ingress and corrosion on electrical resistivity measurements of reinforced concrete: 174 pp. 105

Morris, W., A. Vico, M. Vázquez. (2004). "Chloride induced corrosion of reinforcing steel evaluated by concrete resistivity measurements." Electrochimica Acta 49(25): 4447-4453.

Mussato, B. T., O. K. Gepraegs and G. Farnden (2004). "Relative effects of sodium chloride and magnesium chloride 0n reinforced concrete: state of the art." Transportation research record. (1866): 59-66.

Mutale, L. (2014). An investigation into the relationship between surface concrete resistivity and chloride conductivity tests: 105 pp.

Neville, A. M. (1981). Properties of Concrete. Pitman Publising Limited, London, United Kingdon.

Neville, A. M. (1996). Properties of Concrete: Fourth Edition. 844. Hoboken, NJ, Wiley.

ODOT. (2008). Oregon Standard and Specifications for Construction, Oregon Department of Transportation: 814 pp.

Paul Scherrer Institute. (2013). "GEMS: Gibbs Energy Minimization Software for Geochemical Modeling." From http://gems.web.psi.ch.

Presuel-Moreno, F., Y. Liu, M. Paredes (2009). Understanding The Effect Of Rebar Presence And/Or Multilayered Concrete Resistivity On The Apparent Surface Resistivity Measured Via The Four-Point Wenner Method. Corrosion Conference 2009. Atlanta, GA, NACE International.

Qiang, Y., A. Katrien, S. Caijun, S. Geert De. (2008). Effect of temperature on transport of chloride ions in concrete. Concrete Repair, Rehabilitation and Retrofitting II, CRC Press: 159-160.

Rupnow, T., I. Patrick. (2011). Evaluation of surface resistivity measurements as an alternative to the rapid chloride permeability test for quality assurance and acceptance. Louisiana Transportation Research Center: 68 pp.

Ryu, D, W. Ko, T. Noguchi. (2011). "Effects of simulated environmental conditions on the internal relative humidity and relative moisture content distribution of exposed concrete." Cement and Concrete Composites 33(1): 142-153.

Sadowski, L. (2013). "Methodology for assessing the probabilty of corrosion in concrete structures on the basis of half-cell potential and concrete resistivity measurements." Scientific World Journal. 2013: 8. Article ID 714501.

Salehi, M. (2013). Numerical investigation of the effects of cracking and embedded reinforcement on surface concrete resistivity measurements using Wenner probe. Civil 106 and Environmental Engineering. Ottawa, Ontario, Carleton University. Master of Applied Science in Civil Engineering: 155 pp.

Sengul, O., O. E. Gjorv (2009). "Effect of embedded steel on electrical resistivity measurements on concrete structures." ACI Materials Journal 106-M02 (January/February 2009): 11-18.

Sengul, O., O. E. Gjorv. (2008). "Electrical resistivity measurements for quality control during concrete construction." ACI Materials Journal 105(6): 541-547.

Shariati, M., H. Sulong, M. Arabnejad, P. Shafigh, H. Sinaei. (2011). "Assessing the strength of reinforced concrete structures through ultrasonic pulse velocity and Schmidt Rebound Hammer tests." Scientific Research and Essays 6 (1): 213-220.

Shi, X. (2011). Understanding and mitigating effects of chloride deicer exposure on concrete. Western Transportation Institute. Bozeman, MT, Montana State Univerity.

Shi, X., L. Yajun, M. Mooney, M. Berry, L. Fay, A. B. Leonard. (2010). Effect of chloride-based deicers on reinforced concrete structures. Bozeman, MT, Montana State University: 1-74.

Shi, X., Y. Li., S. Jungwirth, Y. Fang, N. Seeley, E. Jackson. (2013). "Identification and laboratory assessment if best practices to protect DOT equipment from the corrosive effect of chemical deicers." 217 pp.

Sirivivatnanon, V., W. A. Thomas, K. Waye. (2012). Determination of free chlorides in aggregates and concrete. Australian Journal of Structural Engineering. 151-158.

Song, H., V. Saraswathy. (2007). "Corrosion monitoring of reinforced concrete structures - a review." International Journal of Electrochemical Science 2(2007):1-28.

Standard method of test for surface resistivity indication of concrete's ability to resist chloride ion penetration. (2011). American Association of State Highway and Transportation Officials, Washington DC.

Sutter, L., K Peterson, G. Julio-Betancourt, D. Hooton, T. V. Dam, k. Smith. The Deleterious Chemical Effects of Concentrated Deicing Solutions on Portland Cement Concrete. (2008). SD2002-01. Federal Highway Administration: 1-198, Houghton, MI.

Swanstrom, J., T. Rogers, G. Bowling, S. Tuttle (2013). ODOT bridge inspection program manual 2013. Oregon Department of Transportation: 1-381, OR.

Wagner, T., D. A. Kulik ,F. F. Hingerl, S. V. Dmytrieva. (2012). "Gem-Selektor geochemical modeling package: TSolmod library and data interface for multicomponent phase models." Canadian Mineralogist 50(5): 1173-1195. 107

Wang, Q. Z., L. Wang, Y. Yao, K. Li. (2015). "Electrical resistivity of cement pastes undergoing cyclic freeze-thaw action." Journal of Materials in Civil Engineering. 27(1).

Wang, Z., Q. Zeng, L. Wang, Y. Yao, K. Li. (2014). "Effect of moisture content on freeze–thaw behavior of cement paste by electrical resistance measurements." Journal of Materials Science. 49(12): 4305-4314.

Weydert, R., C. Gehlen. (1999). "Electrolytic resistivity of cover concrete: Relevance, measurement and interpretation." Proceedings of the 8th International Conference on Durability of Building Materials and Components. 409-419. NRC Research Press, Vancouver,

3 Second Manuscript

Experimental Investigation of the Effects of Corrosion on Ductile Iron

Silas Shields[1], O. Burkan Isgor[1], Jason H. Ideker[1], Pratik Murkute[1]

Abstract: Ductile iron pipes have been used mostly in water transmission since the 1950s when it replaced the traditional cast iron pipes, due to ductile iron's superior strength properties. More recently, ductile iron pipe has been considered for local power transmission structures. Power utility companies are considering it as a replacement for traditional timber poles. While there are benefits to using ductile iron (such as its strength and sustainability), ductile iron has been reported to be vulnerable to pitting corrosion due to the nodular structure of its free graphite. In this research, ductile iron was tested for its susceptibility to corrosion using a salt fog chamber and electrochemical methods. In the salt fog chamber, samples went through an accelerated corrosion process. After the samples had corroded, mass loss measurements were taken and corrosion rates were calculated. Tensile strength tests were also done before and after corrosion. Stainless steel samples were tested alongside the ductile iron for comparison. In addition to the corrosion chamber and strength tests, electrochemical tests were done on both ductile iron and stainless steel samples in the form of open circuit potential monitoring, electrochemical impedance spectroscopy and cyclic polarization to characterize the corrosion kinetics of ductile iron. In the salt fog tests, stainless steel samples showed almost no change in mass loss and tensile strength after corrosion. Ductile iron samples, on the other hand, had a corrosion rate of approximately 52.6 mpy (1.3 mmy), and a 10 ksi (69 MPa) decrease in ultimate tensile strength after corrosion. Open circuit potential results showed that the ductile iron samples had a higher potential, and thus, lower corrosion resistance than the

stainless steel samples. Similarly, electrochemical impedance spectroscopy showed that stainless steel had a greater impedance than ductile iron, which correlates to increased corrosion resistance. Analysis of cyclic polarization curves showed that the ductile iron samples had much higher corrosion rates than stainless steel samples. However, the corrosion products which formed on the ductile iron samples appeared to be protective in nature. This indicates that ductile iron may have good field performance.

Keywords: Corrosion, Ductile Iron, Stainless Steel, Tensile Test, Electrochemical Tests

_____

[1]Oregon State University, School of Civil and Construction Engineering, Corvallis, Oregon, USA

3.1 Introduction

Pitting corrosion of ductile iron pipe is a significant issue that has been evident since its development and use for water transmission in the 1950s. Today, it is used more than its predecessor, cast iron pipe, and is being considered for use by the power transmission industry. Because of ductile iron's ductility, strength properties, and the fact that it is manufactured using recycled iron, it has become a desirable material in the industry.

Ductile iron was first developed in 1948, and was considered to be one of the most significant breakthroughs in metallurgy of the century (Carpenter 2010). Ductile iron is stronger, more ductile, and can withstand higher impacts than cast iron (Carpenter 2010). DIP is an iron alloy containing approximately 3% carbon and .035% magnesium, and has a unique, nodular microstructure. The reason ductile iron performs better than cast iron is due to its unique microstructure. The addition of magnesium causes the free graphite to form nodular deposits rather than flakes. Figure 3.1 compares the microstructure of cast iron to that of ductile iron.
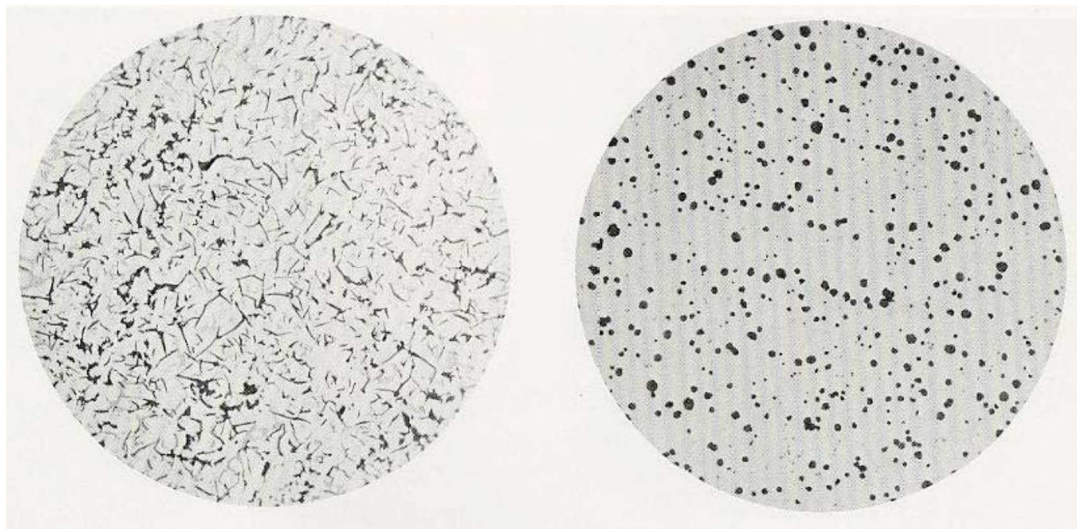

Figure 3.1: Microstructure of cast iron (left) and ductile iron (right) (Carpenter, Ralph 2010).

The figure clearly shows the difference in graphite formation. The cast iron has very flaky graphite, while the ductile iron graphite forms in nodes or spheroids. While this nodular graphite structure gives the ductile iron increased strength and ductility, it is also responsible for ductile iron's propensity towards pitting corrosion.

There are two main forms of corrosion that tend to occur on ductile iron pipe (Uhlig and Revie 2008). The first form is graphitic corrosion. Graphitic corrosion occurs when iron is selectively leached from the alloy, leaving behind the graphite. This leaching is caused by the electrochemical potential difference between iron and graphite. Iron is anodic to graphite, therefore, it is the element that leaches out. The graphite that is left behind is not as strong on its own. This leads to a loss in strength of ductile iron.

Pitting corrosion is the other common type of corrosion that can occur on ductile iron pipe. Pitting corrosion occurs when corrosion is localized in a small anodic area (Marcus 2012). These anodic areas can be caused by alloying metals or microstructural defects. In the case of ductile iron, the graphite nodes are less active than the adjacent iron. Because of this, local action cells develop and the iron will preferentially corrode. This forms pit-like deterioration on the surface of the ductile iron.

Pitting corrosion is a significant problem when dealing with water transmission pipes. In the 1960's the thinnest 12 inch cast iron pipe used in water transmission was 0.54 inches thick (Szeliga 2012). The thinnest 12 inch ductile iron pipe at the time was 0.31 inches thick (Szeliga 2012). The industry at the time believed that since ductile iron had higher strength and ductility that it could be made thinner than the cast iron pipe, while still maintaining the required durability. It was not well understood, however, the effects of pitting corrosion. The thinner pipe allows for pitting corrosion to penetrate through the walls of the pipe much faster. As a

result, since the 1960's there have been many documented cases of ductile iron pipe failing faster than cast iron pipe (Szeliga 2012). This type of corrosion is also a concern if ductile iron pipe is to be used for power transmission since the corroded pits will expose wiring to the outside environment.

Characterization of ductile iron and its corrosion properties is necessary for understanding how it may perform in the field. Many studies on ductile iron pipe have been focused on examining DIP that has already been in use (Szeliga 2012; Kleiner et al. 2013). In one study DIP samples were taken from existing water utilities in four different North American locations (Kleiner et al. 2013). The pitting population as well as the soil property data from each of the locations was analyzed. It was found that the soil property data did not improve their ability to make pitting corrosion property predictions. These studies may be good for observing how DIP performs in those specific environments, but they do not give a general understanding of ductile iron corrosion.

Controlled laboratory studies are critical for understanding how ductile iron behaves in different types of environments. Oke and Ukoba did this type of study on ductile iron over a 6 month period (Oke and Ukoba 2013a). DIP samples were exposed to different corrosion environments to observe and compare corrosion rates. Initial results showed that samples exposed to a salty (sodium chloride) environment had the highest weight loss. The samples in the air-conditioned environment had no corrosion. The ductile iron samples exposed to the outside and sodium chloride environments had the greatest weight loss. Unfortunately, specific environmental conditions such as temperature and relative humidity were not given this paper. This makes it difficult to apply the data to other environmental locations.

This research study will provide more detailed data on how ductile iron performs in a controlled corrosion chamber environment. Characterization through electrochemical tests will also be done so that a better understanding of ductile iron can be developed. Finally, mechanical strength tests will be done to compare the strength and ductility changes before and after corrosion. These experiments will provide information for making decisions on how to use ductile iron pipe and further study it in future research projects.

3.2   Materials and Methods

3.2.1   General Information

The experimental procedure for this study involved accelerated corrosion in a salt fog chamber, mechanical tests, and benchtop electrochemical tests on ductile iron and stainless steel (control) samples. The material properties of ductile iron samples match the properties of the utility poles used by power utility companies.

3.2.2   Materials

The materials used in this study were ordered from commercial sources. The materials received were cut into proper dimensions, and preparation such as polishing was done as described in this following section. The approximate chemical composition for grade 80-55-06 ductile iron and 316 stainless steel is shown in table 3.1.

Table 3.1: Chemical composition of grade 80-55-06 ductile iron and 316 stainless steel (ASTM A536) and (ASTM A240).

	C	Si	Mn	P	Mg	Cr	Ni	Mo	Fe
316 Stainless Steel, % wt.	0.08	0.75	2.0	0.045	2.0	16.0 – 18.0	10.0 – 14.0	2.0 – 3.0	Bal.
80-55-06 Ductile Iron, % wt.	3.0 - 6.0	2.3 - 2.9	0.3 - 0.6	<0.06	0.03 – 0.055				Bal.

3.2.2.1 Ductile Iron

The ductile iron used in this study had a reported yield strength of 55,000 psi (379.2 MPa), and was cast in accordance with ASTM A536 (2017). This standard ensures that all the graphite in the ductile iron is in its characteristic spheroidal shape. Table 3.2 shows the mechanical requirements for different grades of ductile iron. Based on the reported yield strength, the ductile iron samples used in this study are grade 80-55-06.

Table 3.2: Tensile requirements for different grades of ductile cast iron (ASTM A536).

	Grade 60-40-18	Grade 65-45-12	Grade 80-55-06	Grade 100-70-03	Grade 120-90-02
Tensile strength, min, psi (MPa)	60,000 (413.7)	65,000 (448.2)	80,000 (551.6)	100,000 (689.5)	120,000 (827.4)
Yield strength, min, psi (MPa)	40,000 (275.8)	45,000 (310.3)	55,000 (379.2)	70,000 (482.6)	90,000 (620.5)
Elongation in 2 in. min, %	18	12	6.0	3.0	2.0

3.2.2.2 Stainless Steel

The stainless steel used in this study was a highly corrosion-resistant 316 stainless steel with a

yield strength of 30,000 psi (206.8 MPa). This steel was cast according to ASTM A240 (2017) and

contains 16-18% Chromium and 10-14% Nickel. Table 3.3 shows the mechanical properties of

type 316 stainless steel.

Table 3.3: Mechanical properties of stainless steel type 316 (ASTM A240).

UNS Designation	Type	Tensile Strength , min (ksi)	Tensile Strength , min (MPa)	Yield Strength , min (ksi)	Yield Strength , min (MPa)	Elongation 2 in., min %
S31600	316	75	515	30	205	40

3.2.2.3 Sample Preparation

For this study, three different sample types were used based on their dimensions and surface

preparation to satisfy the specific requirements of corrosion chamber, mechanical, and

electrochemical testing.

3.2.2.3.1 Corrosion Chamber Test Samples

The sample dimensions used in the corrosion chamber were decided based on ease of

measurement, observation, and placement in the corrosion chamber. The stainless steel

received commercially were 6x6 in. plates with a .25 in. (6.35 mm) thickness. These samples

were cut into .75 in. (19.1 mm) wide strips. The ductile iron samples came as .75 in. (19.1 mm)

thick cylindrical rods that had a 6 in. (152.4 mm) diameter. These samples were cut across the

top every .25 (6.35 mm) inches so that .25 in. (6.35 mm) thick strips with a 6 in. (152.4 mm)

length were obtained. Figure 3.2 shows these samples after they were cut.
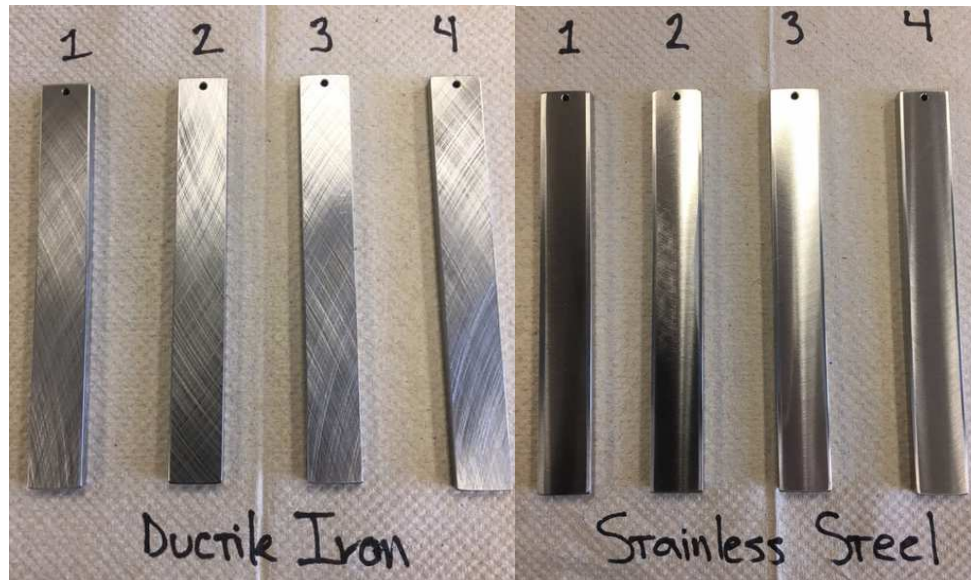
Figure 3.2: Samples after being cut and prepared for accelerated corrosion testing. Each bar is 6 in. (152.4 mm) in length.

After the samples were cut, the surface of each sample was cleaned with ethanol to remove any

grease or other contaminates that were applied during the manufacturing and cutting process.

3.2.2.3.2 Mechanical Test Samples

For tensile strength tests, coupons needed to be made out of the samples. The coupons were

made according to the dimensions described in ASTM E8 (2016). The sub-size was used for the

coupons in this study. Figure 3.3 shows a picture of the coupon specimens used in this study.

Figure 3.3: Coupons used for tensile strength tests. Each coupon is 6 in. (152.4 mm) in length.

Table 3.4 shows the dimensions of each coupon used in this study (ASTM E8).

Table 3.4: Dimensions of sub-size coupons (ASTM E8).

	Gauge Length, in. (mm)	Width, in. (mm)	Thickness, in. (mm)	Radius of fillet, in. (mm)	Overall length, in. (mm)	Length of Grip Section, in. (mm)	Width of Grip Section, in. (mm)
Sub-size coupon	1.00 (25.4)	0.50 (12.7)	0.250 (6.4)	0.250 (6.35)	4 (101.6)	1.25 (31.8)	0.375 (9.5)

The length of each coupon was cut to between 6 and 7 inches. This is within the standard since the specified overall length is a minimum value.

3.2.2.3.3 Electrochemical Test Samples

Circular discs (diameter 0.6 in. (15 mm) and thickness 0.1 in. (3 mm)) of ductile iron and stainless steel were used for all the electrochemical tests. The samples were polished with 1200 grade silicon carbide paper followed by cloth polishing up to 0.03 μm with alumina suspension. Post

sample preparation, samples were ultrasonically cleaned in iso-propyl alcohol. Figure 3.4 shows

the samples before being tested.

Figure 3.4: Stainless steel (Left) and ductile iron (right) samples for electrochemical tests. Both samples have a diameter of 0.6 in. (15 mm).

3.2.3   Test Methods

This study utilized several test methods to better characterize ductile iron. These tests included

accelerated corrosion tests, tensile strength tests, and electrochemical tests.

3.2.3.1 Corrosion Chamber Testing

Accelerated corrosion tests were performed to observe the mass loss of the ductile iron

compared to the mass loss of the stainless steel. Tests were done in accordance with ASTM

B117 (2016).

3.2.3.1.1 Corrosion Chamber Exposure Regime

The corrosion chamber used in this study was manufactured by Q-Fog and is capable of both

continuous and cyclic exposure regimes. The Q-Fog chamber consists of a fog chamber, salt

solution reservoir, heating device, and a system for using compressed air to atomize the solution

so that it gets sprayed as a fog into the chamber. The air pressure and position of the nozzle can

be adjusted so that the salt fog is evenly distributed inside the chamber. To calibrate the salt fog

distribution, graduated cylinders with funnels are placed throughout the chamber. The fog

chamber is then run for a period of time and at the end the cylinders are checked to ensure that

they have equal amounts of salt solution in them. If they are uneven, the nozzle tip can be

redirected, or the spray pressure adjusted accordingly. This process is iterated until an even

distribution is achieved. The optimal spray pressure for this study was found to be 15 psi. Figure

3.5 shows the Q-Fog corrosion chamber.

Figure 3.5: Q-Fog CCT 600 corrosion chamber.

Though it is well understood that the continuous salt fog test specified by ASTM B117 (2016)

does not correlate to natural environment performance, it is often used to produce relative

corrosion resistance information (ASTM B117). The data gathered by this test method cannot be

extrapolated to make predictions about a metal's performance, but it can provide a good

comparison of one metal's susceptibility to corrosion to another. For this study, samples in the

corrosion chamber were exposed to a continuous salt fog spray and temperature of 95°

Fahrenheit (35° Celsius), specified by ASTM B117 (2016). The salt solution was a 5% sodium

chloride solution. The solution was periodically checked to ensure the pH remained in a range of

6.5 to 7.2. Specimens in the chamber were oriented so that they did not drip solution on other

specimens. Figure 3.6 below shows the specimen arrangement inside the chamber.
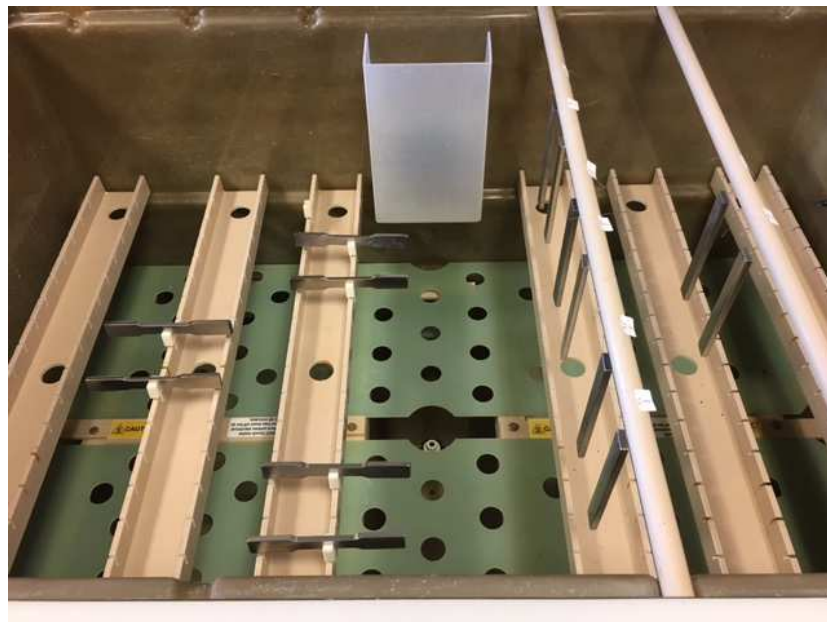

Figure 3.6: Sample placement inside corrosion chamber.

ASTM B117 is a continuous fog test, so the salt fog never ceases throughout the test period. The

test period for this study was 10 days (240 hours). The chamber was only stopped to periodically

examine the specimens.

3.2.3.1.2 Mass Loss and Corrosion Rate Determination

To quantify the corrosion damage after exposure in the corrosion chamber, mass loss

measurements were taken for the ductile iron samples. Samples were weighed prior to the

corrosion test and then again after the corrosion products were cleaned after the test. ASTM

G1-03 was used as a guideline for cleaning the samples after the corrosion test. Mechanical

cleaning with a wire brush was used as the cleaning method for this study. The corrosion

products were scrubbed off and then weighed to determine mass loss of the base ductile iron

material. Cleaning with the wire brush was repeated until the mass loss stabilized at a particular

value and no more corrosion products remained to be scrubbed away. Once the mass loss was

found, the corrosion rate could be determined, using equation 3.1 (ASTM C1617-15).

$$Corrosion\ Rate(CR) = \frac{Mass\ Loss(g) * K}{Alloy\ Density(g/cm^3) * Exposed\ Area(A) * Exposure\ Time(hr)} \qquad (3.1)$$

Where K is a factor that accounts for the desired corrosion rate units. The alloy density is 7.2

g/cm^3. The exposed area is the surface area of the ductile iron samples, and its units depend on

the desired corrosion rate units. The exposure time for this study was 240 hours.

3.2.3.2 Mechanical Testing

Tensile testing of the ductile iron and stainless steel coupons were done according to ASTM E8.

An Instron testing system was used to load the samples, and get stress and strain data. The

samples were loaded at a rate of .05 in/min during the elastic phase. The elastic phase was

determined to end when the strain reached .5%. At this point the load rate increased to 0.2 in/min and remained there until failure.

3.2.3.3 Electrochemical Testing

All the electrochemical tests were performed using Gamry 3000- potentiostat /galvanostat / FRA. The working electrode was the test specimen, counter electrode was the porous graphite electrode and the reference electrode used was standard calomel electrode (SCE). The metal surface area exposed to the electrolyte was 0.18 in^2 (1.15 cm^2). The test samples tested in triplicates to validate the reproducibility of the results. Electrochemical tests constituted of 2 cycles of Initial open circuit potential (OCP) monitoring followed by electrochemical impedance spectroscopy (EIS) and at the end of 2 cycles, the tests were concluded with a cyclic polarization (CP) scan. The electrochemical cell setup is illustrated in figure 3.7.
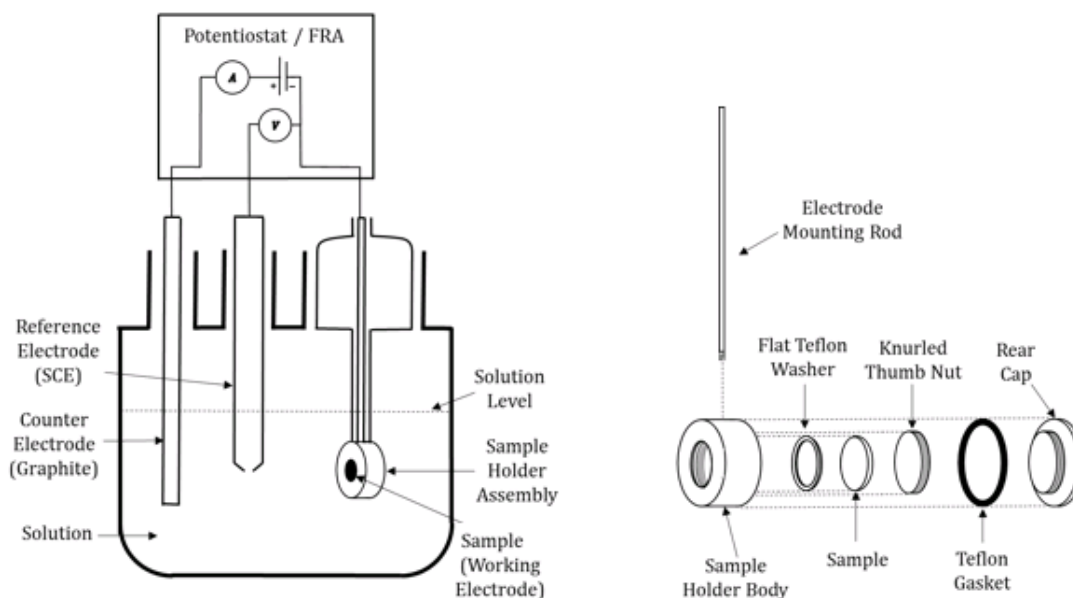
Figure 3.7: Schematic of the experimental setup used for all electrochemical testing (Williamson and Isgor 2016).

All the OCP measurements were made for a period of 1-hour post sample immersion in electrolyte, followed by EIS with an Initial start frequency of 5×10^4 Hz, final frequency of 1×10^{-2} Hz and AC voltage of 5 mV rms at low noise setting. After 2 cycles of OCP-EIS, single CP scan with forward-backward scan rates of 0.166 mV/s, initial-final potential of -0.5 V w.r.t OCP, apex potential of +1 V w.r.t OCP and apex current of 25 mA/cm^2.

3.3   Experimental Results and Discussion

3.3.1   Corrosion Chamber Testing

After 10 days (240 hours) of continuous exposure to 5% sodium chloride spray fog the ductile iron samples showed significant corrosion damage. Conversely, the stainless steel samples showed almost no visible corrosion. Figure 3.8 shows the ductile iron and stainless steel samples after the corrosion chamber test.

Figure 3.8: Ductile iron and stainless steel samples after corrosion (6-inch sample length).

Corrosion products began to develop on the ductile iron samples after just 2 hours of testing. After 4 days of testing the entire sample was completely covered in rust. The stainless steel samples have no visible rusting except for very small amounts on the sides of the sample. Typically when ductile iron corrodes in visible pits, however, the pitting corrosion is so severe on these sample that the corrosion appears uniform. After the ductile iron samples were cleaned the local action corrosion can be more easily seen. Figure 3.9 shows this.
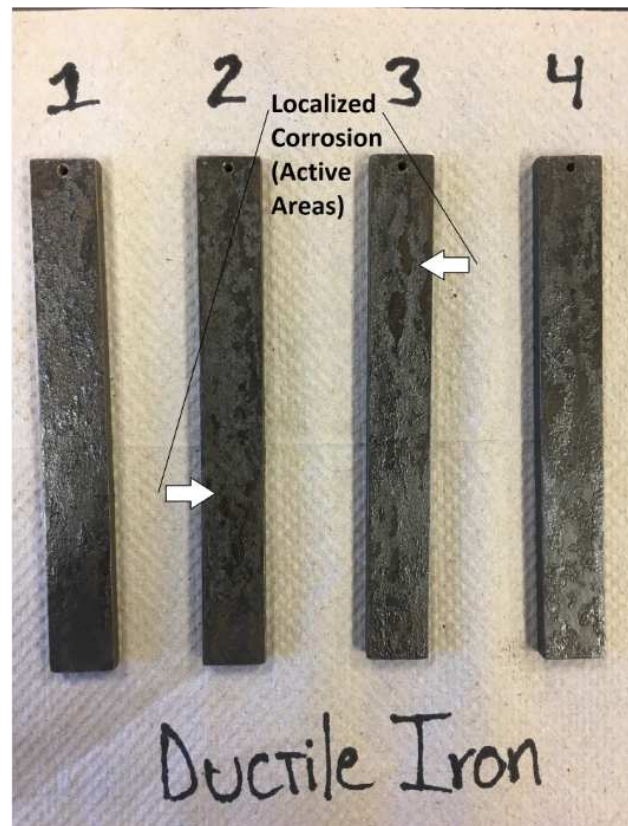
Figure 3.9: Cleaned ductile iron samples after corrosion test.

It can be seen that there are more active areas where the corrosion reaction removed more of the ductile iron material. The samples have pits and ridges across the entire surface area.

3.3.1.1 Mass Loss and Corrosion Rate

The stainless steel samples did not show any corrosion or have mass loss so the corrosion rate was not calculated. The ductile iron samples were repeatedly cleaned until a stable mass loss was found. The mass loss determination can be seen in figure 3.10.

Ductile Iron Mass Loss
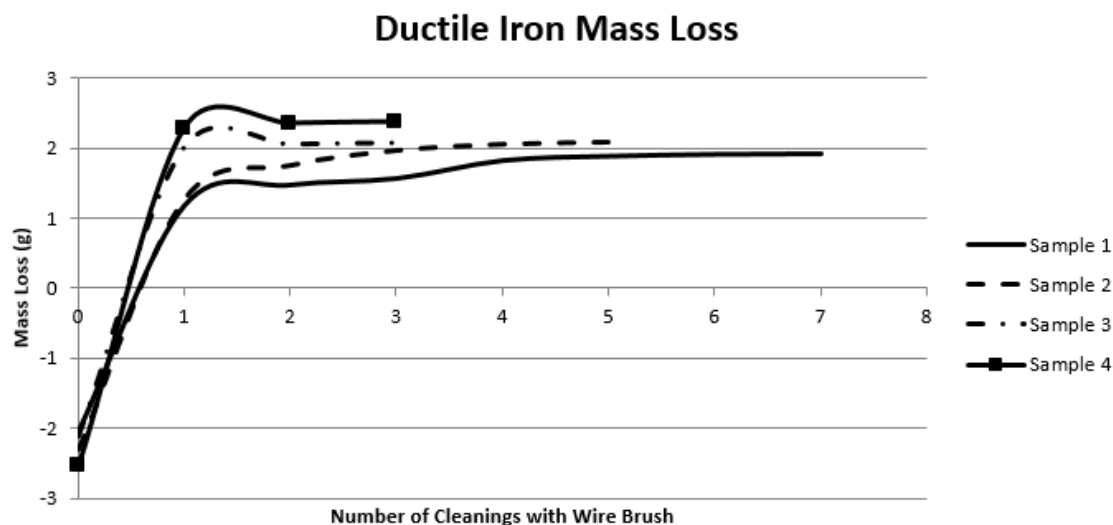
Figure 3.10: Mass loss determination

The samples began to stabilize at a mass loss of about 2 grams. Table 3.5 below shows the exact

measurements taken for each sample.

Table 3.5: Mass loss measurements for ductile iron samples.

Sample	Mass Loss (g)
1	1.908
2	2.081
3	2.062
4	2.373
Average	2.106

These results show a greater mass loss than what was found in the study by Oke and Ukoba. The

ductile iron exposed to a sodium chloride environment in their study had a mass loss 0f 0.8201

grams after 30 days of exposure (Oke and Ukoba 2013). This is expected since the sample size

used in this study was likely different from the sample size used in the Oke and Ukoba, which

was not reported. The salt concentration and temperature of the test was also not reported for

that study so it is likely that the conditions were not as severe. They could have used a lower salt

concentration solution, or tested at a lower temperature.

The corrosion rates were calculated from the measured mass loss for each sample. Table 3.6

shows the results.

Table 3.6: Corrosion rates for ductile iron samples.

Sample	Corrosion Rate (mpy)	Corrosion Rate (mmy)
1	47.6	1.2
2	52.0	1.3
3	51.5	1.3
4	59.3	1.5
Average	52.6	1.3

Corrosion rates were calculated in both mils per year (one mil = one-thousandth of an inch) and

millimeters per year. The exposure conditions inside the chamber were very aggressive, thus the

corrosion rates were considerably high. At this rate of corrosion, there would be about 2.5

inches (65 mm) of metal loss after 50 years. This accelerated corrosion does not correlate with

real world exposure, therefore, electrochemical tests may give a better representation of what

the actual corrosion rate may be for ductile iron exposed to a salty environment.

3.3.2   Mechanical Testing

The tensile strengths of all samples are shown in table 3.7. The data from these test results

show that corrosion did cause a decrease in the tensile strength of ductile iron. There is about a

10 ksi difference in tensile strength between the control samples and the corroded samples. The

ductile iron showed a much more brittle failure than the stainless steel samples. This is due to

the increased carbon content in ductile iron compared to stainless steel. There is very little

variation in performance for the stainless steel samples. The corrosion samples appear to have

not lost any of their mechanical performance. All stainless steel samples exceed the minimum

tensile strength of 75 ksi prescribed by ASTM A240 (ASTM A240).

Table 3.7: Tensile strengths of stainless steel and ductile iron samples.

Sample	Tensile Strength, ksi (MPa)			
	Stainless Steel		Ductile Iron	
	Before Corrosion	After Corrosion	Before Corrosion	After Corrosion
1	95.1 (656)	87.7 (605)	87 (600)	81 (558)
2	91.7 (632)	93.6 (645)	88 (606)	81 (558)
3	91.5 (631)	88.9 (613)	97.4 (672)	82.4 (568)

The ductile iron samples also had tensile strengths above the ASTM standard minimum of 80 ksi

(552 MPa) even after corrosion. This shows that although ductile iron corrodes very easily, it

may still maintain an acceptable tensile strength.

3.3.3   Electrochemical Tests

Figure 3.11 shows the open circuit measurement for stainless steel and ductile iron for 2 hours.

Ductile Iron has a higher open circuit potential (OCP) than stainless steel, implying lower

corrosion resistance of ductile iron. OCP of ductile iron decreases over a period of time, whereas

for stainless steel the potential increases in the positive direction and then stabilizes. This is

strong evidence, that ductile iron has higher corrosion susceptibility and tendency when compared to stainless steel.

Figures 3.12 and 3.13 show impedance and phase angle results of the EIS tests performed on ductile iron and stainless steel in 5% wt. NaCl solution. At lower AC frequencies (0.10 - 0.01 Hz), stainless steel manifests higher impedance in the range $10^5 – 10^6$ ohms, whereas ductile iron impedance is in the range of 103-104 ohms. Higher impedance indicates greater corrosion resistance. This can be attributed to chromium presence in stainless steel, which aids in passive film formation in near neutral solutions, thereby increasing the corrosion resistance. In addition, EIS 2 shows higher impedance than EIS 1, and this is justified, since, over a period of time, the passive film/ corrosion product forming on the metal surface acts as a barrier to charge transfer and thereby increasing the double layer thickness forming at the electrolyte-metal interface.
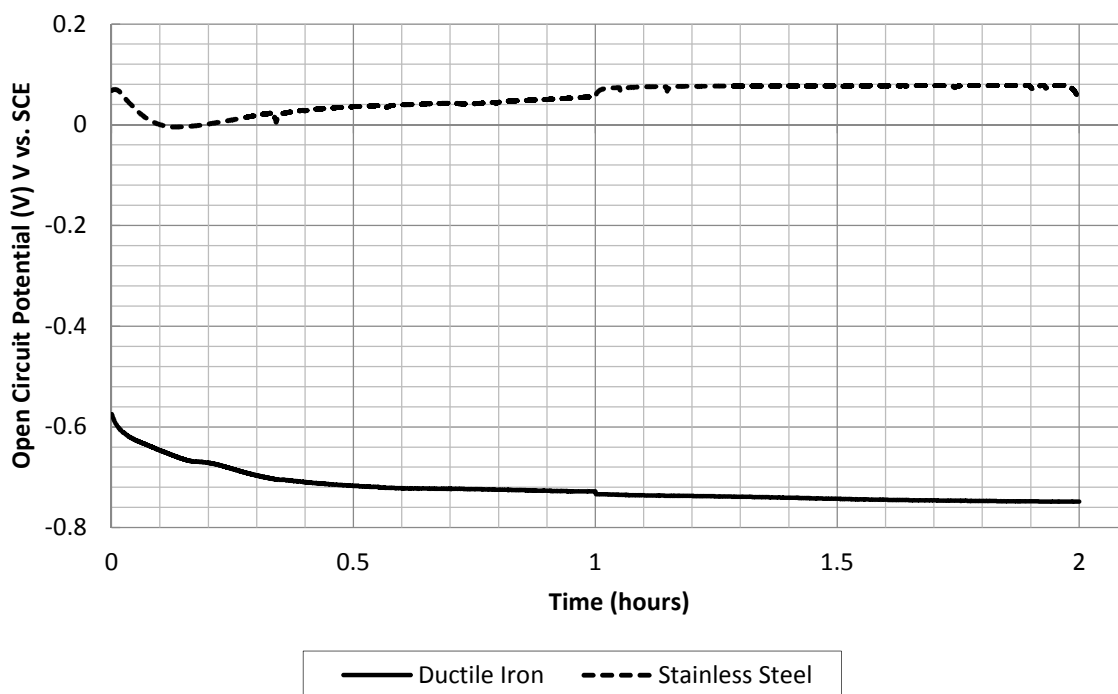
Figure 3.11: Open circuit potentials for ductile iron and stainless steel

As shown in figure 3.13, in mid frequency range, the phase angle for both the alloys approaches a phase angle of -90°, which indicates double layer capacitance at the electrolyte-metal interface. Since negative phase angle is related to the capacitive behavior, stainless steel shows this capacitive behavior over a wider range of frequency as compared to ductile iron, in addition stainless steel has higher negative angle (~84°) than ductile iron (~68°). Also for both the alloys, EIS 2 shows higher negative angle than EIS 1, which is again a confirmation of the results obtained from impedance plots. It can be safely concluded from the impedance and phase angle plots that stainless steel is more resistant to corrosion than ductile iron. The phase angle value for ductile iron, however, indicates that the corrosion product forming is somewhat protective in nature.
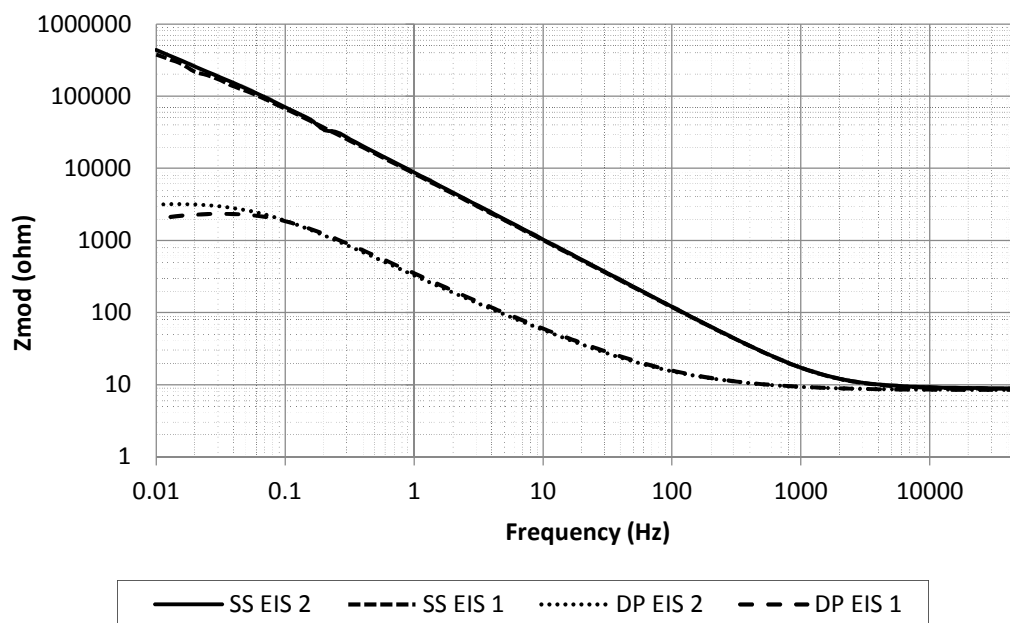
Figure 2.12: Impedance plots for ductile iron and stainless steel
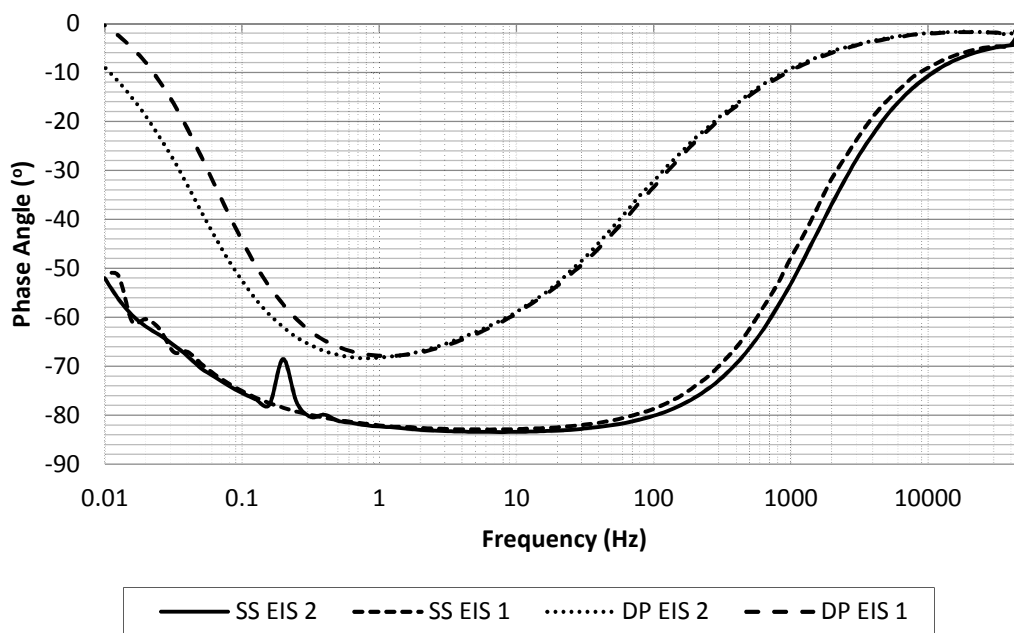

Figure 3.13: Phase angle plots for ductile iron and stainless steel

To validate the EIS results and quantitatively assess corrosion rates, cyclic polarization (CP) tests

were performed after OCP-EIS cycles. Figure 3.14 shows the CP plots for stainless steel and ductile

iron. It is evident that the corrosion current (I_{corr}) for ductile iron (in range of 0.1- 0.01µA) is 2

orders of magnitude less than stainless steel (in range of 1-10 μA). Corroding potential (E_{corr}) for the stainless steel is much higher than ductile iron. The protective nature of the rust forming on the surface decided by the inflection point in the reverse loop as compared to the original E_{oc}. Analyzing the reverse loop of CP plots for both alloys, we can conclude that the nature of rust forming on the ductile iron is protective in nature with respect to the soluble rust products forming on the stainless steel. The corrosion rates were calculated via tafel extrapolation and the corroding currents, potentials, tafel slopes, and corrosion rates for ductile iron and stainless steels are presented in table 3.8. The corrosion rate obtained from tafel extrapolation, quantitatively confirms that the stainless steel is more corrosion resistant than ductile iron in 5 % wt. NaCl solution, which were qualitatively confirmed from the OCP and EIS measurements as well.

The onset of pitting in stainless steel is clearly evident in Figure 3.15 whereas a specific pitting potential for ductile iron cannot be pointed out from the CP plots. Ductile iron shows active behavior in 5 wt. % NaCl solution, with signs of continuous dissolution on anodic arm of CP plots. For stainless steel, pits formation (unstable pits) initiates at the potentials as low as 163 mV, but stable pit forms at about 280 mV which is still higher than ductile iron corroding potential. Figure 3.15 (a) and (b), shows the photographs of the stainless steel and ductile iron samples after electrochemical tests. Ductile iron is homogenously covered with blackish-brown rust layer on the exposed area, whereas wide and deep pits are visible on stainless steel surface.

Table 3.8: Cyclic polarization data for ductile iron and stainless steel.

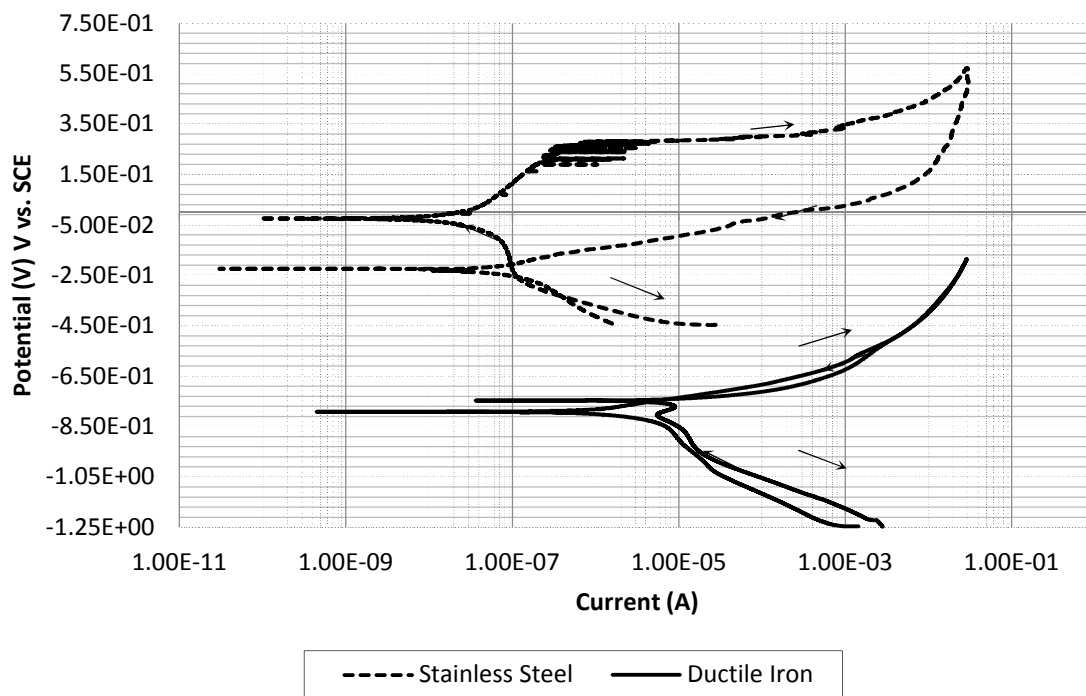| Material	I_{corr} (µA)	E_{corr} (mV)	β_A (V/decades)	β_C (V/decades)	Corrosion Rate (mpy)
Ductile Iron	1.85	-791	0.0869	0.0853	0.7344
Stainless Steel	0.023	-25	1.351	2.0	0.072

Figure 4.14: Cyclic polarization curves for ductile iron and stainless steel.
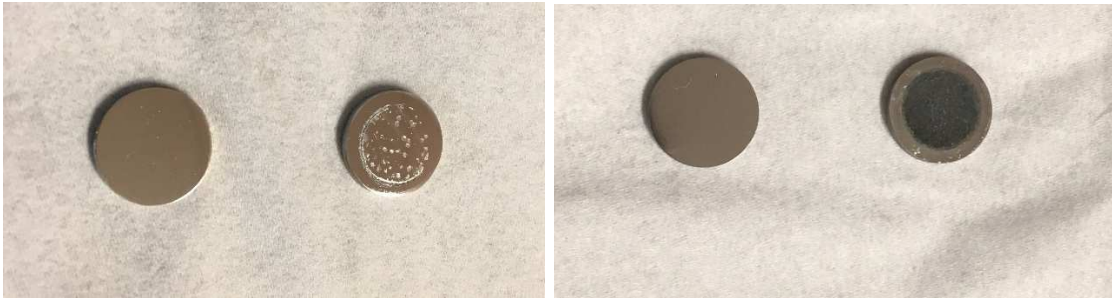
Figure 3.15: Test specimen before and after electrochemical tests (a) stainless steel (b) ductile iron

3.4   Conclusions

This study evaluated the durability and performance of ductile iron when exposed to sodium chloride. The purpose of this was to determine if ductile iron is a feasible material to be used in manufacturing power transmission poles. Accelerated corrosion tests, tensile strength tests, and electrochemical tests were all utilized to gather necessary data. The results from these experimental procedures gave the following conclusions:

- Under accelerated corrosion conditions per ASTM B117, ductile iron samples had an approximate corrosion rate of 52.6 mpy (1.3 mmy), while stainless steel samples experienced no mass loss.

- Tensile strength tests show that there was only about 10 ksi (69 MPa) of strength loss after corrosion for ductile iron. Stainless steel showed no loss in strength. The strength loss in the ductile iron samples was small enough to still be within the minimum standard, according to ASTM A536.

- Electrochemical tests show that ductile iron has a higher corrosion rate and potential for corrosion than stainless steel. Impedance and phase angle plots show that stainless

steel is more resistant to corrosion. Corrosion rates derived from cyclic polarization data show that ductile iron has a higher corrosion rate than ductile iron.

- Analysis of the polarization plots show that the rust formed on the surface of ductile iron is protective in nature as opposed to the soluble rust products, which formed on the stainless steel. This behavior is similar to a weathering steel, and implies that ductile iron may have satisfactory performance in the field.

- To get a better understanding of ductile iron performance in the field, it is recommended that further experiments be done on ductile iron samples that more closely simulate real world environments.

3.5   References

ASTM A240-16a Standard Specification for Chromium and Chromium-Nickel Stainless Steel Plate, Sheet, and Strip for Pressure Vessels and for General Applications1. (2017). ASTM International, West Conshohocken, PA.

ASTM A536-84 Standard Specification for Ductile Iron Castings1 (2017). ASTM International, West Conshohocken, PA.

ASTM B117-16 Standard Practice for Operating Salt Spray (Fog) Apparatus. (2016). ASTM International, West Conshohocken, PA.

ASTM C1617-15 Standard Practice for Quantitative Accelerated Laboratory Evaluation of Extraction Solutions Containing Ions Leached from Thermal Insulation on Aqueous Corrosion of Metals. (2017). ASTM International, West Conshohocken, PA.

ASTM E8-16a Standard Test Method for Tension Testing of Metallic Materials. (2016). ASTM International, West Conshohocken, PA.

ASTM G1-03 Standard Practice for Preparing, Cleaning, and Evaluating Corrosion Test Specimens (2011). ASTM International, West Conshohocken, PA.

ASTM G61-86 Standard Test Method for Conducting Cyclic Potentiodynamic Polarization Measurements for Localized Corrosion Susceptibility of Iron-, Nickel-, or Cobalt-Based Alloys. (2014). ASTM International, West Conshohocken, PA.

ASTM G69-12 Standard Test Method for Measurement of Corrosion Potentials of Aluminum Alloys. (2012). ASTM International, West Conshohocken, PA.

Ahn, Tae-Ho, and Toshiharu Kishi. (2010) "Crack Self-healing Behavior of Cementitious Composites Incorporating Various Mineral Admixtures." Journal of Advanced Concrete Technology ACT 8.2: 171-86.

American pipe manual. (2004). Birmingham, Ala.: American Cast Iron Pipe Co.

Bonds, Richard W. (2015) "Cement-Mortar Linings for Ductile Iron Pipe." Ductile Iron Pipe Research Association.

Carpenter, Ralph. (2010) "Gray Iron and Ductile Iron Pipe—Some Historical Benchmarks Impacting Condition Assessment." World Environmental and Water Resources Congress.

Keil, Brent, and Jack Devletian. (2011) "Comparison of the Mechanical Properties of Steel and Ductile Iron Pipe Materials." Pipelines.

Kleiner, Yehuda, Balvant Rajani, and Dennis Krys. (2013) "Performance of Ductile Iron Pipes. I: Characterization of External Corrosion Patterns." Journal of Infrastructure Systems 19.1: 108-19.

Kleiner, Yehuda, and Balvant Rajani. (2013) "Performance of Ductile Iron Pipes. II: Sampling Scheme and Inferring the Pipe Condition." Journal of Infrastructure Systems 19.1: 120-28.

Kramek, N., & Loh, L. (2007). "The History of Philadelphia's Water Supply and Sanitation System. Lessons in Sustainability of Developing Urban Water Systems." *Master of Environmental Studies. Philadelphia, University of Pennsylvania, Philadelphia Global Water Initiative, junio*.

Liu, Zheng, Marc Genest, and Dennis Krys. (2012) "Processing thermography images for pitting corrosion quantification on small diameter ductile iron pipe." NDT & E International 47: 105-15.

Marcus, P. (2012). "Corrosion mechanisms in theory and practice." Boca Raton: CRC Press.

Noble, H. J. (1940). "History of the Cast Iron Pressure Pipe Industry in the United States of America." Printed at Birmingham publishing Company.

Oke, P.k., and O.k. Ukoba. (2013) "Analysis of Corrosion Growth of Ductile Iron in Different Environments." Advanced Materials Research 824: 327-31.

Oke, P.k., and O.k. Ukoba. (2013) "Analysis of Property Changes of Ductile Iron in Different Environments." Advanced Materials Research 824: 332-38.

Roberge, P. R. (2008). "Corrosion engineering: principles and practice." New York: McGraw-Hill.

Szeliga, Michael J. (2012) "Ductile Iron Corrosion Theories and Science." Pipelines.

Szeliga, Michael J., and Debra M. Simpson. (2003) "Evaluating Ductile Iron Pipe Corrosion." New Pipeline Technologies, Security, and Safety.

Uhlig, H. H., & Revie, R. W. (2008). "Corrosion and corrosion control: an introduction to corrosion science and engineering." Hoboken, NJ: J. Wiley.

Williamson, Jon, and O. Burkan Isgor. (2016) "The effect of simulated concrete pore solution composition and chlorides on the electronic properties of passive films on carbon steel rebar." *Corrosion Science* 106: 82-95

4   General Conclusions

Manuscript 1 provided data that helps further the understanding of the effects of magnesium

chloride deicing solutions and freeze-thaw cycling on the surface resistivity of reinforced

concrete. Routine surface resistivity measurements were taken throughout the entire study

period on both reinforced concrete slabs and their corresponding cylinders. The experimental

results yielded the following conclusions:

- It is recommended that if bulk or surface resistivity are to be used congruently with

  ASTM C666, to use Procedure A in the standard, so as to eliminate the effects that wet

  and dry exposure conditions used in Procedure B may have on the specimens and

  measurements.

- Bulk and SR resistivity measurements taken on the cylinders showed a linear

  relationship which is in line with previous studies that compared the two testing

  methods.

- F-T action had a significant negative impact on the rate of chloride ingress on the slabs.

  The concrete slab with no air entrainment had severe deterioration and allowed for

  substantial chloride ingress after 29 ponding cycles and 240 F-T cycles.

- Although the OPC mixture with air-entrainment visually did not appear to be as

  deteriorated compared to the slab with no air-entrainment, the chloride profiles clearly

  indicate that the penetrability of the slab increased compared to the same slab that did

  not go through F-T action.

- The HPC mixture performed well under F-T action. An increase in transport of chlorides

  was not evident and cannot be seen in the chloride profiles, however, it would be

  beneficial in this study to do a hardened air void analysis on this mixture to verify the air

  void content since the excellent performance of this mixture under F-T action was not

  expected due to the low fresh concrete air content measured.

- It appears that freeze-thaw damage caused an increase in micro-cracking, especially near the surface of the STA slab. This along with the possible decrease in moisture content caused the surface resistivity of STA to increase after ponding was stopped, but freeze-thaw cycles continued.

Manuscript 2 evaluated the durability and performance of ductile iron when exposed to sodium chloride. The purpose of this was to determine if ductile iron is a feasible material to be used in manufacturing power transmission poles. Accelerated corrosion tests, tensile strength tests, and electrochemical tests were all utilized to gather necessary data. The results from these experimental procedures gave the following conclusions:

- Under accelerated corrosion conditions per ASTM B117, ductile iron samples had an approximate corrosion rate of 52.6 mpy (1.3 mmy), while stainless steel samples experienced no mass loss.
- Tensile strength tests show that there was only about 10 ksi (69 MPa) of strength loss after corrosion for ductile iron. Stainless steel showed no loss in strength. The strength loss in the ductile iron samples was small enough to still be within the minimum standard, according to ASTM A536.
- Electrochemical tests show that ductile iron has a higher corrosion rate and potential for corrosion than stainless steel. Impedance and phase angle plots show that stainless steel is more resistant to corrosion. Corrosion rates derived from cyclic polarization data show that ductile iron has a higher corrosion rate than ductile iron.
- Analysis of the polarization plots show that the rust formed on the surface of ductile iron is protective in nature as opposed to the soluble rust products, which formed on the stainless steel.

- To get a better understanding of ductile iron performance in the field, it is recommended that further experiments be done on ductile iron samples that more closely simulate real world environments.

Bibliography

ACI Committee 222R-01: (2001), Protection of Metals in Concrete against Corrosion. Reapproved 2010.

Ahn, Tae-Ho, and Toshiharu Kishi. (2010) "Crack Self-healing Behavior of Cementitious Composites Incorporating Various Mineral Admixtures." Journal of Advanced Concrete Technology ACT 8.2: 171-86. Web.

Alonso, C., C. Andrade, J. A. González. (1988). "Relation between resistivity and corrosion rate of reinforcements in carbonated mortar made with several cement types." Cement and Concrete Research 18(5): 687-698.

American pipe manual. (2004). Birmingham, Ala.: American Cast Iron Pipe Co.

Andrade, C., C. Alonso (2004). "Test methods for on-site corrosion rate measurement of steel reinforcement in concrete by means of the polarization resistance method." Materials and Structures 37(9): 623-643.

Andrade, C., M. Prieto, P. Tanner, F. Tavares, R. d'Andrea. (2013). "Testing and modelling chloride penetration into concrete." Construction and Building Materials 39: 9-18.

ASTM A240-16a Standard Specification for Chromium and Chromium-Nickel Stainless Steel Plate, Sheet, and Strip for Pressure Vessels and for General Applications1. (2017). ASTM International, West Conshohocken, PA.

ASTM A536-84 Standard Specification for Ductile Iron Castings1 (2017). ASTM International, West Conshohocken, PA.

ASTM A615-15a Standard Specification for Deformed and Plain Carbon-Steel Bars for Concrete Reinforcement. (2015). ASTM International, West Conshohocken, PA.

ASTM B117-16 Standard Practice for Operating Salt Spray (Fog) Apparatus. (2016). ASTM International, West Conshohocken, PA.

ASTM C1152-12 Standard test method for acid-soluble chloride in mortar and concrete. (2012). ASTM International, West Conshohocken, PA.

ASTM C1218/C1218M-15 Standard Test Method for Water-Soluble Chloride in Mortar and Concrete. (2015). ASTM International, West Conshohocken, PA.

ASTM C1556-11a Standard test method for determining the apparent chloride diffusion coefficient of cementitious mixtures by bulk design. (2012). ASTM International, West Conshohocken, PA.

ASTM C1617-15 Standard Practice for Quantitative Accelerated Laboratory Evaluation of Extraction Solutions Containing Ions Leached from Thermal Insulation on Aqueous Corrosion of Metals. (2017). ASTM International, West Conshohocken, PA.

ASTM C215-08 Standard Test Method for Fundamental Transverse, Longitudinal, and Torsional Resonant Frequencies of Concrete Specimens. (2014). ASTM International, West Conshohocken, PA.

ASTM C39-15 Standard Test Method for Compressive Strength of Cylindrical Concrete Specimens. (2015). ASTM International, West Conshohocken, PA.

ASTM C457-12 Standard Test Method for Microscopical Determination of Parameters of the Air-Void System in Hardened Concrete. (2012). ASTM International, West Conshohocken, PA.

ASTM C597-09 Standard test method for pulse velocity through concrete. (2010). ASTM International, West Conshohocken, PA. 102

ASTM C666/C666M-15 Standard test method for resistance of concrete to rapid freezing and thawing. (2015). ASTM International, West Conshohocken, PA.

ASTM E8-16a Standard Test Method for Tension Testing of Metallic Materials. (2016). ASTM International, West Conshohocken, PA.

ASTM G1-03 Standard Practice for Preparing, Cleaning, and Evaluating Corrosion Test Specimens (2011). ASTM International, West Conshohocken, PA.

ASTM G61-86 Standard Test Method for Conducting Cyclic Potentiodynamic Polarization Measurements for Localized Corrosion Susceptibility of Iron-, Nickel-, or Cobalt-Based Alloys. (2014). ASTM International, West Conshohocken, PA.

ASTM G69-12 Standard Test Method for Measurement of Corrosion Potentials of Aluminum Alloys. (2012). ASTM International, West Conshohocken, PA.

ASTM WK37880 New Test Method for Measuring the Surfae Resistivity of Hardened Concrete Using the Wenner Four-Electrode Method. (2014). ASTM International, West Conshohocken, PA.

Backus, J., D. McPolin, A. Long, M. Basheer, N. Holmes. (2013). "Exposure of mortars to cyclic chloride ingress and carbonation." Advances in Cement Research 25(1): 3-11.

Basheer, P., P. Gilleece, A. Long, W. Mc Carter. (2002). "Monitoring electrical resistance of concretes containing alternative cementitious materials to assess their resistance to chloride penetration." Cement and Concrete Composites 24(5): 437-449.

Blackburn, R., D. Amsler, K. Bauer (2004). Snow removal and ice control technology. Sixth International Symposium on Snow Removal and Ice Control Technology, Transportation Research Board of the National Academies, Spokane, WA.

Brencich, A., G. Cassini, D. Pera, G. Riotto (2013). "Calibration and Reliability of the Rebound (Schmidt) Hammer Test." Civil Engineering and Architecture 1(3): 66-78.

Bonds, Richard W. (2015) "Cement-Mortar Linings for Ductile Iron Pipe." Ductile Iron Pipe Research Association.

Carpenter, Ralph. (2010) "Gray Iron and Ductile Iron Pipe—Some Historical Benchmarks Impacting Condition Assessment." World Environmental and Water Resources Congress.

Conciatori, D, H. Sadouki, E. Brühwiler. (2008). "Capillary suction and diffusion model for chloride ingress into concrete." Cement and Concrete Research 38(12): 1401-1408.

Concrete materials and methods of concrete construction/Test methods and standard practices for concrete. (2009). Canadian Standards Association, Toronto, ON.

Florida method of test for concrete resistivity as an electrical indicator of its permeability. (2004). Department of Transportation Florida, FL, USA.

Garzon, A. J., J. Sanchez, C. Andrade, N. Rebolledo, E. Menéndez, J. Fullea. (2014). "Modification of four point method to measure the concrete electrical resistivity in presence of reinforcing bars." Cement and Concrete Composites 53: 249-257.

Ghosh, P., Q. Tran. (2015). "Correlation Between Bulk and Surface Resistivity of Concrete." International Journal of Concrete Structures and Materials 9(1): 119-132.

Gowers, K. R., S. G. Millard. (1999). "Measurement of concrete resistivity for assessment of corrosion severity of steel using Wenner technique." ACI Materials Journal 96(5): 536-541.

Gowers, K., S. Millard. (1999). "Measurement of concrete resistivity for assessment of corrosion severity of steel using Wenner technique." ACI Materials Journal 96(5): 536-541. 103

Gucunski, N., I. Arezoo; F. Romero, S. Zanarian, D. Yuan, H. Wiggenhauser, P. Shokouhi, A. Taffe, D. Kutrubes. (2013). Nondestructive testing to identify concrete bridge deck deterioration. Transportation Research Board. Washington, D.C.

Hamilton, H., A. J. Boyd, E. Vivas, M. Bergin. (2007). Permeability of concrete - comparison on conductivity and diffusion methods. No. 00026899. Gainesville, FL, University of Florida.

Hong, K. (1999). Cyclic wetting and drying and its effects on chloride ingress in concrete. National Library of Canada, Ottawa, ON.

Hooton, R.D., A. Shahroodi, E. Karkar. (2012). Evaluating concretes using rapid test methods for fluid penetration resistance, ACI Fall Convention in Toronto, presented in the Emerging Technologies (Part 2); available at aci-int.org.

Hope, B., A. Ip. (1987). "Chloride Corrosion Threshold in Concrete." Materials Journal 84(4): 306-314.

Huang, J., W. Shaowei, J. Chaudhari, S. Soltesz, X. Shi. (2014). Deicer Effect on Concrete Bridge Decks: Practitioners Perspective and a Method of Developing Exposure Maps. Transportation Research Board Annual Meeting: 1-13. Washington, DC.

Hussain, R. R. (2011). "Effect of moisture variation on oxygen consumption rate of corroding steel in chloride contaminated concrete." Cement and Concrete Composites 33(1): 154-161.

Hussain, S., E.,Rasheeduzzafar, A. Almusallam, A. S. Algahtani. (1995). "Factors affecting threshold chloride for reinforcement corrosion in concrete." Cement and Concrete Research 25(7): 1543-1555.

Jackson, L. (2013). "Surface resistivity test evaluation as an Indicator of the Chloride Permeability of Concrete." Tech brief. Publication no. FHWA-HRT-13-024, McLean, VA.

Jaegermann, C. (1990). "Effect of water-cement ratio and curing on chloride penetration into concrete exposed to Mediterranean Sea climate." Materials Journal 87(4): 333-339.

Ji, Y., T. Zan, Y. Yuan. (2009). "Chloride Ion Ingress in Concrete Exposed to a Cyclic Wetting and Drying Environment." American Society of Agricultural and Biological Engineers 52(1): 239-245.

Jiang, J. H. (2013). "Relationship of moisture content with temperature and relative humidity in concrete." Magazine of Concrete Research 65(11): 685-692. 104

Jianhong, C., B. Dylan, J. Frank, H. Dryver. (2008). Concrete bridge deck condition assessment with automated multisensor techniques. Bridge Maintenance, Safety Management, Health Monitoring and Informatics. Burlington, VT, Taylor & Francis.

Julio-Betancourt, J. A. (2009). Effect of de-icer and anti-icer chemicals on the durability microstructure, and properties of cement-based materials. Graduate of Civil Engineering. Toronto, Canada, University of Toronto. Doctor of Philosophy: 854 pp.

Keil, Brent, and Jack Devletian. (2011) "Comparison of the Mechanical Properties of Steel and Ductile Iron Pipe Materials." Pipelines.

Kleiner, Yehuda, Balvant Rajani, and Dennis Krys. (2013) "Performance of Ductile Iron Pipes. I: Characterization of External Corrosion Patterns." Journal of Infrastructure Systems 19.1: 108-19.

Kleiner, Yehuda, and Balvant Rajani. (2013) "Performance of Ductile Iron Pipes. II: Sampling Scheme and Inferring the Pipe Condition." Journal of Infrastructure Systems 19.1: 120-28.

Kessler, R., R. Powers, M. Paredes. (2005). Resistivity measurements of water saturated concrete as an indicator of permeability. NACE International.

Khalim, A. R., D. Sagar, M. D. Kumruzzaman, A. S. M. Z. Hasan. (2011). "Combination of nondestructive evaluations for reliable assessment of bridge deck." Facta universitatis - series: Architecture and Civil Engineering 9(1): 11-22.

Koch, G.H., M. Brongers, N. Thompson, Y. Virmani, J. Payer. (2002). "Corrosion Costs and Preventive Strategies in the United States." FHWA-RD-01-156 (Final Report): 773 pp.

Kosmatka, S. H., M. L. Wilson. (2011). "Design and Control of Concrete Mixtures." 15th Edition: 444, Portland Cement Association, Washington, D.C.

Kramek, N., & Loh, L. (2007). "The History of Philadelphia's Water Supply and Sanitation System. Lessons in Sustainability of Developing Urban Water Systems." *Master of Environmental Studies. Philadelphia, University of Pennsylvania, Philadelphia Global Water Initiative, junio*.

Kulik, D., T. Wagner, S.Dmytrieva, G. Kosakowski, F. Hingerl, K. Chudnenko, U. Berner. (2013). "GEM-Selektor geochemical modeling package: revised algorithm and GEMS3K numerical kernel for coupled simulation codes." Computational Geosciences 17(1): 1-24.

Lingen, R. T. (1998). "Concrete in coastal structures." 301. London, U.K., Thomas Telford Limited.

Liu, Zheng, Marc Genest, and Dennis Krys. (2012) "Processing thermography images for pitting corrosion quantification on small diameter ductile iron pipe." NDT & E International 47: 105-15.

López, W., J. A. González. (1993). "Influence of the degree of pore saturation on the resistivity of concrete and the corrosion rate of steel reinforcement." Cement and Concrete Research 23(2): 368-376.

Lord, B. N. (1988). "Program to reduce deicing chemical usage." Federal Highway Administration: 13 pp., McLean, VA.

Marcus, P. (2012). "Corrosion mechanisms in theory and practice." Boca Raton: CRC Press.

Martin-Perez, B. (1999). "Service life modelling of R.C. highway structures exposed to chlorides." Ph.D. thesis: 168 pp.

Method of test for determination of electrical resistivity of concrete. (2013). Ministry of Transportation Ontario, Toronto, ON.

Morales, M. T. (2015). Experimental investigation of the effects of embedded rebar, cracks, chloride ingress and corrosion on electrical resistivity measurements of reinforced concrete: 174 pp. 105

Morris, W., A. Vico, M. Vázquez. (2004). "Chloride induced corrosion of reinforcing steel evaluated by concrete resistivity measurements." Electrochimica Acta 49(25): 4447-4453.

Mussato, B. T., O. K. Gepraegs and G. Farnden (2004). "Relative effects of sodium chloride and magnesium chloride 0n reinforced concrete: state of the art." Transportation research record. (1866): 59-66.

Mutale, L. (2014). An investigation into the relationship between surface concrete resistivity and chloride conductivity tests: 105 pp.

Neville, A. M. (1981). Properties of Concrete. Pitman Publising Limited, London, United Kingdon.

Neville, A. M. (1996). Properties of Concrete: Fourth Edition. 844. Hoboken, NJ, Wiley.

Noble, H. J. (1940). "History of the Cast Iron Pressure Pipe Industry in the United States of America." Printed at Birmingham publishing Company.

ODOT. (2008). Oregon Standard and Specifications for Construction, Oregon Department of Transportation: 814 pp.

Oke, P.k., and O.k. Ukoba. (2013) "Analysis of Corrosion Growth of Ductile Iron in Different Environments." Advanced Materials Research 824: 327-31.

Oke, P.k., and O.k. Ukoba. (2013) "Analysis of Property Changes of Ductile Iron in Different Environments." Advanced Materials Research 824: 332-38.

Paul Scherrer Institute. (2013). "GEMS: Gibbs Energy Minimization Software for Geochemical Modeling." From http://gems.web.psi.ch.

Presuel-Moreno, F., Y. Liu, M. Paredes (2009). Understanding The Effect Of Rebar Presence And/Or Multilayered Concrete Resistivity On The Apparent Surface Resistivity Measured Via The Four-Point Wenner Method. Corrosion Conference 2009. Atlanta, GA, NACE International.

Qiang, Y., A. Katrien, S. Caijun, S. Geert De. (2008). Effect of temperature on transport of chloride ions in concrete. Concrete Repair, Rehabilitation and Retrofitting II, CRC Press: 159-160.

Roberge, P. R. (2008). "Corrosion engineering: principles and practice." New York: McGraw-Hill.

Rupnow, T., I. Patrick. (2011). Evaluation of surface resistivity measurements as an alternative to the rapid chloride permeability test for quality assurance and acceptance. Louisiana Transportation Research Center: 68 pp.

Ryu, D, W. Ko, T. Noguchi. (2011). "Effects of simulated environmental conditions on the internal relative humidity and relative moisture content distribution of exposed concrete." Cement and Concrete Composites 33(1): 142-153.

Sadowski, L. (2013). "Methodology for assessing the probabilty of corrosion in concrete structures on the basis of half-cell potential and concrete resistivity measurements." Scientific World Journal. 2013: 8. Article ID 714501.

Salehi, M. (2013). Numerical investigation of the effects of cracking and embedded reinforcement on surface concrete resistivity measurements using Wenner probe. Civil 106 and Environmental Engineering. Ottawa, Ontario, Carleton University. Master of Applied Science in Civil Engineering: 155 pp.

Sengul, O., O. E. Gjorv (2009). "Effect of embedded steel on electrical resistivity measurements on concrete structures." ACI Materials Journal 106-M02 (January/February 2009): 11-18.

Sengul, O., O. E. Gjorv. (2008). "Electrical resistivity measurements for quality control during concrete construction." ACI Materials Journal 105(6): 541-547.

Shariati, M., H. Sulong, M. Arabnejad, P. Shafigh, H. Sinaei. (2011). "Assessing the strength of reinforced concrete structures through ultrasonic pulse velocity and Schmidt Rebound Hammer tests." Scientific Research and Essays 6 (1): 213-220.

Shi, X. (2011). Understanding and mitigating effects of chloride deicer exposure on concrete. Western Transportation Institute. Bozeman, MT, Montana State Univerity.

Shi, X., L. Yajun, M. Mooney, M. Berry, L. Fay, A. B. Leonard. (2010). Effect of chloride-based deicers on reinforced concrete structures. Bozeman, MT, Montana State University: 1-74.

Shi, X., Y. Li., S. Jungwirth, Y. Fang, N. Seeley, E. Jackson. (2013). "Identification and laboratory assessment if best practices to protect DOT equipment from the corrosive effect of chemical deicers." 217 pp.

Sirivivatnanon, V., W. A. Thomas, K. Waye. (2012). Determination of free chlorides in aggregates and concrete. Australian Journal of Structural Engineering. 151-158.

Song, H., V. Saraswathy. (2007). "Corrosion monitoring of reinforced concrete structures - a review." International Journal of Electrochemical Science 2(2007):1-28.

Standard method of test for surface resistivity indication of concrete's ability to resist chloride ion penetration. (2011). American Association of State Highway and Transportation Officials, Washington DC.

Sutter, L., K Peterson, G. Julio-Betancourt, D. Hooton, T. V. Dam, k. Smith. The Deleterious Chemical Effects of Concentrated Deicing Solutions on Portland Cement Concrete. (2008). SD2002-01. Federal Highway Administration: 1-198, Houghton, MI.

Swanstrom, J., T. Rogers, G. Bowling, S. Tuttle (2013). ODOT bridge inspection program manual 2013. Oregon Department of Transportation: 1-381, OR.

Szeliga, Michael J. (2012) "Ductile Iron Corrosion Theories and Science." Pipelines.

Szeliga, Michael J., and Debra M. Simpson. (2003) "Evaluating Ductile Iron Pipe Corrosion." New Pipeline Technologies, Security, and Safety.

Uhlig, H. H., & Revie, R. W. (2008). "Corrosion and corrosion control: an introduction to corrosion science and engineering." Hoboken, NJ: J. Wiley.

Wagner, T., D. A. Kulik, F. F. Hingerl, S. V. Dmytrieva. (2012). "Gem-Selektor geochemical modeling package: TSolmod library and data interface for multicomponent phase models." Canadian Mineralogist 50(5): 1173-1195. 107

Wang, Q. Z., L. Wang, Y. Yao, K. Li. (2015). "Electrical resistivity of cement pastes undergoing cyclic freeze-thaw action." Journal of Materials in Civil Engineering. 27(1).

Wang, Z., Q. Zeng, L. Wang, Y. Yao, K. Li. (2014). "Effect of moisture content on freeze–thaw behavior of cement paste by electrical resistance measurements." Journal of Materials Science. 49(12): 4305-4314.

Weydert, R., C. Gehlen. (1999). "Electrolytic resistivity of cover concrete: Relevance, measurement and interpretation." Proceedings of the 8th International Conference on Durability of Building Materials and Components. 409-419. NRC Research Press, Vancouver,

APPENDICES

APPENDIX A: Type II Cement Composition

WYOMING ANALYTICAL LABORATORIES, INC.

November 5, 2014

Chang Li
Oregon State University
220 Owen Hall
Corvallis, OR 97331-3212

WAL #140913-1
Sample ID. Type I/II Cement
PO#:

CHEMICAL ANALYSIS
Wt%, as Rec'd Basis

Silicon Dioxide	SiO_2	19.93
Aluminum Oxide	Al_2O_3	4.77
Iron Oxide	Fe_2O_3	3.50
Calcium Oxide	CaO	63.47
Magnesium Oxide	MgO	0.87
Sodium Oxide	Na_2O	0.29
Potassium Oxide	K_2O	0.33
Total Alkalies as Na_2O		0.51
Titanium Dioxide	TiO_2	0.27
Manganic Oxide	Mn_2O_3	0.12
Phosphorus Pentoxide	P_2O_5	0.07
Strontium Oxide	SrO	0.18
Barium Oxide	BaO	0.11
Sulfur Trioxide	SO_3	3.11
Loss on Ignition		3.09
Total		100.00

Tricalcium Silicate	C_3S	61.33
Tricalcium Aluminate	C_3A	6.61
Dicalcium Silicate	C_2S	10.86
Tetracalcium Aluminoferrite	C_4AF	10.64

*TiO_2 and P_2O_5 not included in Al_2O_3

* No correction has been made for the possible use of limestone.
Analysis per ASTM C 114

Charles R. Wilson,
Division Manager

APPENDIX B: Silica Fume Composition

WYOMING ANALYTICAL LABORATORIES, INC.

14335 W. 44th Avenue
Golden, CO 80403

www.wal-lab.com
Email: walxray@aol.com

(303) 278-2446
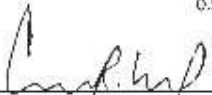Fax: (303) 278-2439

September 29, 2014

Chang Li
Oregon State University
220 Owen Hall
Corvallis, OR 97331-3212

Denver Division #:   140912-1
Sample ID: Silica Fume
PO#:

CHEMICAL ANALYSIS
WT%, DRY BASIS

Silicon Dioxide, SiO2	90.17
Aluminum Oxide, Al2O3	0.48
Iron Oxide, Fe2O3	1.49
Total (SiO2 + Al2O3 + Fe2O3)	92.13
Calcium Oxide, CaO	1.01
Magnesium Oxide, MgO	2.55
Sodium Oxide, Na2O	0.20
Potassium Oxide, K2O	0.78
Titanium Dioxide, TiO2	0.00
Manganese Dioxide, MnO2	0.17
Phosphorus Pentoxide, P2O5	0.11
Strontium Oxide, SrO	0.02
Barium Oxide, BaO	0.00
Sulfur Trioxide, SO3	0.13
Loss on Ignition (950°C)	2.90
Total	100.00
Moisture (105°C), as Received	0.56

Analysis per ASTM C 1240

Charles R. Wilson
Division Manager

MEMBER
ACIL

APPENDIX C: Class F Fly Ash Composition

WYOMING ANALYTICAL LABORATORIES, INC.

14335 W. 44th Avenue
Golden, CO 80403

www.wai-lab.com
Email: walxray@aol.com

(303) 278-2446
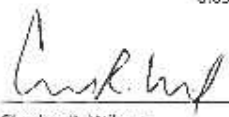Fax: (303) 278-2433

September 29, 2014

Chang Li
Oregon State University
220 Owen Hall
Corvallis, OR 97331-3212

Denver Division #: 140917-1
Sample ID: Fly Ash
PO#:
Project#:

CHEMICAL ANALYSIS
WT%, DRY BASIS

Silicon Dioxide, SiO_2	49.69
Aluminum Oxide, Al_2O_3	17.23
Iron Oxide, Fe_2O_3	5.63
Total ($SiO_2 + Al_2O_3 + Fe_2O_3$)	72.54
Calcium Oxide, CaO	13.94
Magnesium Oxide, MgO	4.48
Sodium Oxide, Na_2O	3.58
Potassium Oxide, K_2O	1.71
Titanium Dioxide, TiO_2	0.98
Manganese Dioxide, MnO_2	0.09
Phosphorus Pentoxide, P_2O_5	0.31
Strontium Oxide, SrO	0.35
Barium Oxide, BaO	0.62
Sulfur Trioxide, SO_3	0.99
Loss on Ignition (750°C)	0.42
Total	100.00

Moisture (105°C), as Received   0.09

Analysis per ASTM C 311

Charles R. Wilson
Division Manager

MEMBER
ACIL

APPENDIX D: Coarse Aggregate Sieve Analysis

Sieve	Sieve Wt. (kg)	Sample Wt. (kg)	Sieve	Opening (mm)	Percent Retained	Sample Weight	Percent Passing	Cumulative Percent Retained
1.5"	8.748	8.748	1.5."	38.10	0.00	0.00	100.00	0.00
3/4"	7.468	8.096	3/4"	19.05	5.45	0.63	94.55	5.45
1/2"	7.324	12.556	1/2"	12.70	45.37	5.23	49.18	50.82
1/4"	8.608	13.712	1/4"	6.35	44.26	5.10	4.93	95.07
No. 4	6.954	7.330	No. 4	4.75	3.26	0.38	1.66	98.34
No.8	6.526	6.696	No.8	2.36	1.47	0.17	0.19	99.81
Pan	6.252	6.274	Pan	0.00	0.19	0.02	0.00	100.00
Total	51.880	63.412		11.53	100.0	11.53		250.52

APPENDIX E: Fine Aggregate Sieve Analysis

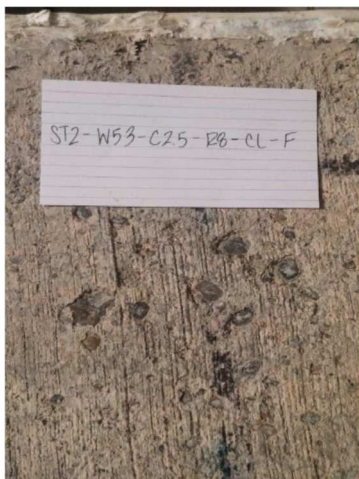| Sieve Opening (mm)	Percent Retained	Sample Weight	Percent Passing	Cumulative Percent Retained
9.525	0.00	0.0	100.00	0.00
4.75	4.55	59.5	95.45	4.55
2.36	18.71	244.5	76.74	23.26
1.18	13.74	179.5	63.00	37.00
0.6	12.53	163.7	50.47	49.53
0.3	34.51	451.0	15.96	84.04
0.15	14.10	184.2	1.86	98.14
Pan	1.86	24.3		100.00
	100.00	1306.7	403.47	
Fineness Modulus		2.97		

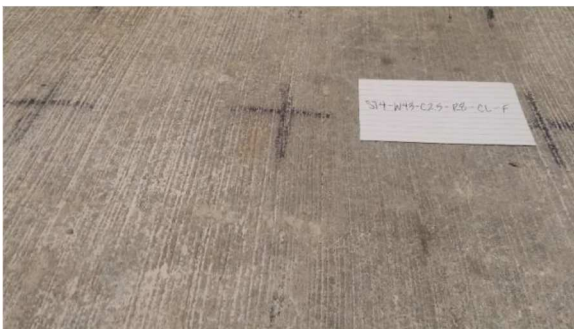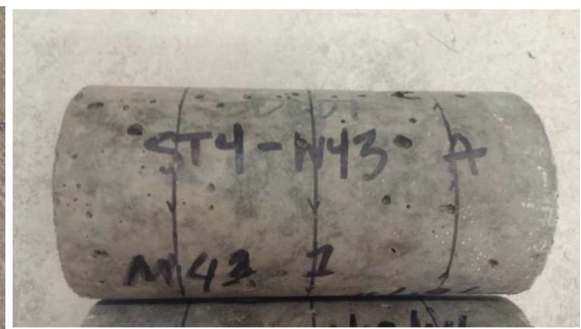APPENDIX F: Deterioration due to Freeze-Thaw Action
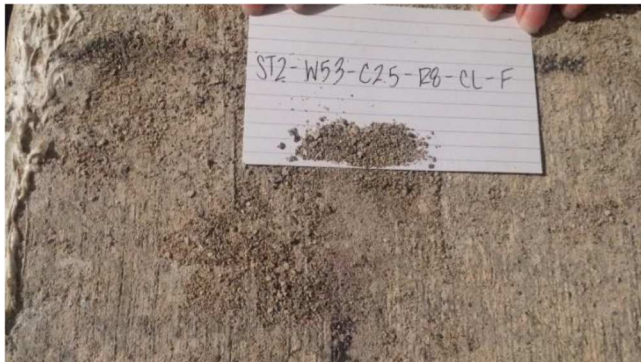
(a)

(b)

(c)

(d)

(e)

(f)

Appendix D - Deterioration due to F-T action. (a)-(d) represent the non-entrained OPC mixture; (e) and (f) represent the HPC mixture.